DOE/JPL 1060-22
GEAEP-54

A Conceptual Design Study on the Application of Liquid Metal Heat Transfer Technology to the Solar Thermal Power Plant

FINAL REPORT

Contract No. 955018

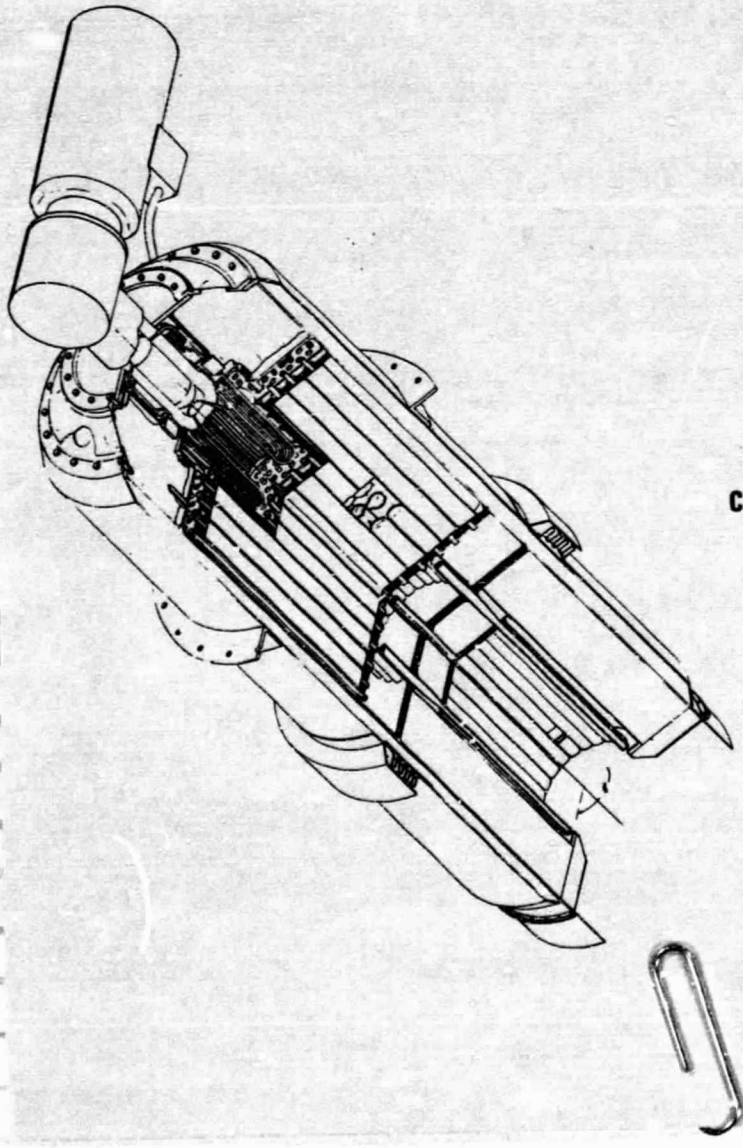

September 25, 1979

Prepared for

JET PROPULSION LABORATORY
CALIFORNIA INSTITUTE OF TECHNOLOGY
Pasadena, California 91103

GENERAL ELECTRIC
ADVANCED ENERGY PROGRAMS
Cincinnati, Ohio 45215

DOE/JPL 1060-28
GEAEP-54

FINAL REPORT

A CONCEPTUAL DESIGN STUDY ON THE APPLICATION OF LIQUID METAL HEAT TRANSFER TECHNOLOGY TO THE SOLAR THERMAL POWER PLANT

by

WF ZIMMERMAN, CS ROBERTSON, CL EHDE,
SM DIVAKARUNI AND LE STACY

for

JET PROPULSION LABORATORY
CALIFORNIA INSTITUTE OF TECHNOLOGY
PASADENA, CALIFORNIA 91103

J.W. STEARNS AND DR. Y.S. WON
PROGRAM MANAGERS

CONTRACT NO. 955018

SEPTEMBER 25, 1979

GENERAL ELECTRIC
ADVANCED ENERGY PROGRAMS
CINCINNATI, OHIO 45215

"This work was performed for the Jet Propulsion Laboratory, California Institute of Technology sponsored by U.S. Department of Energy through an agreement with the National Aeronautics and Space Administration."

ABSTRACT

Alkali metal heat transfer technology was used in the development of conceptual designs for the transport and storage of sensible and latent heat thermal energy in distributed concentrator, solar Stirling power conversion systems at a power level of 15 kW_e per unit. Both liquid metal pumped loop and heat pipe thermal transport were considered; system configurations included (1) an integrated, focal mounted sodium heat pipe solar receiver (HPSR) with latent heat thermal energy storage (TES), (2) a liquid sodium pumped loop with the latent heat storage, Stirling engine-generator, pump and valves located on the back side of the concentrator and (3) similar pumped loops serving several concentrators with more centralized power conversion and storage. The focus mounted HPSR was most efficient, lightest and lowest in estimated cost. Design confirmation testing indicated satisfactory performance at all angles of inclination of the primary heat pipes to be used in the solar receiver. The pumping and flow characteristics of wicking materials and wick joints to be used in the secondary TES heat pipe were confirmed using easy fluids at room temperature. An assessment of the initial conceptual design HPSR has indicated further avenues of performance improvement and cost reduction. Work is continuing under a subsequent contract for the design, fabrication, and test of the HPSR with TES.

TABLE OF CONTENTS

Page No.

LIST OF FIGURES

LIST OF TABLES

SECTION I

SUMMARY

The excellent high temperature heat transfer characteristics of alkali metal thermal transport systems were applied in this study for the purpose of identifying a practical, low cost, and highly efficient thermal transport and storage subsystem for a distributed concentrator solar Stirling power conversion system. It was intended that each concentrator/receiver/engine-generator unit would be capable of providing approximately 15 kW_e and that a large number of units would be operated on one site to produce stand-alone power or power to an electrical grid at total power levels up to 5-10 MW_e.

Both latent heat and sensible heat thermal energy storage (TES) were considered to provide either buffered storage for continued smooth engine-generator operation during periods of cloud cover and/or sufficient energy storage to meet typical utility power load requirements. The various systems alternatives which were studied included single and multiple concentrators, focus mounted and Cassegrainian mounted receivers and TES/engine-generator units at the focus, behind the concentrator, or separately located and shared by several concentrators.

Latent heat storage and sodium heat pipe thermal transport were selected for a fully integrated, compact, and thermally self-regulated focus mounted solar receiver/TES/engine-generator subsystem, called the heat pipe solar receiver (HPSR). This subsystem was selected as the most promising because of its higher efficiency, low pumping and thermal power losses, acceptable weight, mass-producibility, low on-site installation labor, and simple field change-out.

Sodium heat pipes in the receiver delivered thermal energy to a large secondary heat pipe containing both the latent heat TES material in cylindrical metal containers and also the heat exchanger tubes of the Stirling engine. The absence of wicking in the condenser area of the primary heat pipes prevented reverse heat flow from the secondary TES heat pipe back to the receiver during periods of cloud cover. A TES duration of 1.25-2 hours in this design provided for stable, continuous operation of the Stirling engine at near constant temperature. The TES system also provided the capability for simple fossil fuel hybridization of the system using an on-off gas or fuel oil combustor without the need for a high turn-down ratio or complex, variable-combustion control devices.

As an alternative to the compact focal mounted system, a liquid metal pumped loop system powered by an electromagnetic pump was also investigated The latent heat TES, EM pump and liquid metal control valves

were located behind the concentrator where their mass could be utilized to reduce some of the concentrator counterweight mass and where potentially larger quantities of TES material could be incorporated. The system was heavier, more complex, costlier, and less efficient than the focus mounted heat pipe solar receiver (HPSR).

The design of the HPSR was assessed in greater detail for further development and exploitation of its desirable features. Potential improvements in design, weight, and cost were identified. Easy fluid tests were conducted which confirmed the performance of secondary heat pipe wicking of the various types to be used in the design and which confirmed the flow of liquid across wick joints. Primary heat pipes with various internal wick configurations were built and tested satisfactorily at full power under various angles of inclination; the thermal diode effect in these heat pipes was demonstrated; heat pipe tests were run which demonstrated that, after cooling the receiver, the concentrator could be moved to the inverted, stowed position without overnight heat loss through the primary heat pipes.

This work indicated that the focus mounted HPSR has many performance, operational, weight, and cost advantages over alternate thermal transport and storage systems and that it should lend itself favorably and efficiently to hybridization with fossil fuels.

Further development of the HPSR is continuing in a separate contract intended to design, fabricate, and test a 20 kW_e Stirling solar powered conversion system.

SECTION II

INTRODUCTION

A. OBJECTIVES

The objectives of the conceptual design study on the use of liquid metal heat transfer technology in 15 kW_e distributed concentrator solar Stirling power systems were to:

- Indicate the economic viability of alkali metal heat transport for use in the 1985 time period.
- Perform benefit/cost analysis evaluating various promising systems and indicate the relative merit of competing systems.
- Define a promising alkali metal heat transport and storage system.
- Prepare conceptual designs of one or more of the promising systems with the objective of low capital cost in mind.
- Define the necessary developmental effort, including design concept demonstrations required to assure successful implementation of the selected system.

B. SCOPE

The investigations initially considered a broad range of system options as described in Section III. These included:

(1) Sensible and latent heat storage for period of 15 minutes to six hours

(2) Single and multiple concentration systems

(3) Pumped loop and heat pipe thermal transport

(4) Focus-mounted Cassegrainian and fixed-mounted solar receiver configurations

(5) Thermal storage/power conversion subsystems located at the focal point, behind the concentrator or at remote locations served by several concentrators

(6) Thermal transport and storage without the use of liquid metal transport media.

Major effort was placed upon the conceptual design of a compact, focus-mounted heat pipe solar receiver (HPSR) with TES and its integration with a Stirling engine-generator. This system, described more fully below, had the advantages of high efficiency, nearly self-regulated thermal transport and storage, potential incorporation of a simple fuel combustor for hybridization, and amenability to factory production, to simple installation and servicing, and to ready field change-out.

Additional work was undertaken in the experimental verification of design concepts involving heat pipe and wicking design, fabrication, and operating characteristics. This effort is summarized in Section IV-B.6 and 7 and described in separate topical reports*. A brief assessment was also made of current heat pipe technology and operating life experience. This is summarized in Section VII-F and described in more detail in a separate topical report**.

The original design concept integrated the HPSR-TES subsystem with a hypothetical Stirling engine with a specifically calculated heat exchanger configuration. Limited additional work was done in assessing the integration of this subsystem with both a modified P40 United Stirling engine and with a modified 1-98 Phillips type Stirling Engine as described in Section IV-B.9.

Liquid metal pumped loop design concepts, powered by EM or gas lift pumps, were also investigated and assessed. Pumped loop systems have the potential for longer periods of TES because larger TES masses can be located behind the concentrator rather than at the focus. A direct comparison was made between a HPSR and pumped loop system of equivalent TES capacity and operating power.

C. DESIGN GUIDELINES

The design guidelines under which the conceptual designs of the HPSR with TES and the EM pumped loop were prepared are shown in Table 2-1. Earlier work in assessing latent and sensible heat TES options and in characterizing the performance of TES systems was done with earlier design guidelines which differed slightly in such areas as concentrator diameter, receiver aperture diameter, concentrator and receiver efficiency, peak power to TES, Stirling engine efficiency, Stirling engine power, and electrical generator output. For this reason some data reported herein is on a slightly different design basis that the conceptual designs. The conceptual designs are consistant, however.

---

* Divakaruni, S.M., "Heat Pipe Design Confirmation Testing", DOE/JPL 1060-27, GEAEP-55, September 25, 1979.
Divakaruni, S.M., "Easy Fluid Wicking Tests Related to Solar Receiver Heat Pipes", DOE/JPL 1060-26, GEAEP-53, September 25, 1979.

** Zimmerman, W.F. and Stearns, J.W., "Heat Pipe Operating Reliability for the Solar Stirling Receiver", DOE/JPL 1060-29 (to be published).

Table 2-1. Design Guidelines

Concentrator/Solar Receiver:	
Concentrator Diameter	11.5
Concentrator Area	104 m^2
Concentration Ratio	2000
Concentrator Efficiency	70%
Receiver Aperture Diameter	0.257 m
Peak Solar Insolation	1 kW_t
Average Solar Insolation	0.845 kW_t/m^2
Receiver Efficiency	85%
Focal Point Weight	1365 kg
TES:	
Power to TES, Peak	62.1 kW_t
Power to TES and to Stirling Engine, Avg.	52.5 kW_t
Thermal Storage Duration	1.7-2.0 hr.
Sensible Heat Storage Temp. Rise	100°C (180°F)
Latent Heat Storage Temp. Rise	55.5°C (100°F)
Stirling Engine/Generator:	
Nominal Stirling Engine Temp., Max.	827°C (1520°F)
Engine Efficiency	35%
Engine Power, Avg.	18.3 kW
Generator Efficiency	90%
Generator Output, Peak	N.A.
Generator Output, Avg.	16.5 kW_e
Rectifier Efficiency	95%
Power to Grid	15 kW_e
Power To Battery Storage (Before Rectification)	1.5 kW_e

D. WEIGHT AND COST GOALS

As indicated in the design guidelines, the weight limit at the focal point was 1365 kg (3000 lbs.). This weight limit does not include the weight of struts or mounting ring which are normally considered a part of the concentrator itself.

The cost target for the solar heat receiver/TES subsystem was given as $\$400/kW_e$ in mass production quantities. More recently*, production cost goals were specified as $\$6/kW_t$ for the solar receiver and $\$15/kW_e$ + $\$10/kWh_e$ for the benefit of thermal storage; this resulted in a final cost target of $\$110/kW_e$, a significantly lower goal.

E. SELECTION OF THE HEAT PIPE SOLAR RECEIVER

An initial comparative analysis was made of the various system possibilities for the transport and storage of thermal energy for a 15.6-20 kW Stirling engine generator system with 1.7-2.0 hours storage. Of the large number of possibilities considered, the integrated focus mounted system, using sodium heat pipes, was selected as the most promising for preliminary conceptual design. It utilized efficient heat pipes to transport heat from the receiver into the TES and to the Stirling engine heat exchanger over a relatively short distance. No external pumping power was required to move the heat transport fluid. The thermal losses were low because of the compactness of the design. The compactness of the design also reduced weight and cost and rendered the unit mass-producible and easily installed and replaced with minimum field labor.

Latent heat storage was selected over sensible heat storage for the JPSR (and for pumped loop systems) to minimize weight, volume, and cost effects. This selection also eliminated the necessity for the wider range of Stirling engine operating temperatures and the peak materials operating temperatures associated with sensible heat storage. Both LiF and NaF-MgF_2 eutectic were considered in equivalent weight design concepts which produced 1.88 and 1.27 hours, respectively, of thermal storage at nominal design conditions.

The study also considered and found less desirable the use of pumped loops for both focus mounted and dispersed concentrator systems. The dispersed system pumped loop concept was unattractive because of: (1) the large heat losses, pumping losses and operating temperature differentials encountered in such systems; (2) the necessity of both the development costs and the procurement costs of high temperature pumps and valves which are not presently available; and (3) the need for flexible joints in the liquid metal lines at the concentrator. A concentrator mounted pumped loop system without flexible bellows and with the TES and engine affixed to the back of the concentrator was conceptually designed and assessed as the most promising of the pumped loop systems because of its lower heat losses, lower pumping losses, and the opportunity it afforded

*Stearns, J.W., "Dish Stirling Experiment," Advanced Technology Meeting on Advanced Solar/Thermal Power Systems, Long Beach, California, June 19-21, 1979, DOE 5102-129, p. 6.

for larger thermal energy storage than was possible at the focal point. However, it was not as attractive as the HPSR because of its higher weight and cost, its lower thermal efficiency, and the larger system ΔT.

The use of thermal storage for periods up to 15 minutes without the use of heat pipes or pumped loops was also considered but was not as attractive as the HPSR. Initial thermal analysis indicated that inordinately large temperature drops were required to transport heat from the relatively larger volume and surface area of the TES material, through a reasonable distance, to the very limited area of the heat exchanger. A reasonable design concept was later developed for 15 minutes of useful storage, but this concept required extrapolation of Stirling engine heat exchanger design beyond the bounds of conventional practice, requiring the use of a very small number of very long Stirling engine heat exchanger tubes to keep the calculated pressure drops and void volumes within acceptable limits.

The focus mounted HPSR alone appeared to offer the best opportunity to develop, economically, a thermally buffered receiver with the potential for a significant amount of additional TES. A description of that system is presented below.

F. HEAT PIPE SOLAR RECEIVER WITH THERMAL ENERGY STORAGE

The conceptual design of the heat pipe solar receiver/TES/Stirling engine-generator subsystem is shown in Figure 2-1. Its principal features are given in Table 2-2. In the assessment of this conceptual design, several design improvements and the use of alternate materials have been suggested as a means of improving the performance, weight, and, most importantly, the mass production cost of the unit.

The system is comprised of:

(1) A primary sodium heat pipe solar receiver comprised of 27 one-inch diameter heat pipes flattened in the heat receiver area

(2) A large diameter secondary sodium heat pipe containing the TES material in sealed containers

(3) A Stirling engine in which the heater head heat exchanger coils are immersed in the sodium vapors of the secondary TES heat pipe

(4) A 3-phase induction generator connected to the Stirling engine

(5) A thermal insulation system

(6) A structural support system for supporting the various components and mounting the system at the focal point.

The primary heat pipes receive the solar heat and transfer it into the secondary heat pipe. Since these heat pipes are internally

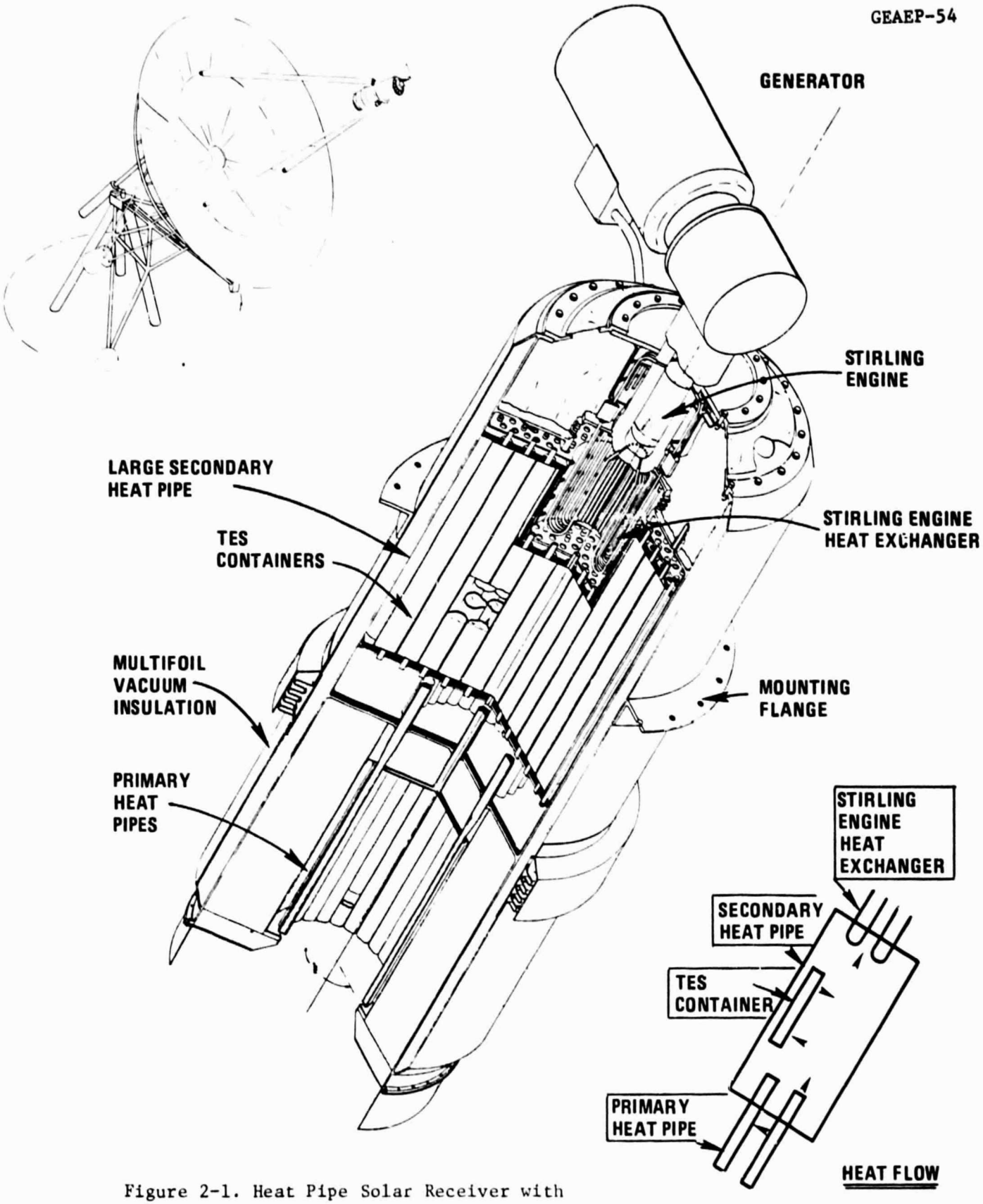

Figure 2-1. Heat Pipe Solar Receiver with TES for Stirling Solar Power

Table 2-2. Principal Features of the Heat Pipe Solar Receiver/TES/Stirling Engine-Generator Subsystem

Diameter	71 cm (28 in.)
Length	231 cm (91 in.)
Weight	1497 kg (3300 lbs.)
Power Output	15.6 kW_e
Thermal Storage Power	98.7 kWh_t
Latent Heat TES Material	LiF or $NaF-MgF_2$
Nominal Operating Temperatures	
Solar Receiver Heat Pipes	856°C (1572°F)
TES Heat Pipe Vapor Space	838°C (1540°F)
Stirling Engine Heat Exchanger	838°C (1540°F)
Heat Pipe Working Fluid	Sodium
Stirling Engine Type	Single Cylinder Rhombic Drive
Stirling Engine Working Fluid	Helium
Stirling Engine Working Fluid Pressure	∿175 atmospheres
Engine-Generator Speed	1800 RPM
Generator Type	Induction
Thermal Insulation	Vacuum-Foil

wicked in the solar receiver area only, sodium liquid cannot flow into the condenser area of the heat pipe under normal operating conditions and thus reverse heat flow in the heat pipe from the TES to the solar receiver is prevented during periods of cloud cover. The primary heat pipe will not operate in a heat loss mode overnight. Prior to overnight shutdown the sodium can be allowed to solidify in the aperture end of the primary heat pipes before the concentrator is moved to the overnight "stowed" position with the receiver aperture pointed upward. This effectively prevents the heat pipe from operating in the inverted position.

The secondary heat pipe operates to transfer heat efficiently, and at near-isothermal conditions, between the primary heat pipe condensers, the TES material sealed in containers, and the surface of the Stirling engine heat exchanger tubes. Liquid sodium is supplied to all surfaces except the Stirling engine heat exchanger by means of screen or fiber metal wicks to assure effective transfer of heat throughout this secondary heat pipe. This heat transfer is promoted by high latent heats of vaporization and condensation, negligible thermal transport pumping power, and very high evaporation and condensing film coefficients. Calculated temperature differentials from the receiver to the Stirling engine heat exchanger tubes are minimal, on the order of 18°C (32°F).

The TES system will require some temperature gradient across the TES containers to thermally charge or discharge the system. However, the magnitude of the temperature gradient is dependent upon the energy transfer rate and the thickness of the solidified salt inside the TES can. Only during the final stages of TES thermal discharge at maximum power levels will the TES can temperature (and the Stirling engine temperature) drop as much as 41-47°C (75-85°F). In most other modes of operation, surface of the TES can will operate at the TES temperature (or slightly above it, depending upon the heat flow into the TES material). Brief variations in solar receiver power will make only relatively minor changes in the TES can temperature and in the Stirling engine operating temperature.

The heat pipe focus mounted subsystem is nearly self-regulating in that the excess power is absorbed in the thermal "inertia" of the TES system; conversely, the engine operates by demand on the TES system during cloud cover or diminished insolation. This thermal transport and storage system operates without valves or controls; it requires only simple temperature measurement instrumentation and relies upon external concentrator controls to defocus the system in case the thermal storage is overloaded. Otherwise, the heat flow is regulated solely by solar thermal inputs and Stirling engine thermal demands. It operates well on the basis of thermal inputs and outputs and demand requirements in various modes of operation throughout a typical day.

Since the 13-hour overnight sensible heat losses result in only a 42°C (76°F) drop when the TES system is fully discharged, the system can be started with a stable, near-normal operating temperature. This can occur once the solar insolation is sufficient to sustain continued operation. Alternatively, the TES system can be partially charged at low solar insolation and an orderly and planned startup of the system can be made at full power before nominal solar insolation is reached.

With the TES partially charged after overnight storage, nominal rated power can be achieved early in the day by calling upon the TES for heat even before the solar insolation has reached its average value and without the need for a supplemental heat source from the combustion of fossil fuel.

When the use of a hybrid heat source is required, the thermal energy storage capability of this heat pipe solar receiver concept will permit full on-off operation of the combustor at full combustor efficiency rather than with carefully proportioned additions of heat to the TES system. The development and use of fossil fueled hybrid heat sources are being considered in a separate contract for the design, fabrication, and test of the HPSR.

The design and operation of this focus mounted system is based upon: (1) a sound technology of heat pipe design prediction methods and operating characteristics, and (2) the prior successful development and operation of somewhat similar high temperature fused salt storage and heat pipe thermal transport applications* for low earth orbit space power and for Stirling engine heat transfer and storage demonstrations**. Additional full-scale design confirmation testing will be required and further design refinements will be necessary under separate contracts to bring a prototype power conversion system of this type to a point of demonstrated life and economic viability.

*Richter, R., "Thermal Energy Storage Demonstration Unit for Vuilleumier Cryogenic Cooler", AFAPL-TR-76-110, Xerox Electro-Optical Systems, Pasadena, CA, February 1977.

**Schubert, K.P., Brost, O., Groll, M., Krähling, H., Mack, H., and Zimmerman, P., "Development of a Heat Pipe Transport and Storage System", Proc. 1st International Heat Pipe Conference, Stuttgart, 1973. See also: Waters, E.O., "A Road Vehicle Thermal Energy Storage Concept and Evaluation", ANL-K78-3983-1, Sigma Research, Inc., Richland, WA, December 1978.

SECTION III

SYSTEMS ALTERNATIVES

A. POTENTIAL SYSTEMS

A number of potential systems using liquid metal for heat transport were identified and evaluated. Table 3-1 shows eleven of these systems.

The first nine cases include use of battery storage for post-insolation power in either heat pipe or pumped loop systems for heat transport. The tenth and eleventh cases involve the use of thermal storage alone for continuous generation of the basic 15 kW_e power beyond the normal insolation period; their development is associated with the need for concentrator designs which permit large thermal storage at a separately supported focal point. The first nine cases require up to a two hour period of thermal storage to accommodate variations in solar insolation and to permit efficient continuous operation of the engine-generator at near-design temperature and load conditions without serious off-design operating inefficiencies and with minimized thermal fatigue implications. In these first nine cases both heat pipes and pumped loops are utilized to transport heat to a single closely coupled storage system in the heat pipe system, and to either an adjacent or remotely located thermal storage system in the pumped loop system. Both sensible and latent heat storage are considered for periods of 15 minutes to 2 hours; the brief storage period is for short cloud cover purposes and the longer period assures much less frequent interruption in the normal operating mode.

Cassegrainian mounting of the receiver, storage, and engine either to the back surface of the concentrator or to a fixed mount behind the concentrator have some potential system advantages which are offset by the additional reflecting mirror losses.

From Table 3-1, and the limits set by the design guidelines given in Table 2-1, the two key trade-offs are the form of TES (latent or sensible) and the heat transport method (heat pipe or pumped loop). These, as well as several other key items are discussed in subsequent sections.

B. ENERGY STORAGE

Energy storage is obviously required for use with solar energy. The simplest storage option is to use the electrical power grid. In this mode, solar generation facilities are analogous to a negative, semi-random load which is managed by the electric utility using their complete mix of power plants. Reasons for not using this option include economics as well as the need to minimize grid demands for solar power shortfalls. Other forms of storage include thermal, chemical, and electrical (battery).

Table 3-1. Preliminary Design Options

PARAMETER	CASE										
	1	2	3	4	5	6	7	8	9	10	11
Generator Power, Average	20 kW_e (16.5 kW_e)*									15 kW_e	
TES Duration, Post Insolation	None									6 Hours	
Other Storage	Batteries									6 Hours TES	
Heat Transport Method	Heat Pipes						Pumped Loop			Heat Pipes	
Concentrator per TES/Engine	1						1	5	10	1	
TES Type	Sensible Heat		Latent Heat		Sensible Heat						Latent Heat
TES Duration (during Insolation)	15 Min.	2 Hrs.	15 Min.	2 Hrs.	2 Hours					6 Hours	
Concentrator/Receiver Type	Focus Mount				Cassegrainian Concentrator Mount	Cassegrainian Fixed Mount	Focus Mount			Fixed Mount	

Basic Parameters:*

- Generator Efficiency, 0.9
- Stirling Engine Efficiency, 0.42 (0.35)
- Heat Receiver Efficiency, 0.9 Overall (.85)
- Concentrator Efficiency, 0.8 (Focal Point Concentrator) (.70)

* Values in parentheses are for the revised system

- Concentrator Size, 11 m (11.5 m)
- Solar Flux, Lancaster, Ca, Data (1 kW/m^2 peak flux, 845 W_t/m^2 avg for 11 hour average day)

Table 3-1. Preliminary Design Options

PARAMETER	CASE										
	1	2	3	4	5	6	7	8	9	10	11
Generator Power, Average	20 kW_e (16.5 kW_e)*									15 kW_e	
TES Duration, Post Insolation	None									6 Hours	
Other Storage	Batteries									6 Hours TES	
Heat Transport Method	Heat Pipes						Pumped Loop			Heat Pipes	
Concentrator per TES/Engine	1						1	5	10	1	
TES Type	Sensible Heat			Latent Heat		Sensible Heat					Latent Heat
TES Duration (during Insolation)	15 Min.	2 Hrs.	15 Min.	2 Hrs.	2 Hours					6 Hours	
Concentrator/Receiver Type	Focus Mount				Cassegrain-ian Concentrator Mount	Cassegrain-ian Fixed Mount	Focus Mount			Fixed Mount	

Basic Parameters:*

Generator Efficiency, 0.9
Stirling Engine Efficiency, 0.42 (0.35)
Heat Receiver Efficiency, 0.9 Overall (.85)
Concentrator Efficiency, 0.8 (Focal Point Concentrator) (.70)

Concentrator Size, 11 m (11.5 m)
Solar Flux, Lancaster, Ca, Data (1 kW/m^2 peak flux, 845 W_t/m^2 avg for 11 hour average day)

* Values in parentheses are for the revised system

Thermal storage enables the Stirling engine to operate when solar insolation is not available, and provides a complete energy system.

Chemical storage requires the conversion of heat energy to some substance which can liberate heat when required. Potential conversion losses plus complex reactions may cause serious problems with respect to areas such as efficiency, control, costs and safety.

Battery storage is the easiest way to add dedicated storage from the standpoint of coupling to the Stirling engine generator, but involves various losses in AC/DC and DC/AC conversions.

This program emphasized thermal energy storage. Almost no work was done on chemical reactions. The battery storage data was supplied by JPL.

1. Thermal Energy Storage

At the beginning of this program, both sensible and latent heat storage were considered. It was thought that a mixture of sodium (for heat transfer) and either a high temperature ceramic like Sialon or a metal like iron (for heat capacity) would provide an inexpensive way to store heat. Although it was recognized that latent heat storage would be lighter, it was thought desirable to avoid the complexities of phase-change materials. Table 3-2 compares several TES storage materials for various storage times.

Figure 3-1 shows the same data plotted for the 15 kW_e cases. With an arbitrary temperature range of 100°C (180°F) allowed for the sensible heat storage, it is clear that latent heat storage materials must be considered for storage times greater than an hour for focus mounted systems because of the weight limit.

The TES temperature range of 100°C (180°F) assumed for sensible heat storage requires that the Stirling engine be operated over a similar range. For a given upper limit on Stirling engine heat exchanger temperature, degraded performance over much of the operating time will occur because of the relatively large ΔT necessitated by sensible heat storage. Although a similar ΔT and performance effect also occurs with latent heat storage, the magnitude of the range is less, only about a half, and the duration of the extreme temperatures is relatively short. This comparison is valid irrespective of the upper limit placed on the Stirling engine heat temperature, or on the shape of the Stirling engine efficiency vs. temperature curve. The operating mode and temperature differences in the latent heat storage heat pipe are discussed more fully under Sections IV and VIII.

Both of the above observations lead to the conclusion that latent heat storage is preferred, if it can be utilized economically and reliably. For focus mounted systems, which are mass limited, only latent heat storage can provide more than a small fraction of an hour of operation. The situation could be changed if future concentrator concepts permitted more

Table 3-2. Thermal Storage Capabilities

Mean Generator Power (kW_e)	Thermal Power To Engine (kW_t)	Storage Time (hrs)	Weight, Volume and Size for TES Materials Alone*		
			Latent Heat 67 NaF-33 MgF_2 (wt %)	70 Sialon - 30 Sodium (Vol. %)	70 Iron - 30 Sodium (Vol. %)
21	55.5	1/4	81 kg 37.9 liter L=D=.364 m	397.7 kg 154 liter L=D=.581 m	594.58 kg 100.2 liter L=D=.503 m
21	55.5	2	648 kg 302.8 liter L=D=.728 m	3181.5 kg 1233 liter L=D=1.162 m	4748 kg 80i liter L=D=1.007 m
15	39.68	1/4	57.9 kg 27.1 liter L=D=.326 m	284.3 kg 110.1 liter L=D=.519 m	424 kg 71.64 liter L=D=.450 m
15	39.68	1	231.6 kg 108.2 liter L=D=.516 m	1137.2 kg 440.4 liter L=D=.825 m	1696 kg 286.6 liter L=D=.715 m
15	39.68	2	463.2 kg 216.4 liter L=D=.651 m	2274.4 kg 880.8 liter L=D=1.039 m	3392 kg 573.12 liter L=D=.900 m
15	39.68	3	694.8 kg 324.7 liter L=D=.745 m	3411.6 kg 1321.2 liter L=D=1.189 m	5088 kg 859.68 liter L=D=1.031 m
15	39.68	6	1389.6 kg 649.3 liter L=D=.939 m	6823.2 kg 2642.4 liter L=D=1.498 m	10,176 kg 1719.4 liter L=D=1.298 m
20	53	1/4	77.3 kg 36.1 liter	379.7 kg 147.1 liter	566.3 kg 95.7 liter
20	53	2	618.7 kg 289.1 liter	3037.9 kg 1176.5 liter	4530.6 kg 765.5 liter

*Sensible heat storage based upon 100°C (180°F) temperature rise.

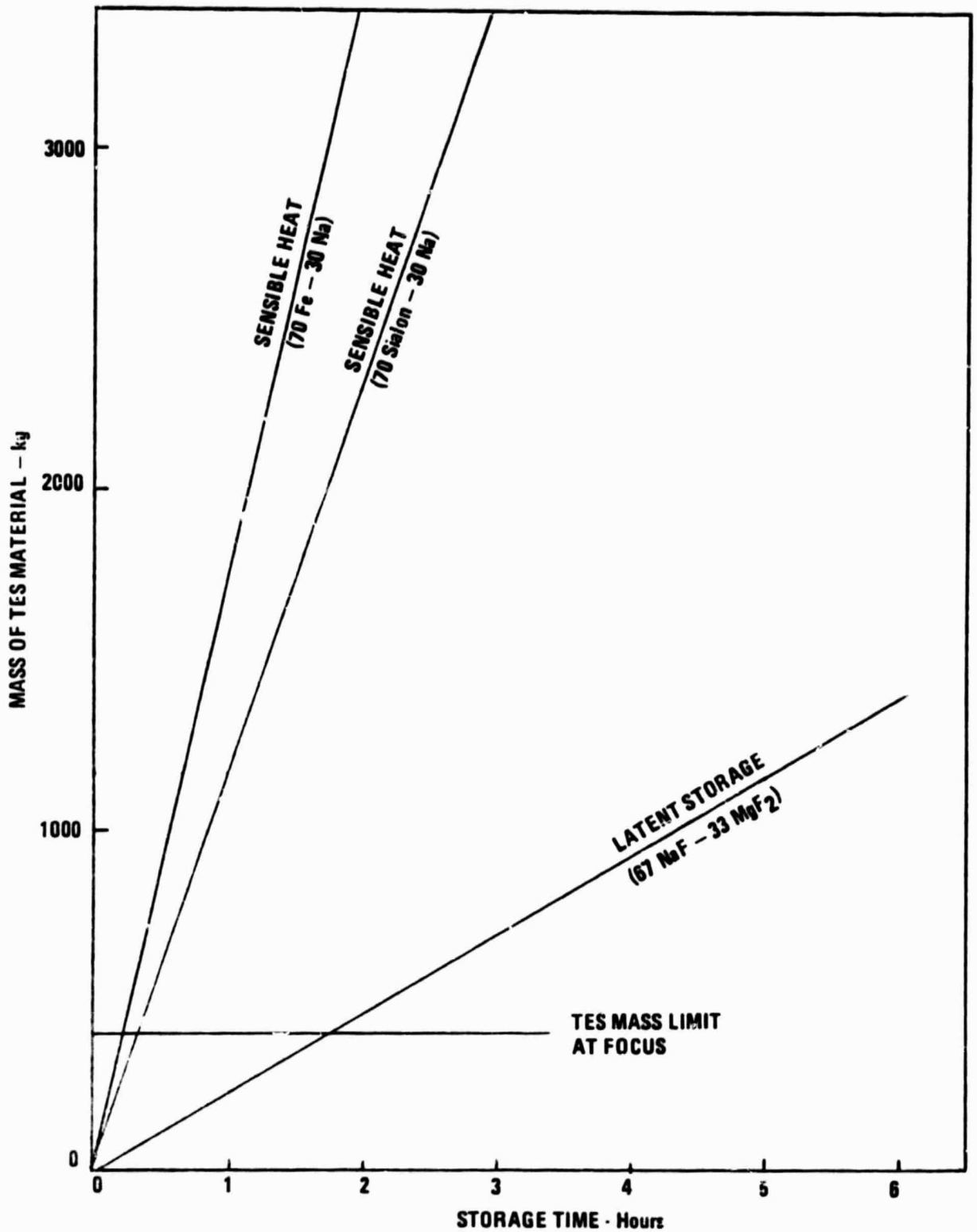

Figure 3-1. TES Mass Required vs. Storage Time

massive TES units. In this case, the low cost of some sensible heat storage media, such as iron/sodium, may outweigh the compactness of latent heat materials. Clearly, however, latent heat storage is preferred for the present design.

2. Chemical Storage

Little work was done in this area. Few possible reactions are well characterized, and cumulative losses through conversion and reconversions tend to lose most of the potential gains. For long term storage of large quantities of energy where TES thermal losses could accumulate significantly, chemical energy storage with lower capital cost and less expensive long term capacity storage cost could provide potential benefits. For small amounts of energy storage and frequent use, the TES approach appears superior.

3. Battery Storage

Battery storage has been studied in detail by JPL personnel. Originally it appeared to be a preferred method, but cost and in-out conversion losses tend to make it less attractive. From the receiver-Stirling viewpoint, the use of batteries is an external or system type of storage, and simply tends to lower the power rating to account for the stored electricity.

4. Energy Storage Assessment

It is clear that some thermal energy storage is necessary to smooth out the operation of the Stirling engine. Beyond this amount, the trade off between different kinds of energy storage is basically economic. Studies conducted under this contract indicate clear advantages for latent heat storage, both operationally and economically, over sensible thermal energy storage.

C. THERMAL TRANSPORT

Thermal transport is the means by which the energy at the receiver surface is transported to the Stirling engine head, as well as into and out of the thermal energy storage system. It serves to allow physical separation of the components, thus allowing separate optimizations and more importantly, it controls the temperature levels and temperature differences between components. Direct coupling of the Stirling engine and receiver is possible, and will be tested experimentally under separate contracts. However, this will require an overall optimization of the combined systems which may degrade the performance and seriously limit the operational flexibility of the system. This program assessed various types of liquid metal heat transport to show how the overall system would benefit by a decoupled system design.

1. Thermal Transport Methods Considered

Thermal transport is needed between the receiver, TES and Stirling engine because the low thermal conductivity of the TES salt combined with the relatively large distances the heat would have to be conducted through

the salt result in such large temperature drops that the efficiency of the Stirling engine is affected too adversely. If the approach is taken of putting the better part of an hour or more of energy storage as TES material in direct contact with the Stirling engine heat exchanger tubes, the average heat transfer conductance distance through the TES material might be on the order of six inches. To extract heat energy at the rates needed to run the Stirling engine would require a temperature drop on the order of hundreds of degrees Celsius. (See IV B.4). Thus, thermal transport is necessary. The two options considered were the use of heat pipes and pumped looped systems.

2. Heat Pipe Thermal Transport

A heat pipe transfers energy over relatively short distances from the hot end to the cold end by the evaporation and condensation of a fluid inside the pipe. The amount of heat that the heat pipe can transfer is dictated principally by the temperatures (and vapor pressures) at the hot and cold end, the latent heat of vaporization of the heat transfer fluid, its vapor density and the ability of the wicking within the heat pipe or of gravity to return the condensed fluid to the evaporator. Heat pipe performance is limited by sonic velocity limits at relatively low temperature, by wicking limitations and by burnout at the evaporator at higher temperatures. Typical heat pipes are capable of transferring many kilowatts of thermal energy with a temperature drop of only a few degrees Celsius. Heat transfer film coefficients are of the order of 57,000 W/m^2-°C (10,000 Btu/hr-ft^2-°F). The heat pipe is self-starting. It will stop when the heat pipe temperature becomes isothermal or when the fluid in the pipe is prevented from returning to the heat source.

Because of the relatively short distances over which heat pipes operate, they provide an excellent, compact and self-regulating thermal transport system for the focus-mounted or Cassegrainian mounted power conversion units cited in the first seven cases and in the massive TES systems which employ a fixed mount focal point power conversion system. Their minimal pumping power is provided by gravity and/or capillary forces in wicks. Thermal flow in the heat pipe is controlled by imposed thermal conditions without the need for additional thermal control devices.

3. Pumped Loop Thermal Transport

The use of electromagnetic, mechanical or gas-lift pumps can be considered for thermal transport by liquid metals. These pumped systems offer excellent thermal control and pumping capacity to transfer alkali metals over a wide range of distances such as system design options numbered seven through nine involving both single and multiple concentrators (see Table 3-1). For the focus mounted system on a single concentrator the pumped loop system could be directly compared with the focus mounted integral system with heat pipe thermal transport. A case not explicitly listed among the design options would involve a single concentrator pumped loop with the TES and power conversion components located at the back surface of the concentrator to minimize focal point mass and to permit larger thermal energy storage behind the concentrator.

In evaluating the use of pumped loops, three areas of concern must be considered; namely, the heat loss from long runs of insulated pipe, the power loss due to the pump and the cost, availability, weight and reliability of pumps and valves.

Table 3-3 shows the estimated heat losses for four different pumped loop configurations, two types of insulation, and two different heat loss rates. The lower heat loss figures represent about 100 W/m (100 Btu/hr-ft) for insulation over pipe, and require either 50 mm (2 inches) of vacuum insulation or 300 mm (12 inches) of a cellular material. Losses from the TES and receiver were not included, being nearly the same for each. Clearly, the losses from the multiple concentrator units are undesirably great, and would eliminate any potential advantage which might be gained by grouping the TES into a more centralized location. For the focus mounted and dish mounted systems, the losses are not necessarily disqualifying. For this reason a pumped loop system involving thermal storage and power conversion units located on the back surface of the concentrator in a single concentrator system was studied as described in Section V.

Pumps and valves for liquid metal service at a nominal 1100-1300°K (1500-1900°F) are not currently available, and represent an area of required development. Although liquid metal loops in this temperature range have been operated successfully, the usual practice has been to put the pumps and valves in a relatively cold leg of the loop. In the present system, no such cold leg exists, and both pumps and valves must be designed for at least 1100°K (1500°F) service. This does not imply that such equipment cannot be developed, only that a development program will be required. A basis of technology for such development is available from prior government sponsored work on alkali metal space power technology*.

Electromagnetic, mechanical and gas lift pumps were considered. EM pumps have the decided advantage of requiring no rotating seals. It is probable that the mass-produced and unattended operation requirements of the overall system will eliminate rotating seals from consideration. Thus, the prime candidate is the EM pump or the gas lift pump. Estimates of the weight and efficiency of EM pumps obtained show weights of 50-250 kg (100-600 lb) depending on efficiency and design voltage, and efficiencies between 8 and 12 percent. System studies showed that approximately 1 kW_e would be required for pumping, including the required cooling air flow for the pump winding.

A further complication of the pumped loop is the requirement for control of a pump and up to six valves. While certainly feasible, the added complexity causes concern with long-term operational reliability in an unattended environment.

The conceptual design and assessment of a single pumped loop system mounted on a single concentrator is given in more detail in Section V.

---

*Zimmerman, W.F., "Alkali Metal Space Power Technology Applicable to National Energy Research and Development", 13th Annual Meeting AIAA, Washington, D.C., January 10-13, 1977.

Table 3-3. System Losses Through Pipe Insulation

Cases	Approximate Pipe Length		Heat Losses			
			51 mm of Vacuum Insulation or Approx. 305 mm Cellular		102 mm of Cellular Insulation or 25.4 mm Super	
	m	ft.	kW	%	kW	%
1 Concentrator Focal Mt. TES	6.1	20	0.6	1.1	1.2	2.1
1 Concentrator Dish Mt. TES	30.48	100	3.0	5.4	5.8	10.4
4 Concentrators Central TES	262.13	860	25.7	11.5	49.7	22.3
8 Concentrators Central TES	609.6	2000	59.7	13.4	116.0	25.9

4. Advantages of Focus Mounted Heat Pipe Thermal Transport

The key reasons for picking the heat pipe concept over the pumped loop concept is that it will be cheaper, lighter, more efficient, and more reliable than pumped loops.

It will be cheaper and lighter in that all the components of a pumped loop are added to similar ones in a heat pump configuration. For example, the TES cans and outer containment shell are required for both systems. However, in the heat pipe concept the functions of the pump and valves are performed by the components of the TES and receiver. The basic simplicity of the design will allow extensive cost cutting as the compact design evolves into mass-produced hardware in factory production lines.

It will be more efficient in that heat losses will be reduced through elimination of large pipe runs and reduced surface area for heat losses; the absence of pumps and valves will minimize parasitic power losses, as well.

It will be more reliable because there will be no need for a control system, pump and remotely operated high-temperature valves. The compactness and simple field change-out will serve to improve on-line availability.

SECTION IV

HEAT PIPE SOLAR RECEIVER WITH TES

A. CONCEPTUAL DESIGN OF THE HEAT PIPE SOLAR RECEIVER

1. Design Approach

The objective of the design was to achieve the highest possible efficiency in a focus mounted system within the permissible weight constraints and at an eventual cost in mass production of $\$400/kW_e$ using current state-of-the-art technology.

To minimize reradiation losses the receiver was designed to emulate a black body as nearly as possible; all the walls of the receiver were cooled by liquid metal heat pipes. Primary heat pipes were designed to operate as one-way thermal valves to minimize reverse heat flow from the secondary TES heat pipe during cloud cover.

The secondary heat pipe was designed in a single cylindrical shape to contain the largest possible amount of stored energy within a given volume at a L/D ratio of 1; this was done to concurrently minimize thermal conduction losses from the secondary heat pipe surface. The thermal energy storage material was distributed in cylindrical containers sized with consideration for the thermal gradient temperature losses which would occur across the solidified salt at various power levels and levels of storage discharge.

Thermal analysis included the heat transfer to the heat pipes in the receiver, the performance of the primary and secondary heat pipes themselves and the transfer of heat between the primary heat pipes, secondary heat pipe TES containers and the Stirling engine. The wicking required to provide liquid metal to all heat sources was studied and the wicking requirements were specified.

Based upon the thermal analysis, the mechanical design was iterated to control the receiver/TES system weight and to provide the other design functions such as structural support, alkali metal containment, thermal insulation and design integration with the concentrator and Stirling engine-generator. Based upon this design concept, layout drawings were prepared and a weight, center of gravity and cost of materials analysis was performed as a basis for assessment of the concept.

2. Thermal Analysis

a. Solar Receiver Thermal Analysis. An analysis was performed to determine the distribution of the thermal energy flux on the inner

cylindrical surface of the receiver cavity. A computer program developed specifically for the thermal analysis of receivers at the focal point of parabolic reflectors was utilized to do the analysis.

As indicated in Figure 4-1, the program integrated the thermal flux impinging on a given increment of a cylinder wall within the solar receiver from various points on the concentrator. Light reflected from each band on the concentrator, at an angle theta (θ), undergoes some spreading through an average conical dispersion angle, phi (ϕ). Phi nominally accounts for all possible errors. But, for this analysis the dish was assumed to be geometrically perfect and the errors, other than the solar disc half angle, were accounted for by using an overall concentrator efficiency of 70%. Phi for this analysis was 0.266 degrees.

In the program the receiver wall was divided into a number of points in the axial or x direction. As the angle theta (θ) was increased to the rim angle, θ_r, the program summed the flux and added it to the points which were within Δx. The results of this analysis are presented in Figure 4-2. The peak incident solar flux is about 500 kW/m^2 which is well below the maximum thermal flux capacity for a liquid metal heat pipe, which is in excess of 2500 kW/m^2.

Figure 4-3 shows the accumulated thermal energy along the length of the solar receiver. Approximately 80 percent of the incident radiation would be absorbed on contact and the rest would be reflected. This reflected radiation would tend to level out the curve shown in Figure 4-3.

A receiver length of 508 mm (20 in.) was chosen because, at a depth of 508 mm, over 80% of the incoming radiation had impinged on the receiver surface at least once. At a given aperture diameter of 256 mm (10.1 in.), this receiver depth was practical from the mechanical design and overall system standpoint. Furthermore, preliminary receiver analysis work done by JPL* indicated that, for a cavity receiver, the efficiency of the receiver leveled off at a ratio of inner wall area/aperture area over 7.

b. Heat Pipe Thermal Analysis. The heat pipes in the solar receiver were designed to transport the thermal flux which impinges upon the walls of the solar receiver. The thermal flux impingement was estimated as described above.

The heat pipe design was based upon transferring a peak power of 62.1 kW$_t$ from the receiver to the TES secondary heat pipe at a maximum local flux of 500 kW/m^2. The design was predicated upon heat pipe cooling of all the interior walls of the solar receiver. Axially arrayed tubular heat pipes were used to cool the cylindrical surfaces of the receiver on which about 88% of the incident energy impinged. A single circular flat plate was initially considered as a means of absorbing

*Anon., "Advanced Technology Development, Semi Annual Progress Report-Thermal Power Systems R&D Project", Jet Propulsion Laboratory, Report No. 5102-67, June 1978, pp. 4-24.

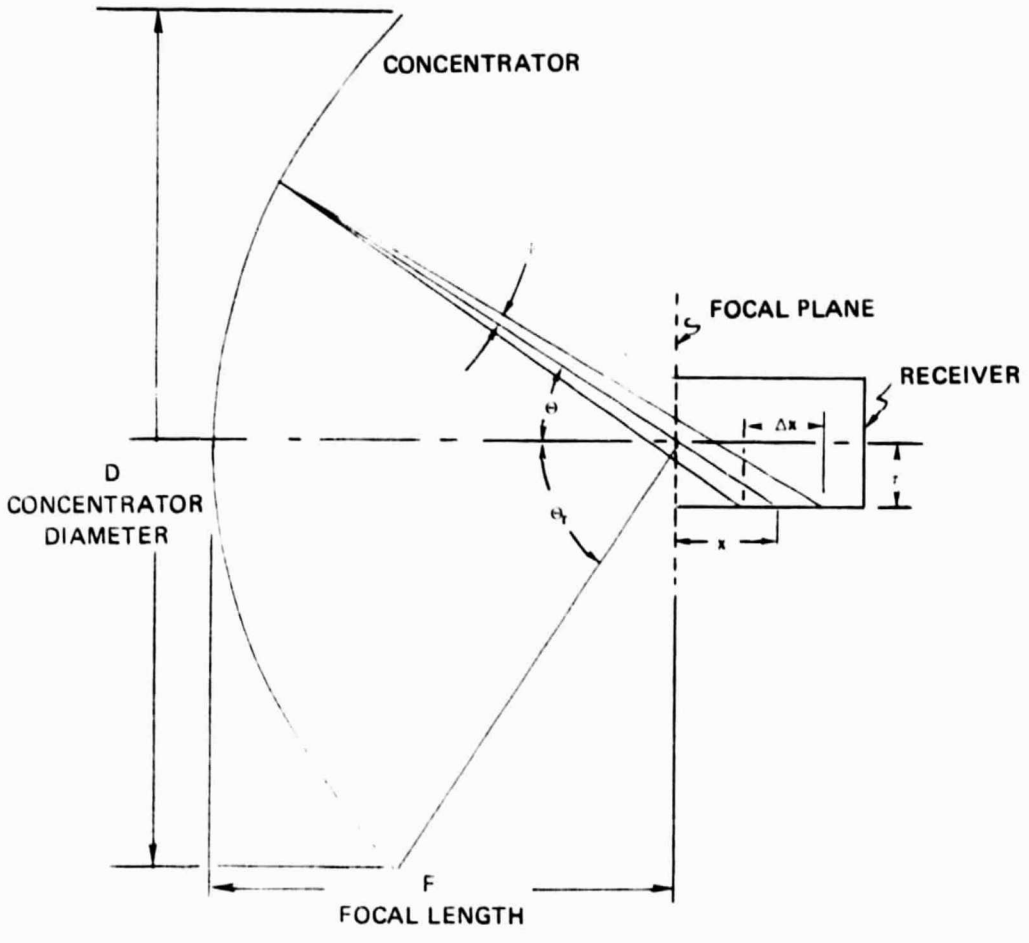

Figure 4-1. Physical Description of Solar Receiver Thermal Flux Analysis Model

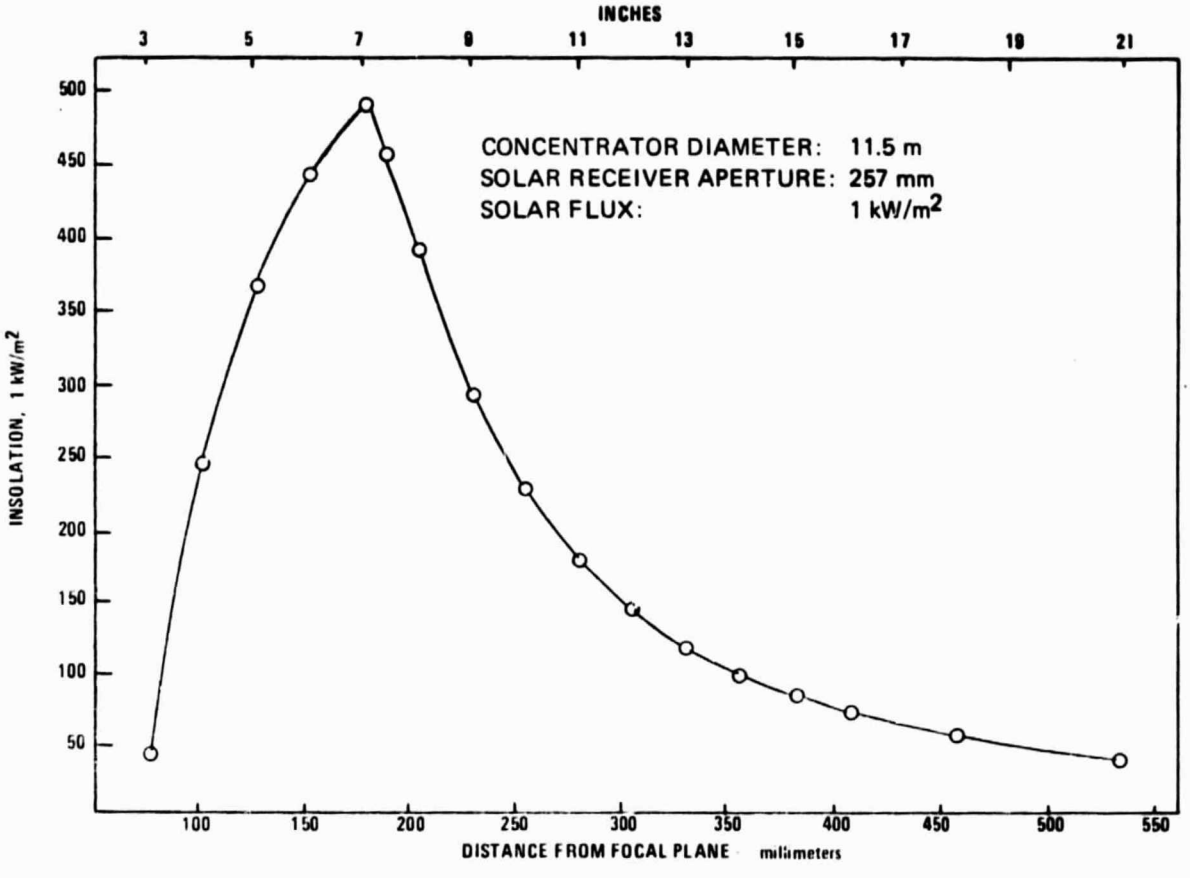

Figure 4-2. Local Impinging Heat Flux Along The Solar Receiver Cooled Wall

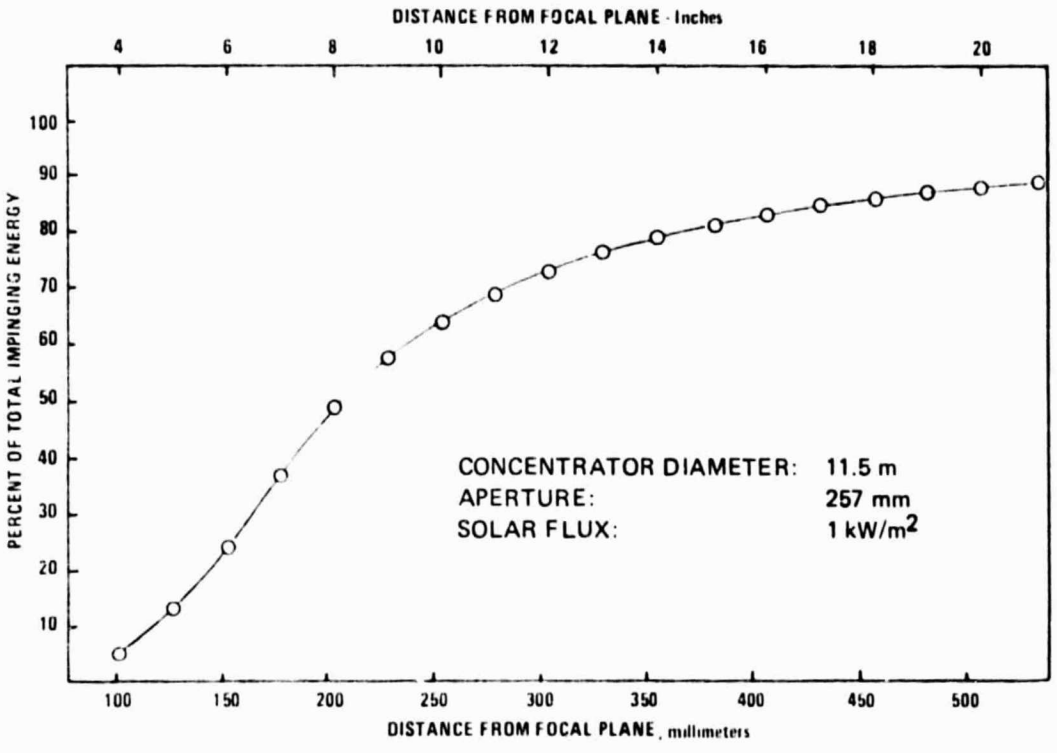

Figure 4-3. Cumulative Impinging Thermal Energy Along Solar Receiver Cylindrical Cooled Wall

heat energy at the end of the receiver but this heat pipe was deleted from consideration in the design. The remaining thermal energy from the back surface of the solar receiver was reflected and transferred by the primary heat pipes to the TES containment vessel.

Several sizes and numbers of tubular heat pipes were considered for use on the cylindrical wall, as indicated in Table 4-1. Thirty-four 25 mm (1 in.) OD heat pipes, each having a length of 508 mm (20 in.) and a wall thickness of 0.86 mm (0.035 in.) (for minimum temperature drop), could be used to transfer heat from the cylindrical wall; nevertheless, mechanical design considerations suggested that 27 such tubes, flattened in the receiver area, should be used to facilitate weld assembly at the TES secondary heat pipe header. The thermal transport capacity of each heat pipe was well above the required transport capacity of 2.31 kW_t per heat pipe.

These heat pipes are wicked in the solar receiver area with a single layer of 60 mesh 304 SS screen. Threaded or knurled inside diameter surfaces have also been considered as an alternative wicking method to distribute condensate return.

All the heat pipes have a 101.6 mm (4 in.) adiabatic length to allow for thermal insulation between the TES secondary heat pipe and this receiver. This insulation is needed since the solar receiver cools during cloud cover or absence of solar insolation. The primary heat pipes will be inoperative and will conduct heat only by thermal conduction from the thermal storage area to the solar receiver during this period. The heat pipes provide a one-way heat flow path eliminating any other type of control. A total length of only 127 mm (5 in.) of condenser section was needed to transfer heat from the primary heat pipes into the secondary heat pipe.

The thermal capacity of each heat pipe was above 2.31 kW_t and was limited by wicking capacity; the local maximum fluxes of 500 kW/m^2 could be readily absorbed. The sodium inventory required was just sufficient to saturate the wick in the primary heat pipes.

The small number of tubes in the solar receiver and their thin walls promote both economy of manufacture and low temperature loss across the metal wall.

The wicking in the secondary, thermal energy storage heat pipe was designed to provide fluid, as required, to all heat sources in the heat pipe and was subdivided as:

(1) The container wicking along the I.D. surfaces of the secondary heat pipe.

(2) The fore and aft capsule radial wicking.

(3) TES capsule wicking.

(4) The header plate radial wicking.

Table 4-1. Primary Heat Pipe Data

O.D.		Wall Thickness		ΔT^*	
mm	Inches	mm	Inches	°C	°F
25.4	1.0**	0.864	0.035	17.8	32
38.1	1.5	1.651	0.065	25.0	45
50.8	2.0	2.413	0.095	35.0	63
63.5	2.5	3.759	0.146	51.7	93

*Calculated values; later experimental verification indicated ΔT = 33°C (60°F).

**Chosen for preliminary design because of minimum temperature gradient.

Heat Pipe Lengths

Evaporator	508 millimeters	20 inches
Adiabatic	102 millimeters	4 inches
Condenser	127 millimeters	5 inches
	737 millimeters	29 inches

Material

Containment	321 Stainless Steel, ASTM 269-69
Wicking	In the lower 508 mm (20 in.)of Receiver Heat Pipes
	Material 304 SS, 1 Layer, 60 Mesh Screen
	Thickness - 0.43 mm

(5) Wicking on the primary heat pipes O.D. evaporation surfaces.

It is essential that neither the TES capsules nor the primary heat pipe heat sources suffer from lack of liquid sodium at the heat input end and also that the condensed liquid returning from the Stirling engine end is distributed circumferentially in a uniform manner. In the configuration where Stirling engine tubes are horizontal, the condensed liquid will tend to drain to the bottom of the TES container unit. The wicking along the inside of the TES secondary heat pipe distributes the liquid circumferentially and axially, the radial wicking on either end of the TES capsules pumps the liquid radially and provides the liquid inventory for the TES capsule wicking which in turn distributes the fluid axially along the individual TES capsules. The header plate radial wicking and the primary heat pipe O.D. wicking provide liquid sodium to the heat source from the solar receiver. The radial wicking has gravity assisting the radially inward flow of condensate in the upper portion of the container, whereas, the capillary forces have an opposing gravity force to counteract in the lower portion of the TES.

In designing the thickness of the wick or in determining the number of layers of screen wick necessary, the wicking limit is used as the design constraint. The wicking limit $(QL)_{max}$ is given in Btu-ft/hr or kW-m, for the given wick geometry and thickness. The wicking limit is expressed as:

$$(QL)_{max} = \frac{P_c \pm P_g}{F_\ell + F_v}$$

where P_c and P_g are the capillary pressure and gravity force terms and F_ℓ and F_v are the liquid and vapor frictional pressure drop factors. The capillary forces increase with the increase in the mesh size for a screen wick and, correspondingly, frictional forces increase. Also the cost/ft of the wick matrix increases very sharply for the small pore screen structures. The estimated wicking capabilities of wire screen and fiber metal type wicks are indicated in Table 4-2. Both from manufacturing and cost considerations, fiber metal wicks have advantages over wire mesh screens. Sintered metals did not appear to be economically acceptable as complex wicks.

The space available between the TES capsules provides the area for vapor flow either from the primary tube heat source or from the TES capsules to the condenser tubes. Sufficient amounts of sodium are provided in the TES system to saturate all the wicks.

c. TES Thermal Analysis. Two fused salt materials were selected for evaluation in the thermal design; the highly volume efficient LiF salt and the much less expensive NaF-MgF_2 eutectic. The thermal design properties and 1978 prices for these materials are shown in Table 4-3. Both salts have melting points in the temperature range appropriate to the proposed Stirling engine heater head temperature. Design calculations used a higher value of thermal conductivity for the NaF-MgF_2 eutectic than for the LiF salt.

Table 4-2. Radial Wicking Capabilities of Wire Screen and Fiber Metal Wicks For 0.46 m (18 in.) Effective Pumping Length

Wick Type	Porosity	Permeability $m^2 \times 10^{-10}$	Capillary Radius (μm)	Thickness (m)	Max. Wicking Capability (kW)
Wire Screens:					
200 Mesh	0.604	0.427	64.00	0.0127	32.4
250 Mesh	0.670	0.3716	50.90	0.0127	64.7
300 Mesh	0.629	0.2136	42.67	0.0127	58.0
400 Mesh	0.670	0.1459	30.48	0.0127	67.9
Fiber Metals:					
FM1101	0.9	0.56	26.5	0.0038	64.65
FM1102	0.8	0.087	13.5	0.0038	25.33
FM1103	0.7	0.028	7.5	0.0038	16.02
				0.0127	74.17
				0.01016	59.33
FM1104	0.6	0.013	5.0	0.0038	11.55
FM1105	0.5	0.0009	2.3	0.0038	18.00

Table 4-3. Properties of LiF and $67NaF-33MgF_2$

TES Material	Melting Temp. °C	Heat of Fusion kJ/kg	Specific Heat kJ/kg-°C $c_{p(s)}$	Specific Heat kJ/kg-°C $c_{p(\ell)}$	Density at 25°C kg/m³	Volume Decrease on Fusion %	Thermal Conductivity W/m-°C	Cost $/kg	Cost ($/lb)
LiF	857[2]	930.4[2]	2.34[2]	2.51[2]	2323[2]	22.7[2]	5.77[3](a)	6.93	3.15
$67NaF-33MgF_2$	832[1]	616.4[1]	1.42[1]	1.38[1]	2140[1]	22.8[1]	4.2-8.3[1] 4.66[1]	1.00	0.45

Data Sources:

1. H.C. Maru, et al., Molten Salt Thermal Energy Storage Systems: Salt Selection, ERDA Report No. COO-2888-1, Contract No. E(11-1)-288, August 1976
2. F.P. Bundy, et al, The Status of Thermal Energy Storage, Technical Information Exchange, Report No. 76CRD041, PO Box 43, Bldg. 5, Schenectady, NY 12301, April 1976
3. J.R. Gintz, Technical and Economic Assessment of Phase Change and Thermochemical Advanced Thermal Energy Storage (TES) Systems, EPRI, EM-256, No. 77EPR305, December 1976

Notes: (a) A value as low as 0.57 W/m °C have been reported. Value reported is estimated from electrical resistivity characteristics.

Table 4-3. Properties of LiF and $67NaF-33MgF_2$

TES Material	Melting Temp. °C	Heat of Fusion kJ/kg	Specific Heat kJ/kg-°C $c_{p(s)}$	Specific Heat kJ/kg-°C $c_{p(\ell)}$	Density at 25°C kg/m3	Volume Decrease on Fusion %	Thermal Conductivity W/m-°C	Cost $/kg	Cost ($/lb)
LiF	857[2]	930.4[2]	2.34[2]	2.51[2]	2323[2]	22.7[2]	5.77[3](a)	6.93	3.15
$67NaF - 33MgF_2$	832[1]	616.4[1]	1.42[1]	1.38[1]	2140[1]	22.8[1]	4.2-8.3[1] 4.66[1]	1.00	0.45

Data Sources:

1. H.C. Maru, et al., Molten Salt Thermal Energy Storage Systems: Salt Selection, ERDA Report No. COO-2888-1, Contract No. E(11-1)-288, August 1976

2. F.P. Bundy, et al, The Status of Thermal Energy Storage, Technical Information Exchange, Report No. 76CRD041, PO Box 43, Bldg. 5, Schenectady, NY 12301, April 1976

3. J.R. Gintz, Technical and Economic Assessment of Phase Change and Thermochemical Advanced Thermal Energy Storage (TES) Systems, EPRI, EM-256, No. 77EPR305, December 1976

Notes: (a) A value as low as 0.57 W/m °C have been reported. Value reported is estimated from electrical resistivity characteristics.

During heat extraction and as the salt is solidifying within the container, a temperature gradient will develop between the molten salt and the sodium vapor heat source at the container surface. This temperature gradient will depend upon the thermal conductivity and the thickness of the solidified salt and the power extraction rate. For thermal design purposes the maximum temperature difference was arbitrarily limited to 56°C (100°F) at the end of the solidification process; over this span of temperature there is only a relatively minor drop in the performance of a typical Stirling engine. A typical parametric analysis chart of the number of capsules, the capsule dimensions and the maximum temperature drops is shown in Figure 4-4 for a system with 2 hours energy storage at 39.68 kW_t.

For production simplicity and to permit adequate provisions for sodium wicking of the exterior of the salt containers, the containers were selected as thin walled metal cylinders. These cylinders were, in turn, contained within the cylindrical secondary heat pipe with a L/D ratio of about 1.0 to maximize the heat pipe volume to surface area.

Using the above design criteria and selected design inputs, the thermal design was developed through the use ot an iterative design computer program which calculated the maximum temperature gradient, the storage time, the weight and physical dimensions of the secondary heat pipe and the number, length and diameter of the salt containers.

d. Stirling Engine Thermal Analysis. A logical point for the thermal interface between the heat pipesolar receiver and the Stirling engine relies upon a definition of the Stirling engine heat exchanger, particularly its surface area, surface temperature and the total heat transfer required. Since the alkali metal condensing heat transfer coefficients are very high, on the order of 60,000 W/m^2-°C, the temperature drop between the sodium vapor and the outer surface of the heat exchanger tubing is very low. The heat transfer is much more limited by the gas side heat transfer coefficients, on the order of 6000-12000 W/m^2-°C, and by the other Stirling engine heat transfer requirements. Thus, the Stirling engine design itself controls the definition of the heat exchanger; consideration must be given to such factors as gas flow, pressure drop, void volume, heat transfer surface area, tube wall thickness (for stress capability and thermal resistance), system operating temperature and total heat flow requirements.

A limited analysis was made by General Electric Stirling Engine development personnel of the design of a 52.5 kW_t, 1.76 x 10^7 Pa (2550 psia) helium gas heat exchanger for a Stirling engine with 42% efficiency operating at 1800 RPM. The results are shown in Figure 4-5. The 24 tube configuration with a 67°C (120°F) temperature drop between the condensing sodium and the helium working fluid was selected. This was a reasonable balance between the desire for economy and manufacturability on the one hand and for thin wall small tube diameter on the other hand. The latter aims at low wall ΔT and high gas side coefficient which are important in minimizing the temperature drop across this heat exchanger.

e. Thermal Losses. For the conceptual design, the principal thermal losses occur by radiation and convection from the receiver during

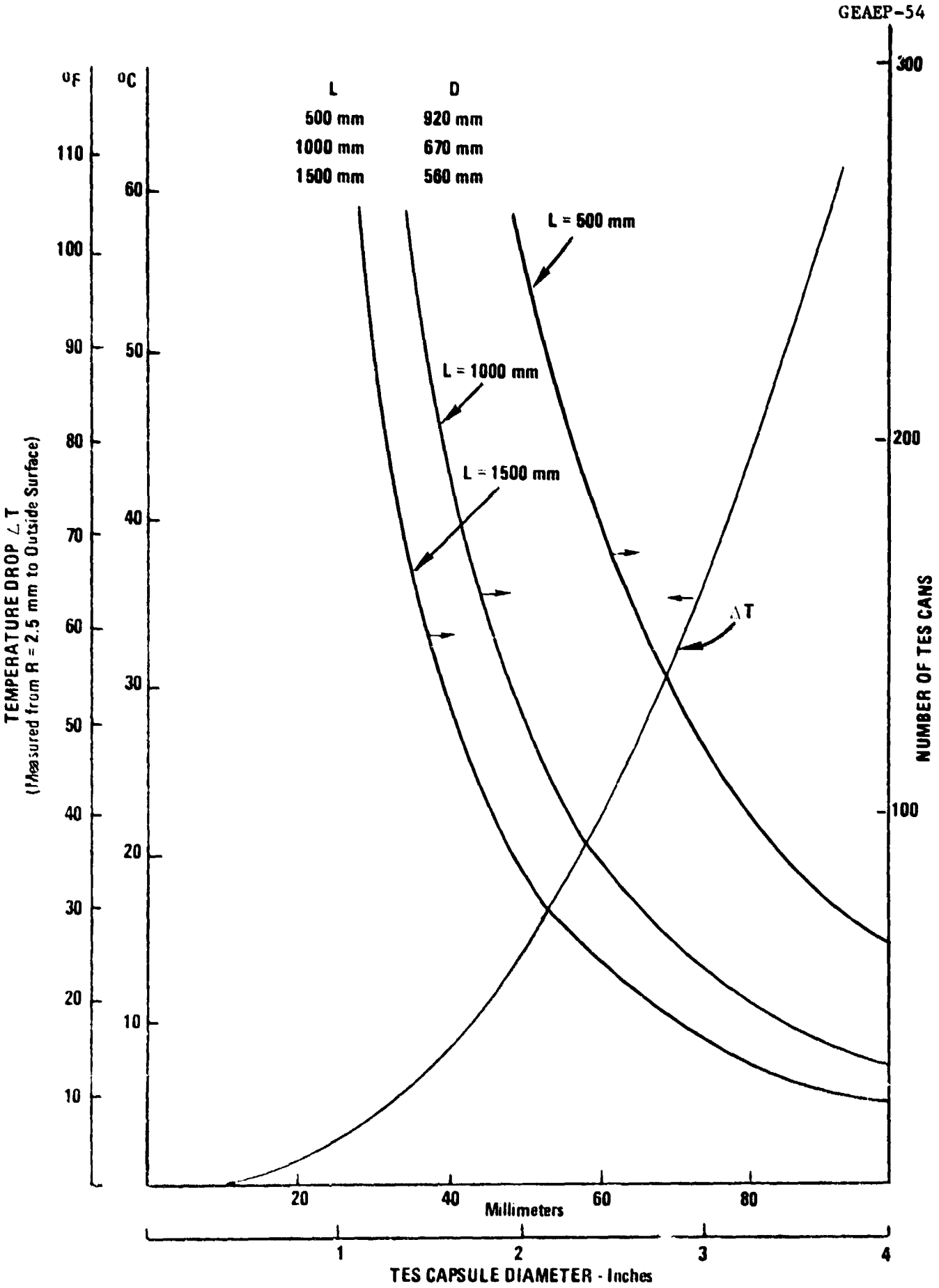

Figure 4-4. 2 Hour Latent Heat TES Requirements at 39.68 kW_t for 67 NaF - 33 MgF_2

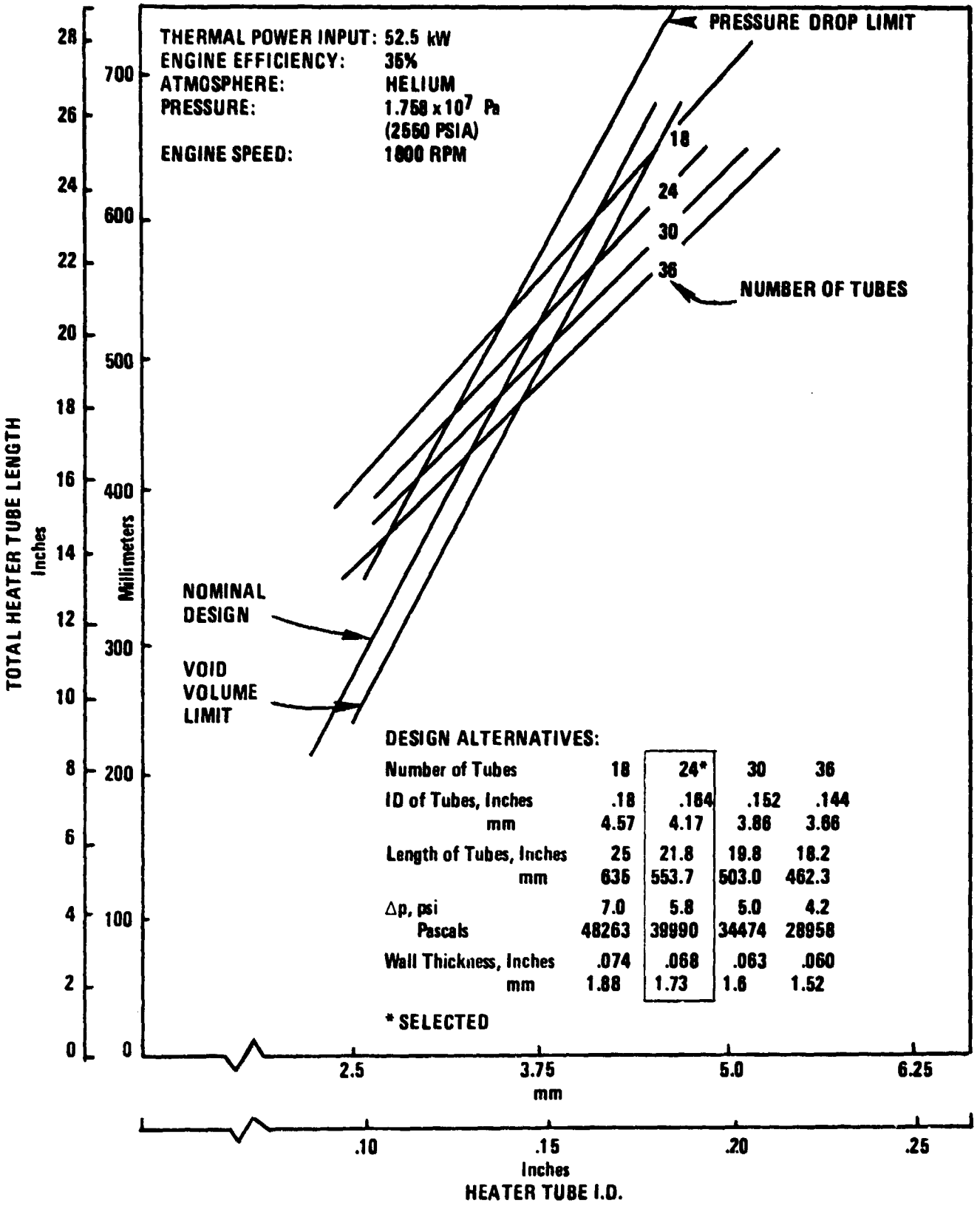

DESIGN ALTERNATIVES:

Number of Tubes	18	24*	30	36
ID of Tubes, Inches	.18	.164	.152	.144
mm	4.57	4.17	3.86	3.66
Length of Tubes, Inches	25	21.8	19.8	18.2
mm	635	553.7	503.0	462.3
Δp, psi	7.0	5.8	5.0	4.2
Pascals	48263	39990	34474	28958
Wall Thickness, Inches	.074	.068	.063	.060
mm	1.88	1.73	1.6	1.52

* SELECTED

Figure 4-5. Stirling Engine Heat Exchanger Optimization Curves

normal daytime operation and by radiation and conduction through the vacuum multifoil insulation at night. The former loss is inherent with all receivers operating at high temperature and the latter loss is a function of the type and amount of insulation used around the TES area.

Reverse heat losses from the secondary TES heat pipe through the primary heat pipes and then by convection and radiation from the receiver during periods of cloud cover or overnight shutdown are minimized by the "thermal valve" characteristics of the primary heat pipe design. Since the condenser end is not wicked, the condensed sodium in the primary heat pipes cannot reach the hot condenser end of the primary heat pipes and reverse heat flow is prevented. Such reverse heat flow from the TES along this same route is prevented during the overnight period while in the "stowed" position by the prior solidification of the sodium in the aperture end of the solar receiver, as discussed in Section VII-B.

The daytime thermal losses from the receiver and TES were calculated to be 8.5 kW_t by a one-dimensional analysis. This analysis did not include Stirling thermal losses. The various daytime heat losses and their percentage of the total loss are shown in Figure 4-6. The largest component of the daytime losses is reradiation from the receiver aperture. This loss can be reduced significantly only by the use of a better, and probably more costly concentrator which in turn would reduce the aperture diameter. The possibility of using aperture windows to reduce radiation and convection losses was discarded because of a 10 percent loss of incoming radiation due to window reflection.

Overnight and cloud cover losses are also shown in Figure 4-6 and were calculated to be 1.6 kW_t by the same procedure. It is under these conditions that the initial investment in insulation is critical in controlling the losses since the primary loss is directly through the insulation. During a typical 13 hour overnight shutdown, approximately 21.7 kW_t can be lost from the TES heat pipe. Were the TES to be fully discharged at the end of the normal solar operating period, the TES heat pipe temperature would drop approximately 42°C (76°F) overnight. This temperature loss would not impair immediate restart the following morning. These TES thermal losses are controllable and can be reduced further by increased thermal insulation and increased TES system outer diameter.

Outside surface temperatures for the unit would be on the order of 65°C (150°F) under normal conditions. While this temperature could cause burns to bare skin, it would not be too great for many forms of weather and oxidation protection.

3. System Engineering Definition

The above thermal analyses resulted in a definition of the key engineering factors that provided the guidelines for the mechanical design of the initial concept heat pipe solar receiver/TES engine-generator subsystem.

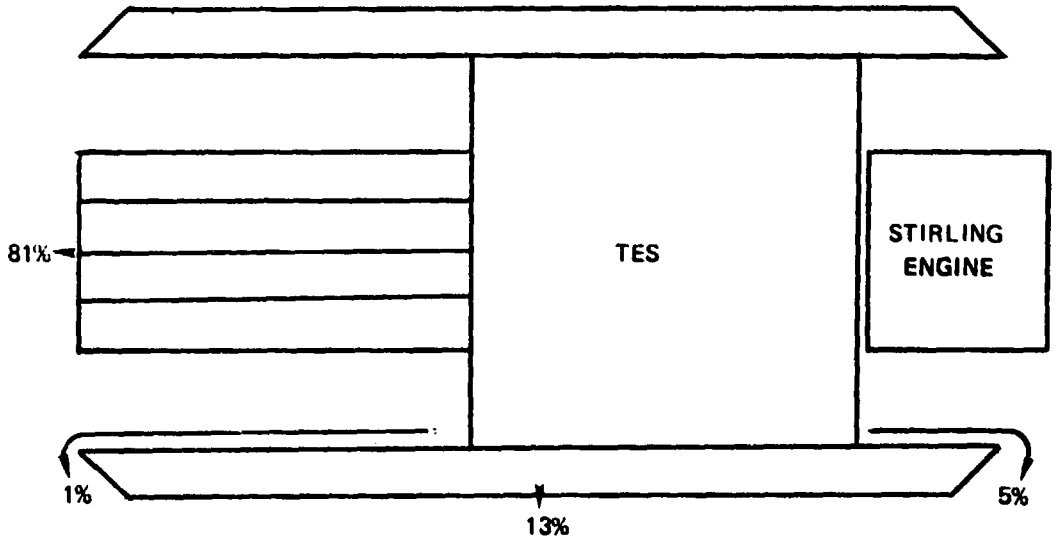

A. Daytime Losses

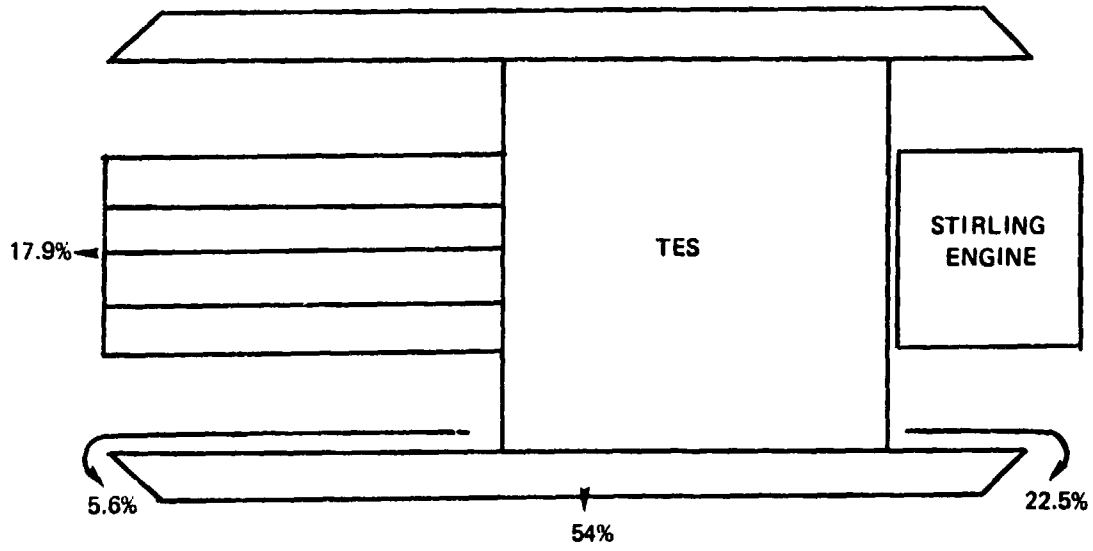

B. Nighttime Losses

Figure 4-6. Receiver/TES Thermal Losses

a. Solar Receiver Definition. Engineering definition of the receiver is given in Table 4-4. The heat pipes would be flattened to the extent that they would fit around the 805 mm (31.7 in.) circumference of the receiver aperture which would mean that each heat pipe would be flattened so the major axis was on the order of 30 mm (1.2 in.). Wicking was specified for the length of the primary heat pipes in the receiver to ensure that adequate wetting could be maintained all around the heat pipe. Under normal operating conditions, there would be no need for a wick to return sodium from the condenser section of the primary heat pipes. The adiabatic section length of 102 mm (4 in.) was specified for insulative purposes between the receiver and TES units.

b. TES Definition. Table 4-5 shows the key design factors resulting from the iterative study of the TES area by the computer design program. Data is given for systems with two salts that were considered, LiF and NaF-MgF_2 eutectic. These results provided the basis for the mechanical design; during the mechanical design it was necessary to modify these design elements slightly since the relationship between number and diameter of small cans and the diameter of the large outer shell is an empirical approximation.

The liquid metals are the only attractive working fluids in the heat pipes operating above 600°K (1100°R). The surface tension, vapor pressure, latent heat and viscosity are the principal properties which make the liquid metal heat pipes high performance devices. Sodium was chosen for the heat transfer fluid in both heat pipes because its low vapor pressure, high latent heat, low viscosity and high surface tension are attractive for heat pipe purposes in the 815°C (1500°F) temperature range. It has good thermal transport properties, it is inexpensive and it is available in abundance.

The operation of the secondary TES heat pipe system as a single heat pipe tends to promote uniform temperatures since heat will be transported to the coldest point. A sufficient amount of sodium working fluid is present in the form of a liquid pool, or contained on wicking surfaces, to transfer the required thermal energy to the Stirling engine.

Gravity return of condensate is of considerable assistance in the proper distribution of sodium to hot surfaces from which heat must be extracted. The use of wicks, however, is essential to pump returning condensate to appropriate surfaces. A wicked system assures radial and axial sodium supply which tends to insure uniform temperature and operating reliability which might not be obtained in an unwicked, simple reflux boiler. Thermal transport in the TES secondary heat pipe relies upon the use of various kinds of wicking to return the condensate along the cylinder walls and TES capsules toward the solar receiver end. These wicks include those located on the surface of the TES containers, on the capsule plates which support the fore and aft ends of the capsules, on the header plate at the receiver end of the TES heat pipe, on the outside surfaces of the condenser ends of the primary heat pipes and along the large inside diameter of the TES heat pipe. The definition of this wicking is given in Table 4-6 and is based upon both initial calculation and analysis and upon the results of later experimental effort on the measurement of the wicking capabilities of various wick structures.

Table 4-4. Receiver Engineering Definition

Aperture Diameter	256 mm (10.1 inches)
Cavity Depth	508 mm (20.0 inches)
Heat Pipe Data:	
Total Power	62.1 kW_t
Power/Heat Pipe	2.31 kW_t
Maximum Power/Heat Pipe	>10.0 kW_t*
Number of Heat Pipes	27
Outer Diameter (unflattened)	25 mm (1.0 inches
Wall Thickness	0.889 mm (0.035 inches)
Evaporator Length	508 mm (20 inches)
Adiabatic Section Length	102 mm (4 inches)
Condenser Section Length	127 mm (5 inches)
ΔT (Total)	18°C (32°F)
Wicking Data:	
Material/Mesh Size	304 SS/60 Mesh
Number of Layers	1
Thickness - Each Layer	0.43 mm (0.017 inch)

*Experimentally tested to 4.5 kW_t.

Table 4-5. Initial TES System Definition

Parameter	Thermal Storage Material			
	$67NaF-33MgF_2$		LiF	
Power Level	53 kW		53 kW	
Melting Point	827°C (1520°F)		857°C (1575°F)	
Storage Time (Latent + Sensible)	1.27 hr		1.88 hr	
Approximate Container ΔT	41.6°C (74.9°F)		40.3°C (72.5°F)	
Weight	kg	lbs	kg	lbs
Total	550.0	1212	550.0	1212
TES Material	346.3	736	346.1	763
Cans	68.3	151	75.7	167
Containment Vessel	114.9	253	107.7	237
Wire Mesh and Sodium	12.4	27	13.0	29
Can Support	8.1	18	7.5	16
Dimensions-Containment Vessel	mm	in.	mm	in.
Length	653	25.7	653	25.7
Diameter	646	25.4	624	24.6
Thickness	6.35	0.25	6.35	0.25
Dimensions-TES Cans	mm	in.	mm	in.
Length	622	24.5	605	23.8
Diameter	58.4	2.3	48.2	1.89
Thickness	0.76	0.03	0.76	0.03
Number of TES Cans	97		135	

Table 4-6. TES Secondary Heat Pipe Wicking

Wicking Location	Effective Pore Size ($m \times 10^{-6}$)	Wick Thickness (mm)	Type
Primary Heat Pipes	0.74	0.32	200 Mesh SS Screen 3 Layers
TES Capsules	0.74	0.213	200 Mesh SS Screen 2 Layers
TES Containment Cylinder (Circumferential)	0.74	0.32	200 Mesh SS Screen 3 Layers
Header Plate (Radial)	17.51	3.175	FM1108 SS 1/8" Thick
Front End (Radial)	20.1	1.59	FM1103 SS 1/16" Thick
Aft End (Radial)	20.1	1.59	FM1103 SS 1/16" Thick

Analysis of the heat flow in the system considered its temperature regulation by the molten salt, the effect of container ΔT at full power extraction and the influence of operating the salt storage over a temperature range 8°C (15°F) above the melting point and 5.6°C (10°F) below the melting point. The maximum operating temperature range of the various components as a result of these temperature gradients and allowable excursions is given in Table 4-7.

c. Engine-Generator. The engine-generator disign was not a part of the scope of work covered by this contract. However, to complete the conceptual design of the solar receiver and TES systems some basic definition for these units was necessary. Certain requirments were stipulated by the JPL guidelines as indicated above in Table 2-1 and from these guidelines further component definitions were generated by Stirling engine development personnel at General Electric Company, Valley Forge Space Center. These engineering definitions were based on assumptions which may or may not prove valid after more concentrated studies in this area. They were, however, utilized in the preparation of conceptual design layout and are indicated in Table 4-8.

In addition to a definition of the engine-generator components, other considerations with regard to interfacing the engine-generator with the TES system must be reviewed. The mechanical interface requires a means of making the Stirling HX tubes accessible to condensing sodium vapors and providing a return path for condensate to the TES. Methods of mounting, supporting and attaching the engine to the TES and in incorporating means of compensating for thermal expansion, provisions for leak tight sodium joints, and insulation to reduce TES containment heat loss at the aft end were all vital design factors which were considered in subsystem integration and overall system definition.

d. Focal Mount Support. The concentrator design was not included in the scope of work covered by this study contract. To complete the conceptual design some definition of the concentrator focal mount support was, however, necessary. Guidelines were furnished by JPL defining the concentrator capabilities as indicated above in Table 2-1.

It was further determined that the concentrator would include a focal mount system support structure capable of supporting a 1365 kg (3000 lb.) load at or near the concentrator focal point. A structural support ring with a diameter of 762 mm (30 in.) was prescribed to accommodate the support of the solar receiver/TES system.

All services to the focal mounted system and electrical power from the system would interface at the support ring. Assembly and disassembly of the focal mounted system from the concentrator system would also be at the support ring.

No structural analysis, vibration analysis, etc., of the heat pipe solar receiver/TES engine-generator, as regards the concentrator mounting, was a part of the initial design requirement.

Table 4-7. Maximum and Minimum Component Operating Temperature Range*

	TES Material							
	$NaF-MgF_2$				LiF			
	Maximum		Minimum		Maximum		Minimum	
	°C	°F	°C	°F	°C	°F	°C	°F
Temperature Range								
Receiver Tube, OD	868	1595	863	1585	899	1650	893	1640
Condenser Tube, OD	835	1535	779	1525	866	1590	860	1580
TES Vapor Space	835	1535	779	1435	860	1590	810	1490
Stirling Engine HX Tube, OD	835	1535	779	1435	860	1590	810	1490
Stirling Working Fluid	768	1415	713	1315	799	1470	743	1370

*Based on melting point of TES salt, maximum ΔT across salt container, 8°C (15°F) salt superheat and 6°C (10°F) salt subcooling.

Table 4-8. Engine Generator Definition

Engine:

Kinematic Type, Rhombic Drive	
Working Fluid	Helium
Operating Pressure Level	17.3 MPa (2500 psia)
Speed	1800 RPM
Swept Volume	244 cm^3 (14.9 $in.^3$)
Bore	76 mm (3.0 in.)
Stroke	53 mm (2.1 in.)
Phase Angle	90°
Swept Volume Ratio	1.0
Pressure Ratio	1.82
Dead Volume	610 cm^3 (37.2 $in.^3$)
Displacer	∿152 mm (6 in.) long
Cylinder	∿356 mm (14 in.) long
Power Piston	76-100 mm (3-4 in.) long
Estimated Weight	136-160 kg (300-350 lbs.)
ΔP	0.13 MPa (18.9 psi)
Coolant System	Not Defined
No. of Heat Exchanger Tubes	24
I.D. of Heat Exchanger Tubes	4.2 mm (0.164 in.)
Length of Heat Exchanger Tubes	554 mm (21.8 in.)
* Heat Exchanger Tube Wall Thickness	1.7 mm (0.068 in.)
Heat Exchanger Wall ΔT	67°C (120°F)
Heat Exchanger Tube ΔP	0.04 MPa (5.8 psi)
Heat Exchanger Tube Void Volume	177 cm^3 (10.8 $in.^3$)

* Based on HS-188 Material.

Generator:

Direct Drive	1800 RPM
Induction Type	
Est. Weight	90 kg (200 lbs)
Cooling	Integral Fan
120/208 Volt, 3 ϕ. 60 Hz	

4. Mechanical Design

The basic design for the focus mounted system is shown in Figures 4-7 and 4-8. This system, for descriptive purposes, will be broken down into four subsystems as follows:

- The Primary Heat Pipe Solar Receiver (HPSR)
- The Thermal Energy Storage System (TES)
- The Stirling Engine/Generator
- The System Mounting or Concentrator Mounting Ring

A parts list for the entire focus mounted system is shown in Table 4-9. The part numbers called out in the table correspond to numbers on the drawing, Figure 4-7. The parts list provides a brief description, indicates the number required, specifies the presently selected material and lists the material configuration, approximate dimensions and weight.

a. Primary Heat Pipe Solar Receiver. The primary heat pipe solar receiver, as shown in Figure 4-7, consists of twenty-seven 25 mm (1 in.) diameter heat pipes located on a diameter slightly greater than the 0.26 m (10.1 in.) diameter aperture. As shown in Section AA, the tubes are flattened for approximately 0.51 m (20 in.) over their overall 0.74 m (29 in.) length. Prior to flattening, a 60 mesh tubular stainless steel wire screen would be inserted inside the tube and expanded along the entire length of the evaporator section. A manufacturing process for producing the tubular screen and expanding the screen inside of the heat pipe has been developed. A description of the fabrication and testing of primary heat pipes is given in Section IV-B6.

The pressure inside the heat pipe will range from a vacuum at ambient conditions to approximately 1.03×10^5 Pa (15 psia) at operating temperature. At the operating temperature, circumferential and longitudinal stresses due to internal pressure will be negligible. Stresses due to the long cantilever length of the pipes are approximately 2.76×10^6 Pa (400 psi). Fatigue stresses due to vibration which might be imposed by the Stirling engine cannot be analyzed at this time. The low stresses imposed on the heat pipes, therefore, allow considerable latitude in the selection of a material. Oxidation and sodium corrosion resistance will be the primary factors in material selection. A stainless steel, such as AISI Type 310 (or Type 321) has been indicated in the parts list.

The rear face of the cavity type solar receiver was originally conceived to contain a single flat plate type heat pipe. A later decision was reached not to incorporate this heat pipe but to allow that uncooled surface to reflect and reradiate heat to the heat pipes which form the cylinder wall.

The heat pipe cluster is surrounded by a can type cavity inner wall liner. This liner is supported at the rear by the heat pipes and at the front by the low thermal expansion Cordierite ceramic ring. It is free to exapnd thermally along its axis. AISI Type 310 stainless steel approximately 0.8 mm (0.030 in.) thick has been selected for the material because of its oxidation resistance.

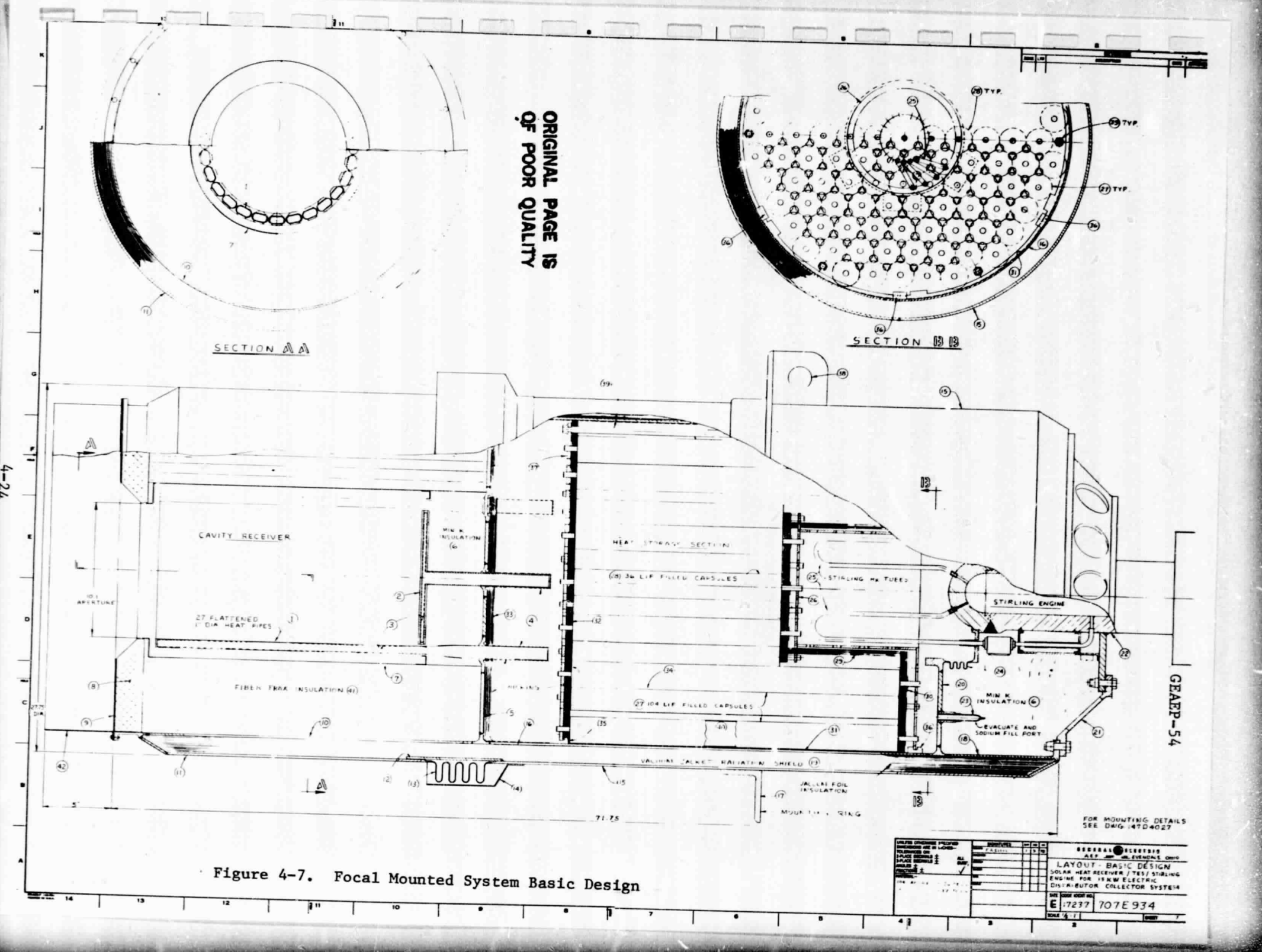

Figure 4-7. Focal Mounted System Basic Design

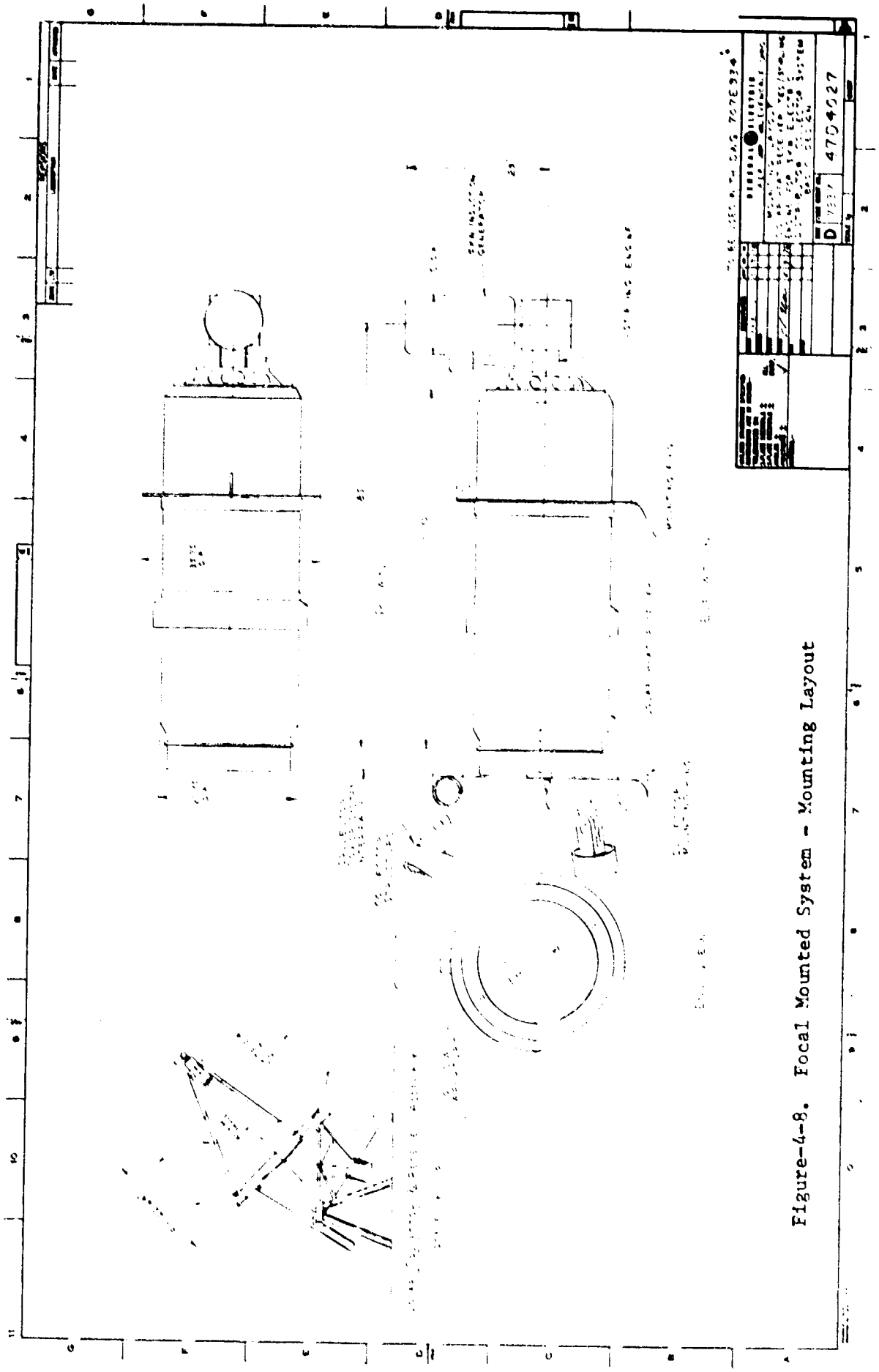

Figure-4-8. Focal Mounted System - Mounting Layout

Table 4-9. Parts List for the Focal Mounted System Basic Design

Part No.	Description	No. Req'd.	Material	Configuration	Size	Weight Lb.
1	Primary Heat Pipes	27	310 SS	1" OD Tube	0.035" wall	85.3
2	Flat Plate Heat Pipe	1	310 SS	1" OD Tube & plate	0.035" wall 1/8" plate	2.9
3	Wicking, Primary HP Evap. End	1 layer	304 SS	60 Mesh 0.239 lb/ft^2	124 ft^2/27 pts.	29.6
4	Wicking, Primary HP Cond. End (outside)	3 layers	304 SS 0.0075" wire dia.	60 mesh	9.2 ft^2/28 pts.	2.2
5	Flat Head (Front of containment vessel)	1	HA-188	Forging	1/4 to 1/2" thick	33.2
6	MIN-K Insulation	AR	MIN-K	Block	0.0116 lb/in^3	169.9
7	Receiver Internal Wall	1	310 SS	Sheet	0.030" thick	4.1
8	Cordierite Front Ring	1	Cordierite	Cast	2" thick	67.7
9	Convection Shield	1	310 SS	Sheet	0.030" thick	2.9
10	Front Inner Vacuum Casing	1	INCO 617	Sheet	1/8" thick	117.4
11	Front Outer Vacuum Casing	1	C Steel	Plate	3/16" thick	145.1
12	Bellows Guide Ring	1	C Steel	Sheet	3/16" thick	
13	Bellows	1	C Steel	Sheet	-	19.1
14	Bellows Shroud	1	C Steel	Sheet	0.030" thick	
15	Aft Outer Vacuum Casing	1	C Steel	Sheet	3/16" thick	200.0
16	TES Containment Cylinder	1	INCO 617	Sheet	1/8" thick	107.0
17	Mounting Ring	1	C Steel	Angle	1/2" thick	32.3
18	Aft Inner Vacuum Casing	1	INCO 617	Sheet	1/8" thick	35.7
19	Multifoil Radiation Insulation	AR	304 SS	Foil	0.0015" thick	443.4
20	Aft Flat Head	1	HA-188	Forging	3/8" thick	48.5
21	Stirling Engine Support Cone	1	C Steel	Plate	1/4" thick	∿ 20.0
22	Stirling Engine	1	-		-	-
23	Sodium Fill Port	1	321 SS	Tube	0.035" thick wall	-
24	Expansion Bellows	1	HA-188	Sheet	-	∿ 4.0
25	Stirling Engine Heat Exchanger	1	-	Multiple-Tube	-	-
26	Rear Capsule Support Plate	1	HA-188	Sheet	1/8" thick	48.5
27	TES Capsule	104	316 SS	Tube	1.9" dia., 24" ln. 0.030" wall	173.5
28	TES Capsule	36	316 SS	Tube	1.9" dia., 15" ln. 0.030" wall	w/o LiF
29	Aft Capsule Support Wicking	1	FM1101	Fibermetal SS Sheet	Porosity 0.9, 0.15" thick, 25" dia.	31.0
30	Wick Containment Washers	AR	304 SS	Sheet	N/I	
31	TES Containment Cylinder Wicking	4 layers	304 SS	60 mesh	81 ft^2	19.4
32	Forward Capsule Support Wicking	1	FM1101	Fibermetal SS Sheet	Porosity 0.9, 0.15" thick, 25" dia.	16.7
33	Forward Flat Head Wicking	1	FM1103	Fibermetal SS Sheet	Porosity 0.7, 0.40" thick, 25" dia.	48.7
34	TES Capsule Wicking	2 layers	304 SS	60 mesh	275 ft^2	65.7
35	Front Capsule Support Mount	1	INCO 617	Bar	-	48.5
36	Rear Capsule Support Mount	1	INCO 617	Bar	-	-
37	Front Capsule Support Plate	1	HA-188	Plate	1/4" thick	34.0
38	Lifting Eye	1	C Steel			-
39	Capsule Assy. Tie Bolt & Sleeve	4	C Steel	Assembly Tools		-
40	Lithium Fluoride	AR	LiF	Bulk	In TES Tubes	792.0
41	Insulation	AR	Fiberglas	Blanket	12 lb/ft^3	
42	Wind Shield	1	310 SS	Sheet	0.030	
43	Sodium, Primary HP		Sodium	Liquid Metal	-	0.7
44	Sodium, Secondary Heat Pipe		Sodium	Liquid Metal	-	12.5

The annulus between the cavity liner and the front inner vacuum casing is filled with low thermal conductivity insulation. The drawing indicates MIN-K 2000 insulation at a density of 320 kg/m^3 (20 lbs/ft^3). This material is a mixture of inorganic oxides, with silica and titania being the most prevalent compounds. It can be provided in block or powdered form. Its thermal conductivity at a mean temperature of 538°C (1000°F) in air is approximately 0.036 W/m-°C (0.21 Btu/hr-ft-°F). This material is very expensive compared to insulations such as Fiberfrax® or Cerafelt®, the latter, however, are not as good insulators. Since the outer vacuum insulation jacket extends the entire length of the cavity receiver, the need for MIN-K insulation is questionable and it is more likely that Fiberfrax® or some cheaper material would actually be used. To prevent excessive heat losses from the TES containment vessel, MIN-K insulation in block form would be employed at the far end of the solar receiver cavity.

The front inner vacuum casing (PN 10) supports the Cordierite aperture ring and contains the solar receiver cavity insulation. The parts list indicates this material as INCO 617; however, as this shell extends further from the TES containment front head its temperature decreases. On the basis of design analyses, it appears stainless steel AISI Type 321 could be utilized at a point where this shell extends approximately 0.2 m (8 in.) forward of the TES front head. This would require a weld joint and the economics of a weld joint vs. extending the INCO 617 all the way forward to the front outer vacuum casing would be the determining factor.

The front outer vacuum jacket casing (PN 11) carries the solar receiver and a portion of the TES weight back to the mounting ring. An expansion bellows with guide ring compensates for thermal expansion between the inner and outer shells. Multifoil radiation insulation in the vacuum jacket reduces heat losses from the solar receiver and TES system to a minimal amount (alternative thermal insulations are discussed under Section IV-B which assesses the design). The outer jacket further provides a method of supporting the entire focus mounted system without allowing direct heat conduction paths from the TES system or other hot parts to the mounting ring. It also provides a secondary containment for a portion of the TES containment vessel (i.e., shell only).

b. Thermal Energy Storage System (TES). The TES system consists of a cylindrical containment vessel with flat front and rear heads. The solar receiver heat pipes are welded in the forward head and the Stirling heat exchanger protrudes through the rear head. The Stirling engine cylinder is sealed to the rear head with an expansion bellows. One-hundred forty LiF-filled tubular capsules supported by front and rear support plates are located in a hexagonal pattern inside the cylindrical shell. Capsules are approximately 51 mm (2.0 in.) in diameter, 36 of which are 0.38 m (15 in.) long and 104 of which are 0.61 m (24 in.) long. All surfaces are wicked as described previously. The front and rear capsule support plates contain holes into which the capsule support pins are inserted during assembly and holes for vapor passage. The interstitial spaces between capsules provide an axial path for sodium vapor to travel throughout the TES system.

® Registered Tradename

The TES capsules and their front and rear support plates, along with wicking, would be assembled as a packaged core and then inserted into the containment vessel. Temporary tie bolts would contain the capsule core during assembly. The capsule assembly is supported from mounts welded to the inside of the cylindrical containment vessel. Rotating the capsule assembly locks this unit into the containment vessel. Thermal expansion of capsules relative to the containment vessel is taken up by the rear capsule pins sliding in the rear support plate. The rear wicking is held in contact with the aft end of the capsules by washers welded to the rear capsule pins.

The TES front head sees little, if any, pressure differential at operating temperatures, and at ambient temperatures is subjected to a differential pressure of 1.0×10^5 Pa (14.7 psi). Since the vapor pressure of sodium rises at a very slow rate with increasing temperature, and material allowable stress decreases with temperature at a faster rate, a plot of head wall thickness vs. temperature for INCO 617 and HA-188 was prepared; see Figure 4-9. These curves indicate the need, at this point in the design study, for HA-188 if reasonable wall thicknesses are to be utilized in head construction. Trends in the cost of cobalt alloys have, since the design, excluded the use of this material. Pressure differentials were obtained from data on sodium vapor pressure and from material allowable stresses as indicated in Figure 4-10. Wall thickness calculations were based on formulas for Unstayed Flat Heads as found in Section VIII of the ASME Code. No effort was made to calculate ligament strengths (i.e., area between heat pipes); however, additional metal thickness in this area will be necessary to keep stresses within the allowable value. A much more rigorous stress and thermal analysis of the head would be conducted in a detailed design phase. Oxidation and corrosion allowances would also be factored into calculations at that time. Although the design does not require ASME Code approval due to the low operating pressure, ASME code design, fabrication and test procedures would be utilized wherever possible.

The cylindrical shell of the TES containment vessel sees no differential pressure at ambient conditions since it is surrounded by a vacuum jacket but sees a differential pressure of approximately 0.8×10^5 Pa (12 psi) at maximum operating temperature. Using formulas for circumferential and longitudinal stress from Section VIII of the ASME Code and assuming a joint efficiency of 1.0, a wall thickness of approximately 2.5 mm (0.100 in.), utilizing INCO 617, is indicated. This does not include loads imposed by the TES capsule supports, bending mounts or vibrational loads imposed by the Stirling engine.

The rear head is exposed to the same pressures as the front head. The large opening for the Stirling engine heat exchanger will require adequate reinforcement as shown on the drawing. Like the front head and cylindrical shell, this structure will require a detailed thermal and stress analysis. The forward and rear heads are both depicted as welded assemblies on the drawing; however, a forging might actually be utilized in mass production.

The TES tubular capsules containing LiF are made from 0.76 mm (0.030 in.) thick Type 316 stainless steel. Similar size capsules have

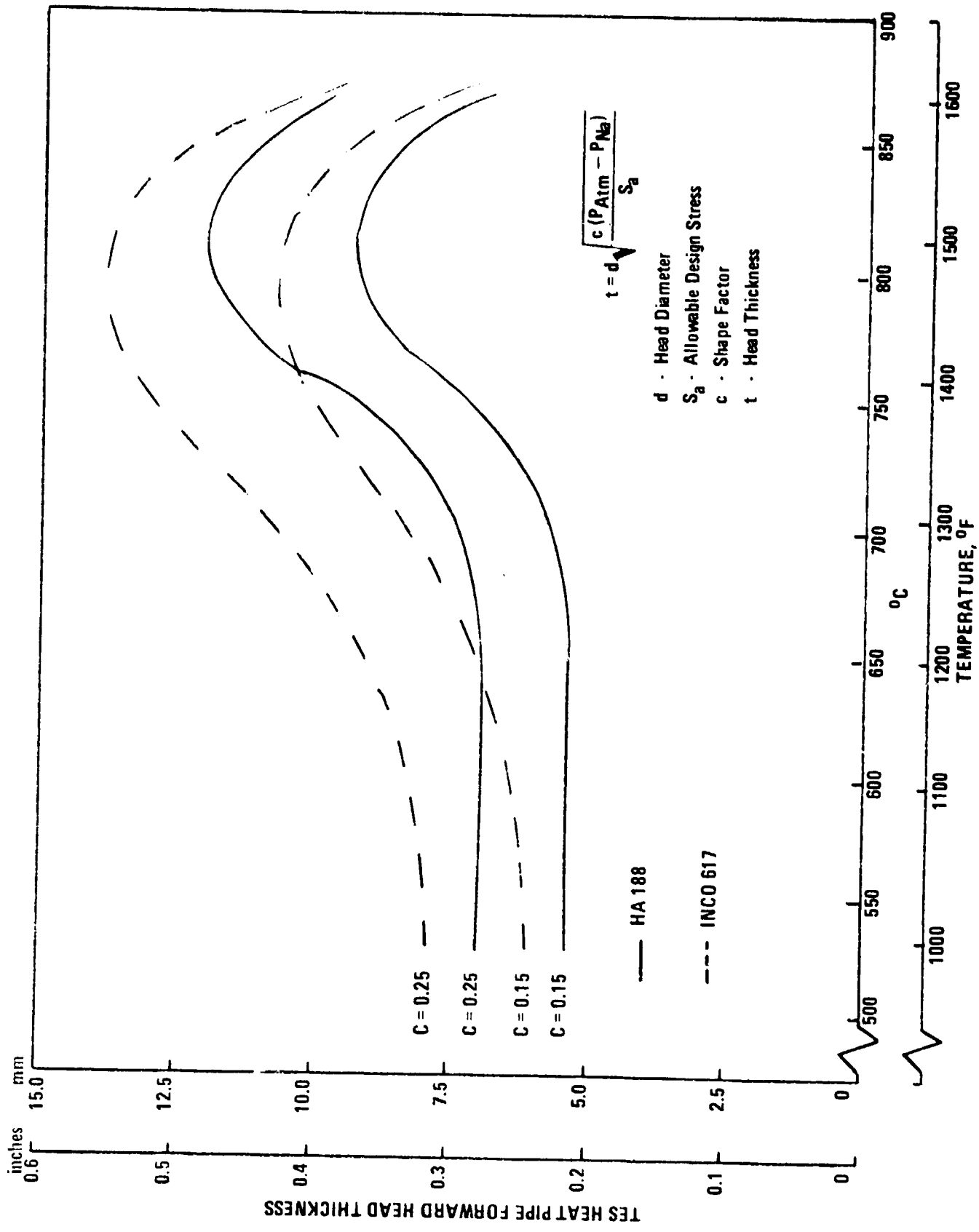

Figure 4-9. Thickness Required for TES Heat Pipe Forward Head vs Operating Temperature.

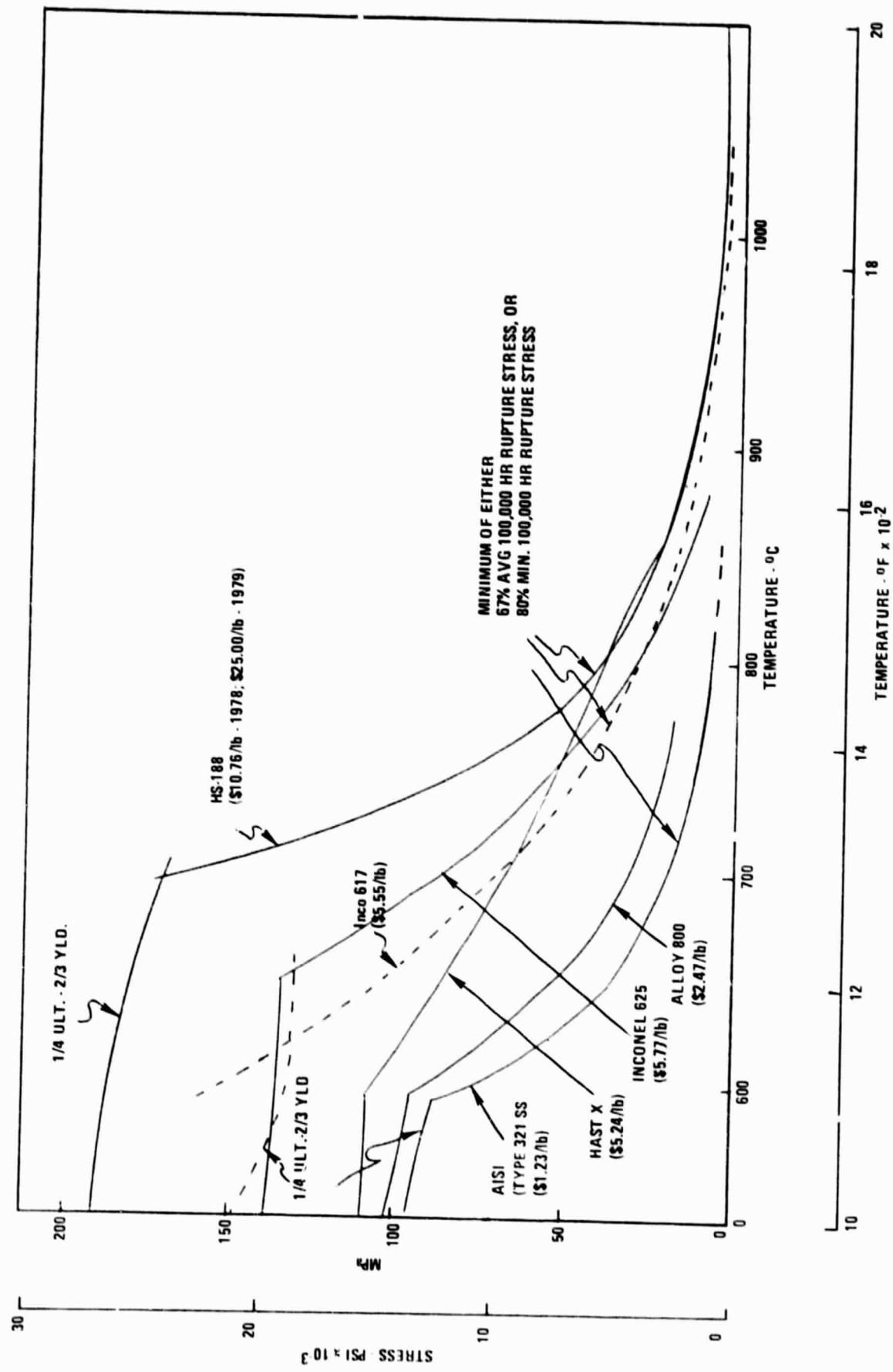

Figure 4-10. Allowable Design Stresses (ASME Design Criteria)

been manufactured from Cb-1Zr for low earth orbit space power applications and tested initially for over 5000 thermal cycles and, more recently, for tens of thousands of hours. The capability of using more economic materials must be established.

The front capsule support plate carries the entire TES capsule load of about 454 kg (1000 lbs.) at high sun angles. This load is transferred to the TES system containment vessel through the locking supports. Its thickness is indicated as 6.4 mm (0.25 in.). A simple, flat, circular plate uniformly loaded with edge supports was assumed in calculating the plate thickness. Capsule front support pins are welded to this plate so that thermal expansion is in the aft direction. When the concentrator is in the stowed position the TES capsule weight is also taken by the front support plate.

The major uncertainty in the design is the ability of wicking to transport adequate sodium liquid to the condenser section of the heat pipes and outer surfaces of the heat storage containment capsules. At low sun elevations (the worst condition), the wicking must be capable of pumping sodium approximately 0.45 m (18 in.) high against the force of gravity. Before proceeding with more extensive design effort, experimental demonstration of the wicking concept in a configuration similar to the basic design would be highly desirable. Easy fluid wicking tests are reported herein under Section IV-B7 for design verification purposes and additional modular experimental work in this area using sodium heat pipes and fused salt storage has since been initiated under a separate contract.

c. Stirling Engine-Generator. This study was intended to rely upon a separate Stirling engine program for definition of the Stirling engine. Since that program had not started, it was necessary to base the Stirling engine-generator configuration on other available, but more generalized, information for this initial conceptual design. The layout drawing and isometric for the basic design depict a horizontal cylinder rhombic drive type crankcase with a direct connection to an 1800 RPM, 3-phase induction generator. A mounting flange on the lower portion (i.e., power piston area) of the cylinder is indicated. This flange is attached to the junction of outer and inner cylindrical casings with a bolted conical structure. Lightening holes in the case provide a means of installing MIN-K insulation to insulate the cylinder and rear TES system head. The lightening holes would be covered with sheetmetal to prevent weather penetration. A metallic bellows assembly attaches the Stirling cylinder head to the TES system rear head. A double or triple ply bellows with a sensor for detecting leaks would probably be employed. The Stirling engine-generator loads are transmitted through the outer casing (vacuum jacket) into the focal point system mounting ring. Differences in thermal expansion between the inner and outer casing are compensated for by the metal bellows in the outer casing. A slip type bellows guide-ring removes lateral loads from the bellows.

d. System Mounting. Figure 4-8 indicates the configuration for mounting the focal point system to a 762 mm (30 in.) diameter concentrator mounting ring. The tubular type ring is merely a concept and no attempt to analyze stress in such a system has been made. The focus mounted sys-

tem mounting ring would be bolted to the concentrator ring after the assembly is lifted into position. The focal system mounting ring would be welded to the vacuum jacket casing at the center of gravity of the focus mounted system. As the system heats up, thermal expansion would cause the aperture (focal point) to move forward (toward the concentrator) slightly.

Electric power wiring and other required engine-generator services would be clamped to the side of the focus mounted system and led forward to the concentrator mounting ring. These service lines would then be run down to the concentrator through the tubular struts.

e. Weight and CG Analysis. The weight analysis of the TES system was important not only in and of itself but also for cost analysis purposes. The whole system was broken down into parts; the material, density, and volume were then calculated and from that the weights were determined. Table 4-10 presents a breakdown of weight by components for the system.

The weights used for the Stirling engine and generator are estimates based on the Phillips 1-98 engine and an induction generator of approximately 20 kW rating. A more detailed breakdown of weights was given above in the parts list, Table 4-9.

The center of gravity for the primary design heat pipe heat transport system is located 279 mm (11.0 in.) aft of the forward flat head welded assembly on the centerline of the system.

The weight of this initial design concept was higher than the initial target of 1365 kg (3000 lb.); design assessments discussed below point to the possible design modifications for weight and cost reductions.

B. DESIGN ASSESSMENT OF THE HEAT PIPE SOLAR RECEIVER

1. Design Assessment Objectives

The conceptual design of the heat pipe heat receiver with TES was assessed in various areas for potential future improvements in weight, cost, performance and reliability. As design guidelines were expected to change in the use of specifically selected Stirling engine-generators and concentrator systems during the course of further prototype development work, these assessments were expected to provide guidance to later progressive improvements in the design of prototypes which could be designed and built for near-term development and for the later design of mass producible, low cost, advanced units which would be required in deployment of more fully developed systems.

2. TES Materials Alternatives

Alternative thermal energy storage materials have been considered including, in decreasing order of thermal storage efficiency and relative cost, LiF, 67NaF-33MgF_2 and Na_2CO_3. A comparison of the relative costs of these materials per kWh for the basic material and for the additional cost of containment in stainless steel containers according to the design concept is shown in Table 4-11. Basic salt costs are given for current large quantity purchase and for future mass production costs of the fluoride salts using lower cost fluorosilicic acid in place of hydrofluoric acid.

Table 4-10. Weights for the Heat Pipe Heat Transport TES System

Item	Mass kg	Mass lb	% of Total Weight
Receiver	210	462	16
TES Area Structured	181	399	14
TES Salt	359	791	28
TES Cans	79	174	6
TES Area Wicking and Sodium	86	190	7
Multifoil Insulation	201	443	16
Outside Steel Shell	157	346	12
Total	1273	2805	
Stirling Engine (Estimate)	147	324	
Generator (Estimate)	68	150	
Total	1488	3279	

Table 4-11. Relative Thermal Energy Storage Materials Costs

TES Material	LiF		$67NaF-33MgF_2$		Na_2CO_3
Melting Point	857°C (1575°F)		827°C (1520°F)		851°C (1564°F)
Density	144.9 lb/ft^3		108.8 lb/ft^3		156.6 lb/ft^3
Latent Heat of Fusion	400 Btu/lb		265 Btu/lb		120 Btu/lb
TES Material Cost Basis	Current	Future	Current	Future	Current/Future
TES Materials Cost	$ 3.15/lb	$ 1.17/lb	$ 0.45/lb	$ 0.08/lb	$ 0.03/lb
Materials Costs/kWh					
Salt	$26.89	$ 9.98	$ 5.80	$ 1.03	$ 0.84
Can and Wicking	8.32	8.32	10.78	10.78	16.54
Other Structural (est. 2 x can/wicking)	16.42	16.42	21.66	21.66	33.08
Total	$51.63	$34.72	$38.24	$33.47	$50.46

As initially contained, the costs per kWh for the more expensive high efficiency LiF are greater than those for the NaF-MgF_2 salt. The Na_2CO_3 salt, because of its comparatively lower latent heat, apparently cannot compete with the mixed fluoride salt. The current cost advantage of the contained wicked and structurally supported mixed fluoride is about twice that of the LiF, but, as the cost of both salts can be expected to drop significantly in the future, this advantage can be expected to be reduced to near equivalency. Furthermore, the higher efficiency TES materials offer cost advantages in the reduced amount of wicking, structural support and external heat pipe containment costs which must be attributed to total TES costs. Design efforts to reduce the ratio of non salt to salt weights and costs will move the reduced cost systems toward the selection of the less expensive mixed fluoride.

Other material properties, such as the higher thermal conductivity of the mixed fluoride which was utilized in the calculation of thermal gradients and in the selection of containment cylinder diameter and cost, can effect TES costs per kWh. More accurate thermal property data is needed in order to continue to assess more accurately the relative merits of various materials.

Lower costs in future designs will also require minimization in both the amount and cost per pound of additional materials used in structural wicking and containment. More advanced design concepts beyond the initial prototype demonstration designs can address the opportunities of providing multifunctional uses to various components in order to achieve this. For example, the wicking might be provided integrally with the TES containment system, structural support might be provided in alternate ways and significant wicking might be eliminated.

3. TES Duration

A determination of the incremental cost of thermal energy storage requires a consideration of not only the change in the amount of salt and salt containment but also of the changes that can be expected in the total heat pipe wicking, structural support, sodium containment and thermal insulation. To determine this total design cost sensitivity to changes in TES duration, a 15 minute duration TES system with its solar receiver was designed and costed using, as a basis of comparison, the 1.27 hours TES duration design featuring NaF-MgF_2. The analysis was performed in the same manner as the cost analysis that was performed earlier and used the same cost data. The quarter-hour system, shown in Figure 4-11, is essentially a reduced length version of the initial conceptual design. For direct cost comparison purposes, materials of construction remain the same. This is an initial concept system, involving the use of alloys such as HA-188, and does not reflect the use of cost-cutting techniques. Costs of the parts were based solely on their weights, which is a reasonable assumption for mass produced items.

It should be noted that, when going to a smaller thermal storage time, by removing TES cartridges, the power extracted from each cartridge increases, thus increasing the temperature gradient in the cartridge. Thus, the diameter of each TES material cartridge had to be reduced to retain about the same temperature drop, as shown in Table 4-12. This

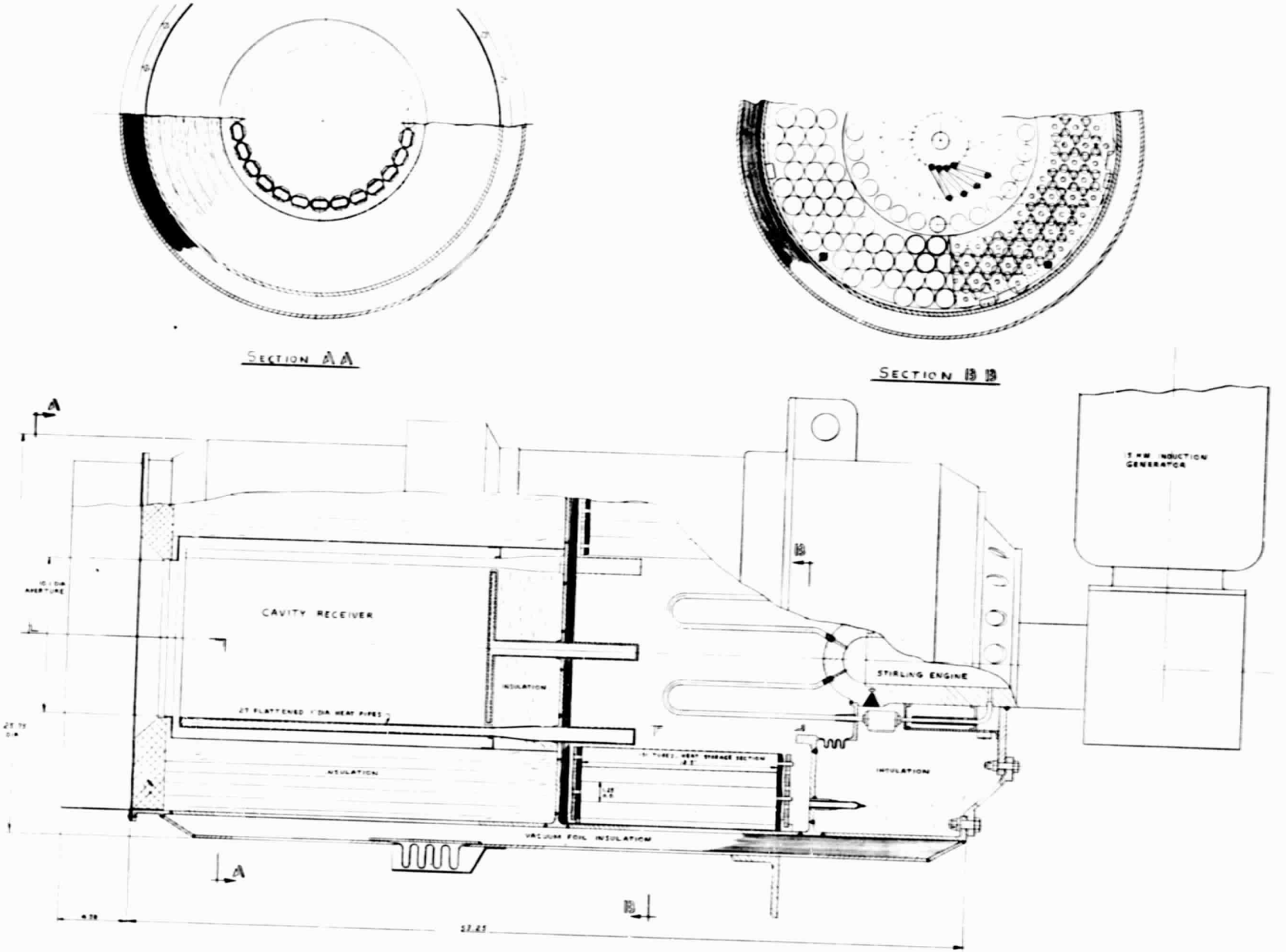

Figure 4-11. Heat Pipe Solar Receiver with 15 Minutes $NaF-MgF_2$ Latent Heat Storage

Table 4-12. Comparison of Thermal Energy Storage With Differing Duration

	1/4 Hour (Nominal) TES System	1.27 Hour TES System
Capsule Size	318 x 32 mm (12.5 x 1.3 in.)	622 x 58.4 mm (24.5 x 2.3 in.)
Weight of Salt (67%NaF-33%MgF_2)	81 kg (178 lbs)	330 kg (728 lbs)
Weight of Overall System (without engine or generator)	680 kg (1500 lbs)	1124 kg (2478 lbs)
Number of Capsules	151	97
Discharged Capsule Temperature Gradient	31°C (56°F)	40°C (72°F)
Center of Gravity of Solar Receiver/TES (distance from the primary heat pipe bulkhead)	20 mm (0.8 in.)	279 mm (11 in.)
Material Cost	$6400	$10,400
Storage Time*	0.30 hr	1.27 hr

*Includes latent heat plus 56°C (100°F) sensible heat for structure and 1/4 of salt.

had the effect of greatly increasing the amount of structure associated with each unit of TES material and tended to keep the total cost from decreasing at the same rate as the storage time. Obviously, alternate and unique design concepts should be used for very short duration TES designs for optimization purposes. The elasticized design presented here was done for the purpose of establishing cost trends for the TES duration within the comparable constraints of a fixed design concept.

When the materials costs for the 15 minute system are compared to those for the 1.27 hour system, as shown in the materials cost vs. storage time plot of Figure 4-12, the slope of the line tends to represent the storage cost per hour for a 52.5 kW_t system. Thus, the materials cost of all components affected by a change in TES storage is of the order of \$79.50/kWh_t. It is apparent that the storage cost per kWh_t is not linear with storage time and that the deviations are greatest at storage times below 15 minutes and must deviate significantly at times beyond 1.27 hours.

The above comparison illustrates the requirements that an ideal salt must have. Since a thermal energy storage system must have some structure associated with it, it is desirable to have as high a latent heat for the salt as possible and thus maximize the "heat storage per unit of structural weight". Additionally, it is desirable to minimize the ratio of structure/containment/wicking to salt by multifunctional design. On the other hand, allowing the cost of the salt to be too large makes the TES system too expensive and the cost per kWh_t again goes up.

A second point which is apparent from the above analysis is that the cost of energy storage for a small unit and for short time periods may be high when compared to much larger systems. The rules of scale probably apply to TES, and especially for closely coupled systems. At low storage periods the real gain may turn out to be due to the economics of closely coupling the source of heat, the storage medium, and the power conversion system (thus greatly reducing the costs of other heat transport portions of a competing system such as pumps, valves, pipes, insulation, controls, etc.) rather than to the cost of the TES, itself.

It is clear from the above discussion that these preliminary costs for thermal energy storage are too high for attractiveness in mass production. Most of the cost is associated with the containment and support hardware rather than with the TES material. This is the area where cost improvement can be effected by means of both design improvements and, eventually, reduced cost in mass production. This improvement requires both development of a workable system and a considerable amount of effort by manufacturing engineers downstream as these units become commercialized. Even with a great deal of development, much necessary and predictable cost reduction can only be accomplished as experience is gained both in design improvements and in manufacturing methods.

4. TES Without Heat Transport

Thermal energy storage without heat transport is limited by the large temperature gradients that develop within the TES material which are necessary to extract the thermal energy at the required rates. Generally, nonmetallic TES materials have rather poor thermal conductivi-

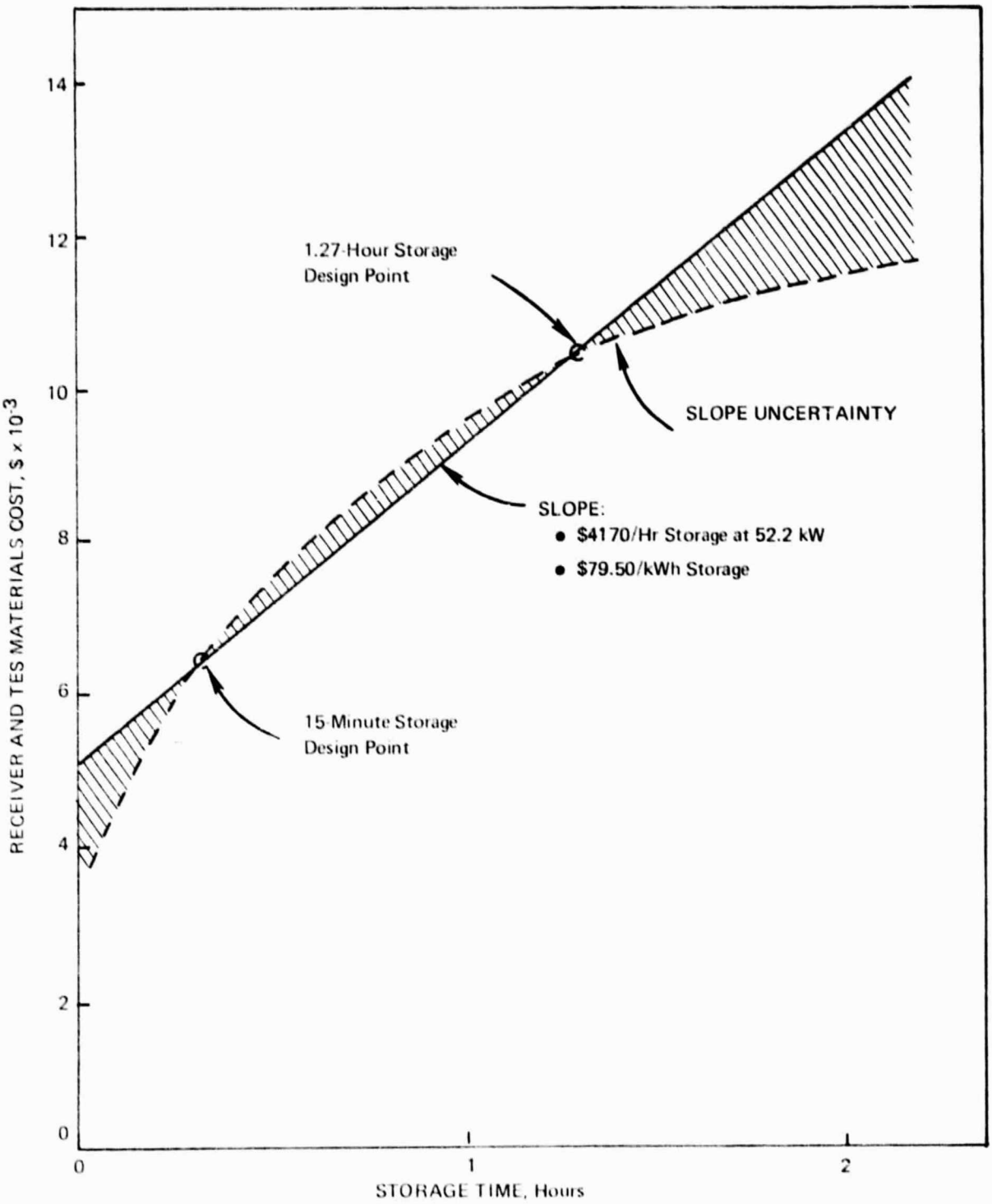

Figure 4-12. Receiver/TES Materials Costs vs. Storage Time Using $NaF-MgF_2$

ties which means that a large temperature gradient is necessary to move the heat a distance more than a very few inches through the materials. The problem then becomes one of creating the geometry such that the distance through the TES material is short and/or improving the thermal conductivity of the TES material. Both of these options were investigated.

Based on a very limited analysis of the Stirling engine heat exchanger, it was determined that the engine exchanger could be designed for direct TES purposes to consist of only 12 tubes, each 762 mm (30 in.) in length. This would permit a much deeper penetration of the TES material by the Stirling heat exchanger tubes and it would allow more material to be wrapped around the tubes than is possible for the type of shorter tube heat exchanger that was used with the conceptual heat pipe design; thus a longer thermal energy storage could be achieved.

Two overall system geometries were investigated. The first, shown in Figure 4-13 has the finned Stirling engine heat exchanger tubes (fins not shown for clarity) running circumferentially around the wall of the receiver in the middle of an annular region filled with salt. This arrangement would probably have the most uniform temperature in the TES material around the exchanger tubes and therefore the minimum thermal expansion induced stresses. In the second system, depicted in Figure 4-14, the heat exchanger tubes run radially outward which allows the wall of the receiver to be scalloped; this in turn, increases the surface area of the receiver and improves the absorption of the solar energy.

Both systems have storage times on the order of 15 minutes. Their temperature drop between the receiverwall and the helium in the exchanger tubes is approximately the same as the heat pipe solar receiver/TES unit. Both designs also assume that the thermal conductivity of the TES material may be increased either by the use of fins or by imbedding the TES material with another material of higher thermal conductivity.

In order for this type of system to be successfully developed, it is important that sufficient flexibility in the Stirling engine heat exchanger design be available to permit the optimization of the combined receiver-heat exchanger. The finned tube heat exchanger configuration and either the convoluted or cylindrical wall solar receiver/TES cavity design impose unique fabrication problems and, particularly, the requirement for extensive heat transfer and stress analysis to evaluate performance and operating reliability under low cycle fatigue conditions.

5. Thermal Insulation

Cost analysis of the conceptual design indicated that the insulation was a significant part of the overall cost. It was also realized that, though the vacuum multifoil insulation accomplished in only an inch or two what other insulations required approximately 200 mm (8 in.) to accomplish, the high cost of steel foil made this option prohibitively expensive. In addition, the cost of maintaining a good vacuum over the life of the system was in doubt. Since limits on the diameter of the system were not of major significance to the concentrator system, the opportunity of making a major reduction of the cost for the thermal in-

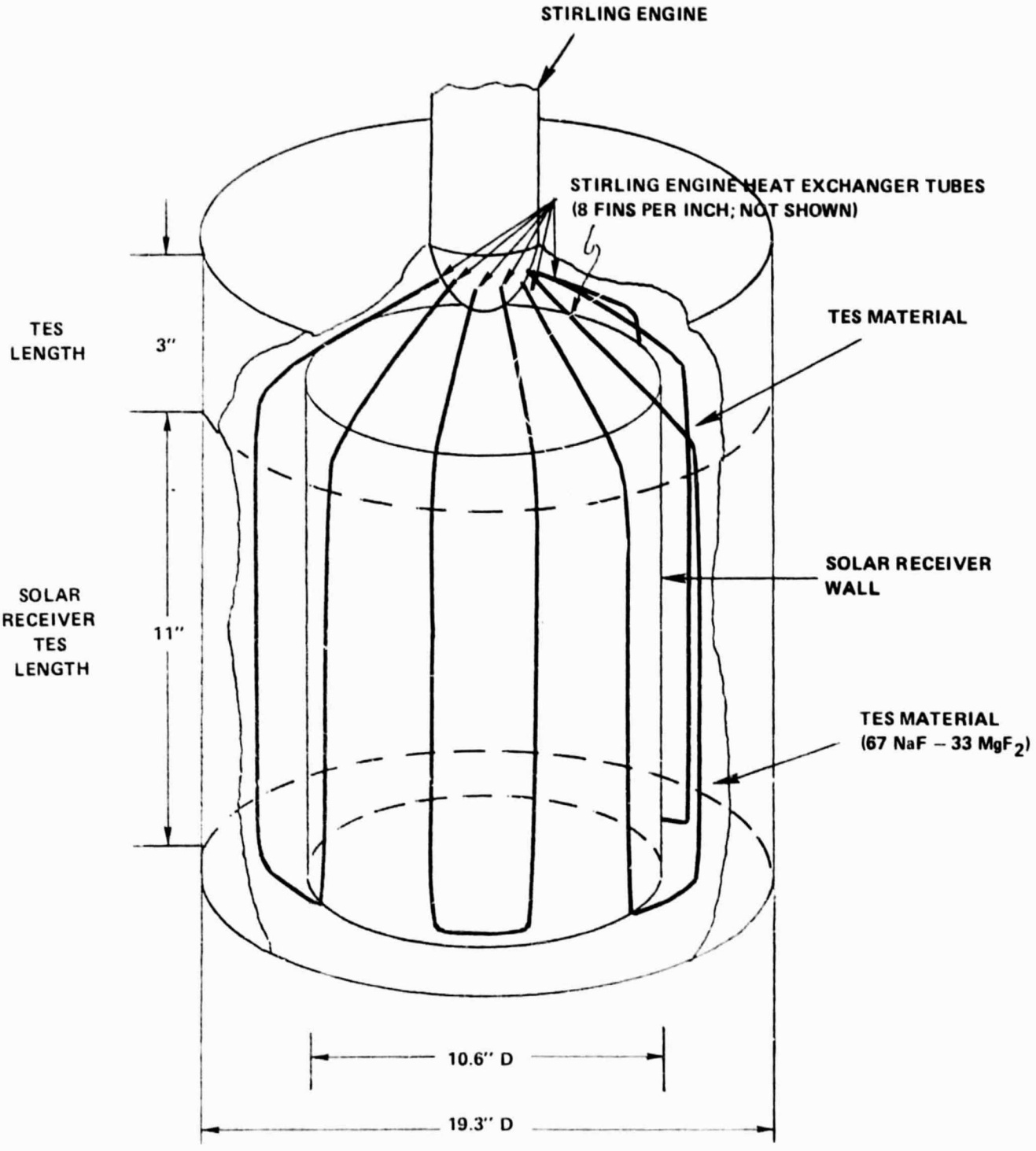

Figure 4-13. 15 Minute TES Finned Tube Stirling Engine Solar Heat Receiver Concept (Circumferential Tube Configuration)

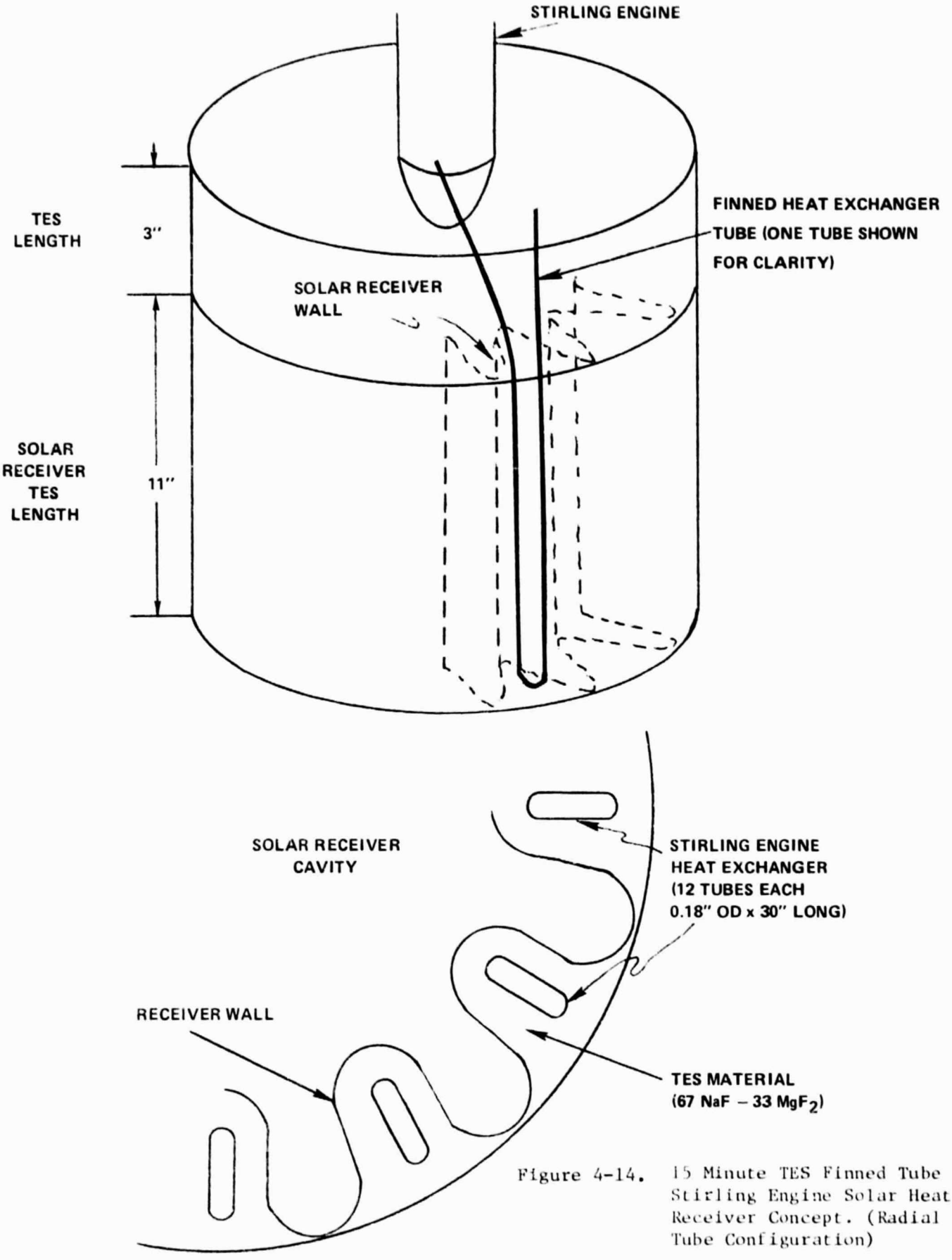

Figure 4-14. 15 Minute TES Finned Tube Stirling Engine Solar Heat Receiver Concept. (Radial Tube Configuration)

sulation was investigated. The use of more bulky, but lighter weight and less expensive fibrous insulation was then considered.

Since the costs for fibrous insulation generally decrease with decreasing maximum service temperature (until cryogenic temperatures are reached), the cheapest insulation package would consist of two or more layers of commercial insulation. The inner, more costly insulation would have relatively high temperature capability and would extend only so far as needed to bring the temperature down to the point where a less costly insulation, such as fiberglass could be used. The definition of the insulation package is a function of the energy lost through it, the inner radius, interface temperature between the two types of insulation, the thermal conductivities of the insulation materials and the total allowable insulation thickness. A parametric analysis was performed to optimize the insulation package. This analysis was performed to include all the combinations of two high temperature, two low temperature, and one intermediate temperature insulation and to calculate the cost, weight, and thicknesses necessary for a range of heat losses.

Relationships between the cost, thickness, weight, and energy lost through the four lowest cost insulation combinations are given in Figures 4-15, 4-16 and 4-17. It should be noted that the loss rate through multifoil insulation, as currently designed, is about 1.07 kW (3650 Btu/h). Also, the cellular insulation was assumed to consist of a 1016 mm (40 in.) long cylinder with an inside diameter of 616 mm (24.25 in.), similar to the multifoil insulation. To insulate this section with multifoil insulation costs about $1100 for the foil alone. Figure 4-15 clearly shows that substantial savings can be achieved either in cost (below $1100) or in thermal loss (below 1.07 kW) by going to a two layer fibrous insulation without the use of vacuum. Several important conclusions were drawn from the analysis which would be valid regardless of which brands of insulation were ultimately used.

First, significant savings over vacuum multifoil type insulation can be achieved in the areas of weight and cost at the expense of thickness. While the data is provided for insulation thickness up to 660 mm (26 in.), some tradeoff will have to be performed to establish the cost effects of the shadowing and of increased outer structure and mounting that are incurred as the diameter of the receiver/TES increases.

Second, cellular type insulations, in reasonable thicknesses of around 150 to 200 mm (6 to 8 in.), can perform as well or better than the current multifoil design. In the current design about half of the losses are through the side wall insulation. Should the thickness of insulation prove to be of lesser importance than the thermal losses, the performance of the insulations can be improved by increasing the thicknesses.

Third, the overall cost of the insulation package is extremely dependent on the price that can be obtained in large orders for the insulation materials. The analysis performed here was based on current list prices and costs are therefore probably higher than those which would occur in mass production.

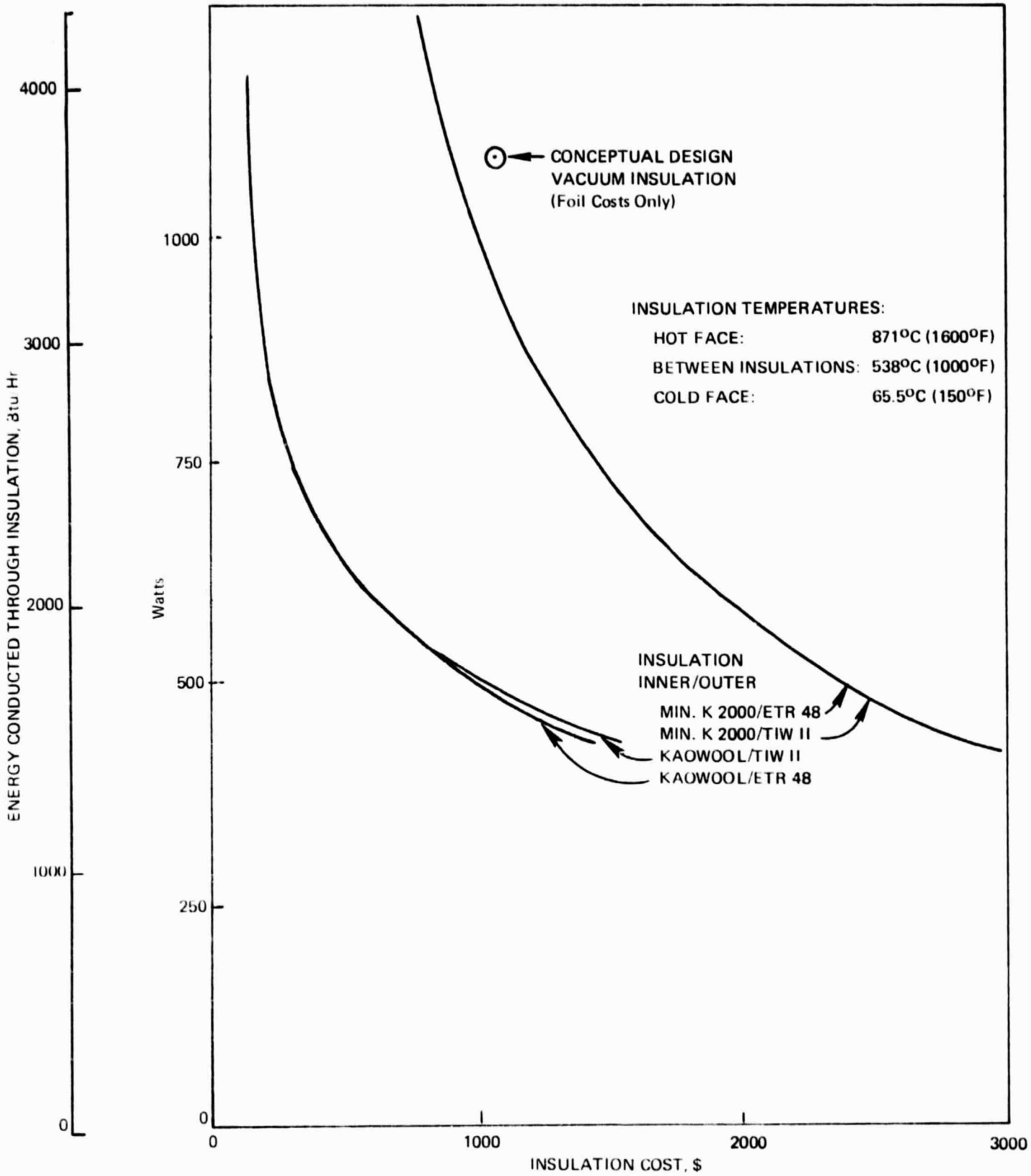

Figure 4-15. Insulation Cost Versus Heat Loss

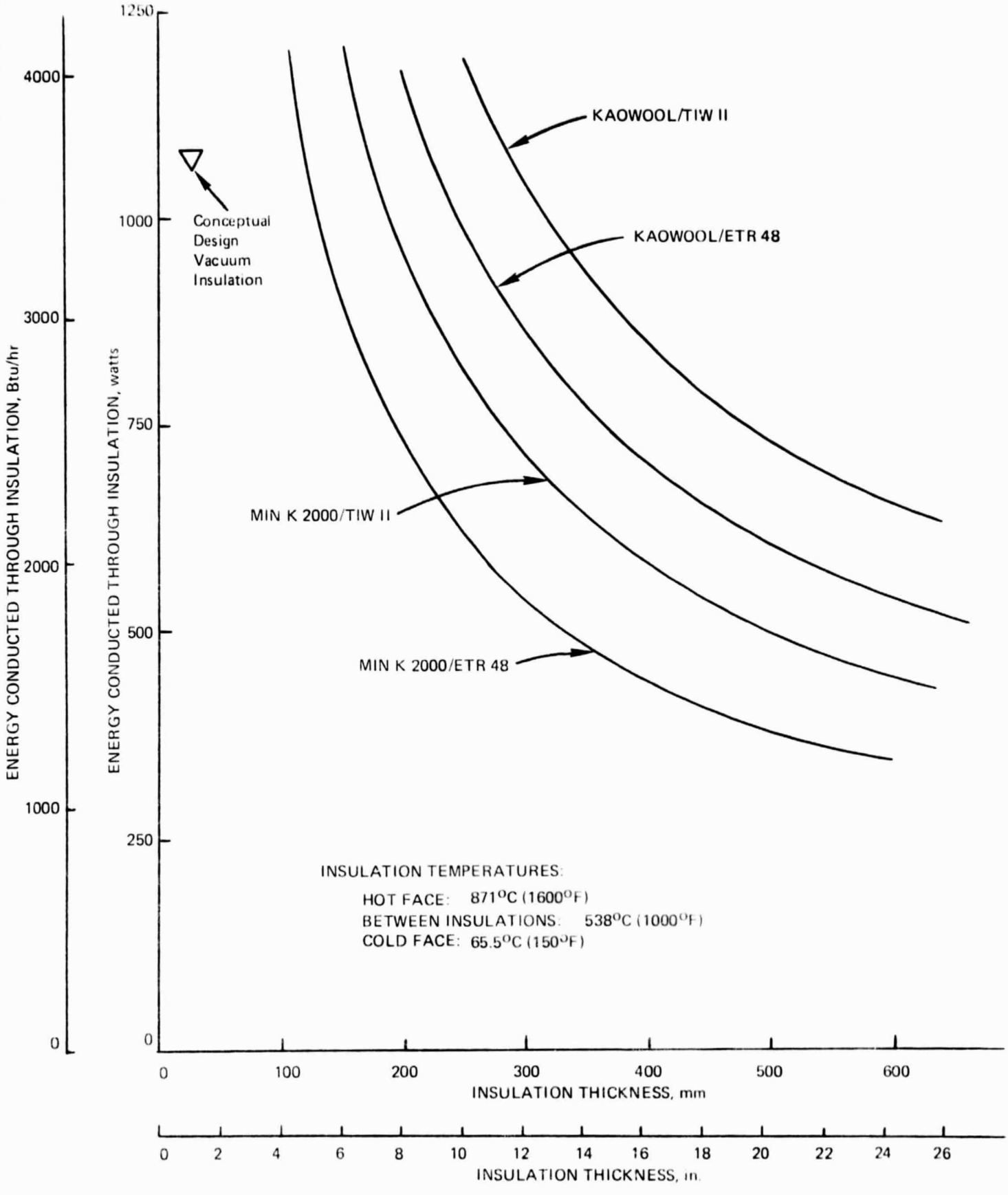

Figure 4-16. Insulation Thickness vs. Energy Lost

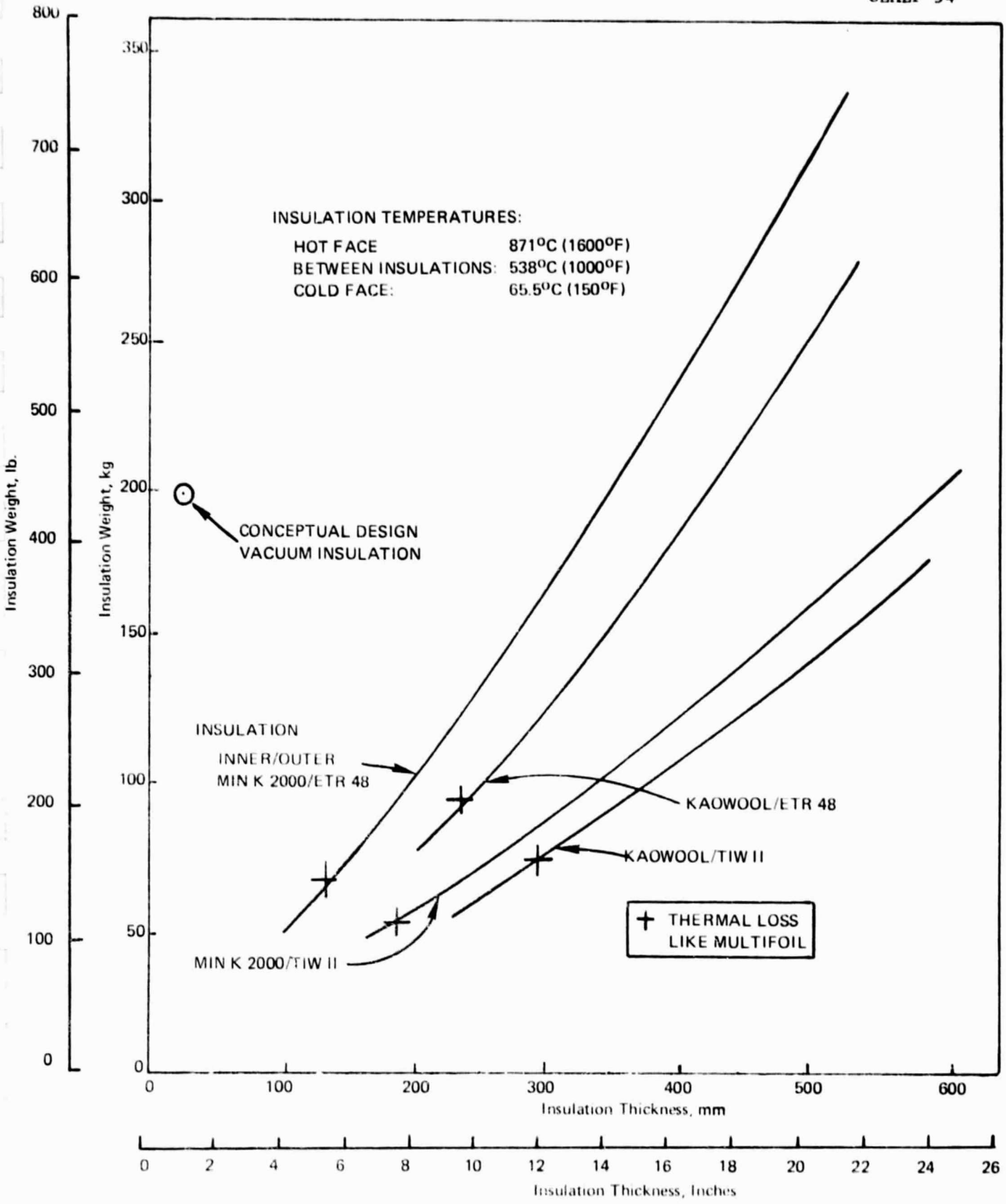

Figure 4-17. Insulation Weight Versus Thickness

Finally, the overall weight of the cellular insulation system would only be about half that of a steel vacuum multifoil system for the current design thermal loss. This opens up the option of reducing this thermal loss without any additional weight penalty or of providing other design improvements with the weight saved.

6. Heat Pipe Confirmation Testing

The primary heat pipes in the receiver were designed to transfer 2300 watts each at maximum solar heat flux conditions. Experimental tests were conducted to verify the power transfer capabilities of these heat pipes at various angles of inclination to the horizontal and at various heat flux conditions. The tests also served as a means to identify performance during startup.

Five heat pipes were fabricated, assembled and filled with sodium. The various components of the heat pipes,excluding internal wicking already installed within the pipes,are shown in Figure 4-18. The five heat pipes with wicking installed and ready for final vacuum bake-out are shown in Figure 4-19. These heat pipes included:

(1) The reference design heat pipe with 60 mesh stainless steel wicking in the evaporator section.

(2) A similar heat pipe with 3.8/mm (96/in.) spiral grooves, 0.25 mm (0.010 in.) deep in the evaporator area.

(3) A heat pipe similar to the second, but with additional longitudinal grooves 0.25 mm (0.010 in.) deep and 1 mm apart.

(4) A flattened heat pipe similar to the reference design but with 60 mesh wick extending the full length of the heat pipe.

(5) A circular cross section heat pipe with 60 mesh wicking in the evaporator area.

Prior to filling with sodium these heat pipes were baked-out in vaccum at 982°C (1800°F) for 1/2 hour and retained in sealed polyethylene bags filled with a protective argon atmosphere. They were then filled with sodium, sealed in vacuum and mass spectrograph helium leak tested after being pressurized in helium. The sodium filling procedure and the manufacturing procedures for the heat pipes are included in a separate Topical Report*.

The heat pipes instrumented with several sheathed thermocouples were installed in the heat pipe test facility. The heat pipes were cooled by the high velocity air at the condenser and were heated by clam shell heaters. These features and the installation of the heat pipes in the test facility are shown in Figures 4-20, 4-21 and 4-22. Primary heat pipe and the test facility drawings are shown in Figures 4-23 and 4-24.

---

*Divakaruni, S.M., "Heat Pipe Design Confirmation Testing", DOE/JPL 1060-27, GEAEP-55, September 25, 1979.

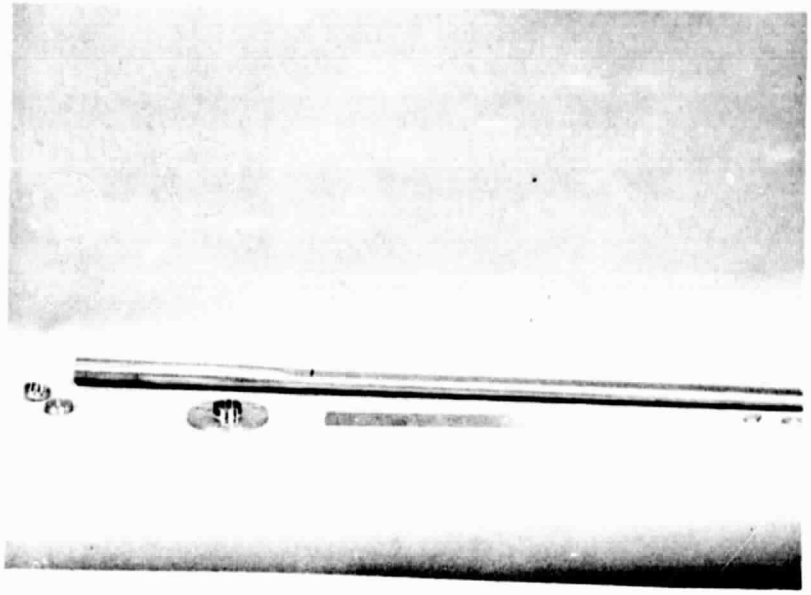

Figure 4-18. Heat Pipe Components (Excluding Wicking)

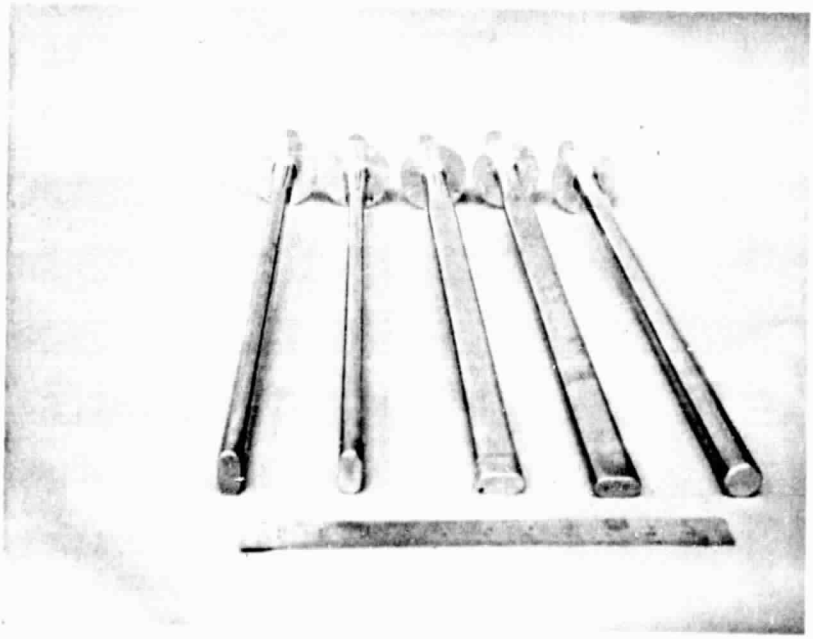

Figure 4-19. Heat Pipes Prior to Vacuum Bakeout

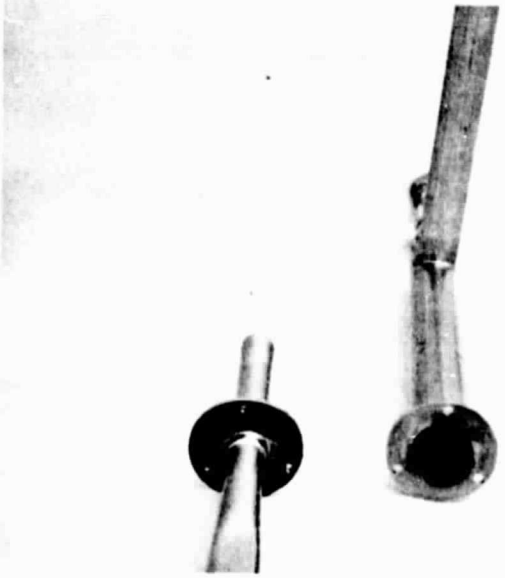

Figure 4-20. Heat Pipe and Reverse Flow Condenser Cooler

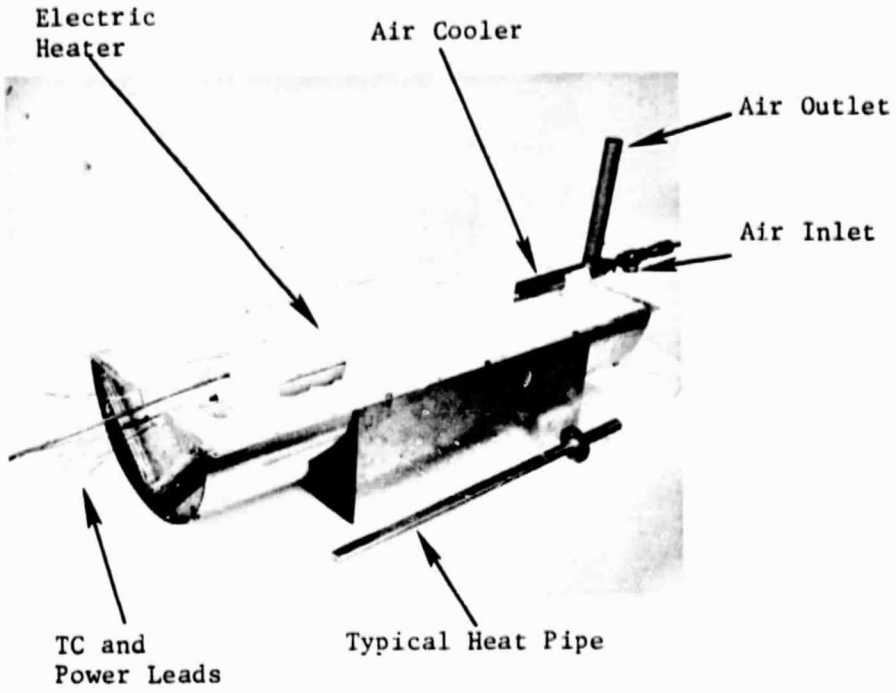

Figure 4-21. Instrumented Heat Pipe in Test Facility. (Additional Heat Pipe in Foreground for Reference)

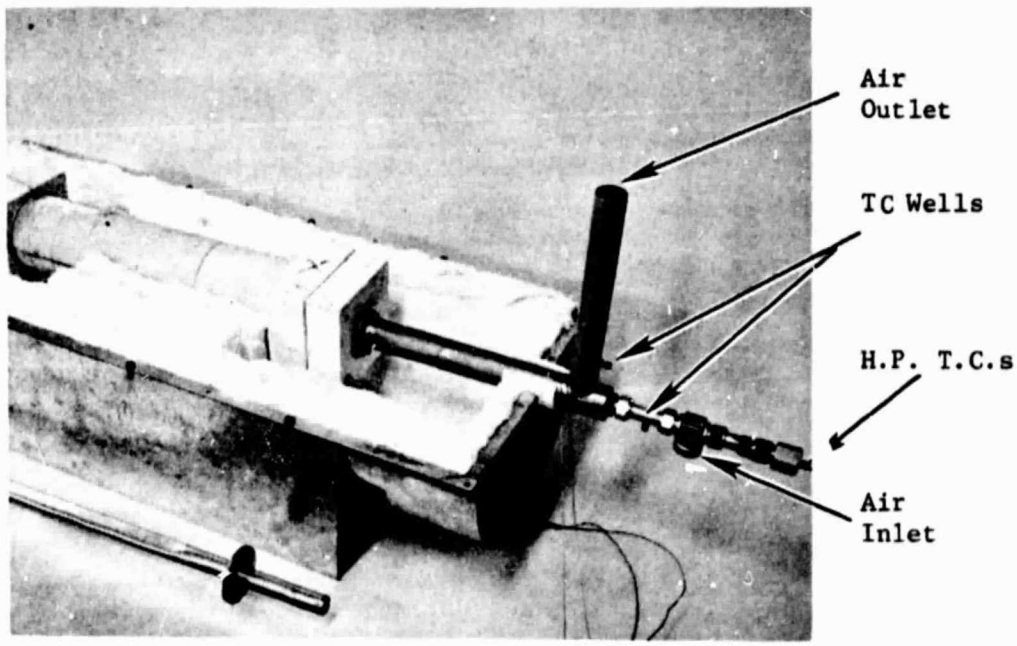

Figure 4-22. Condenser End of Heat Pipe Test Facility

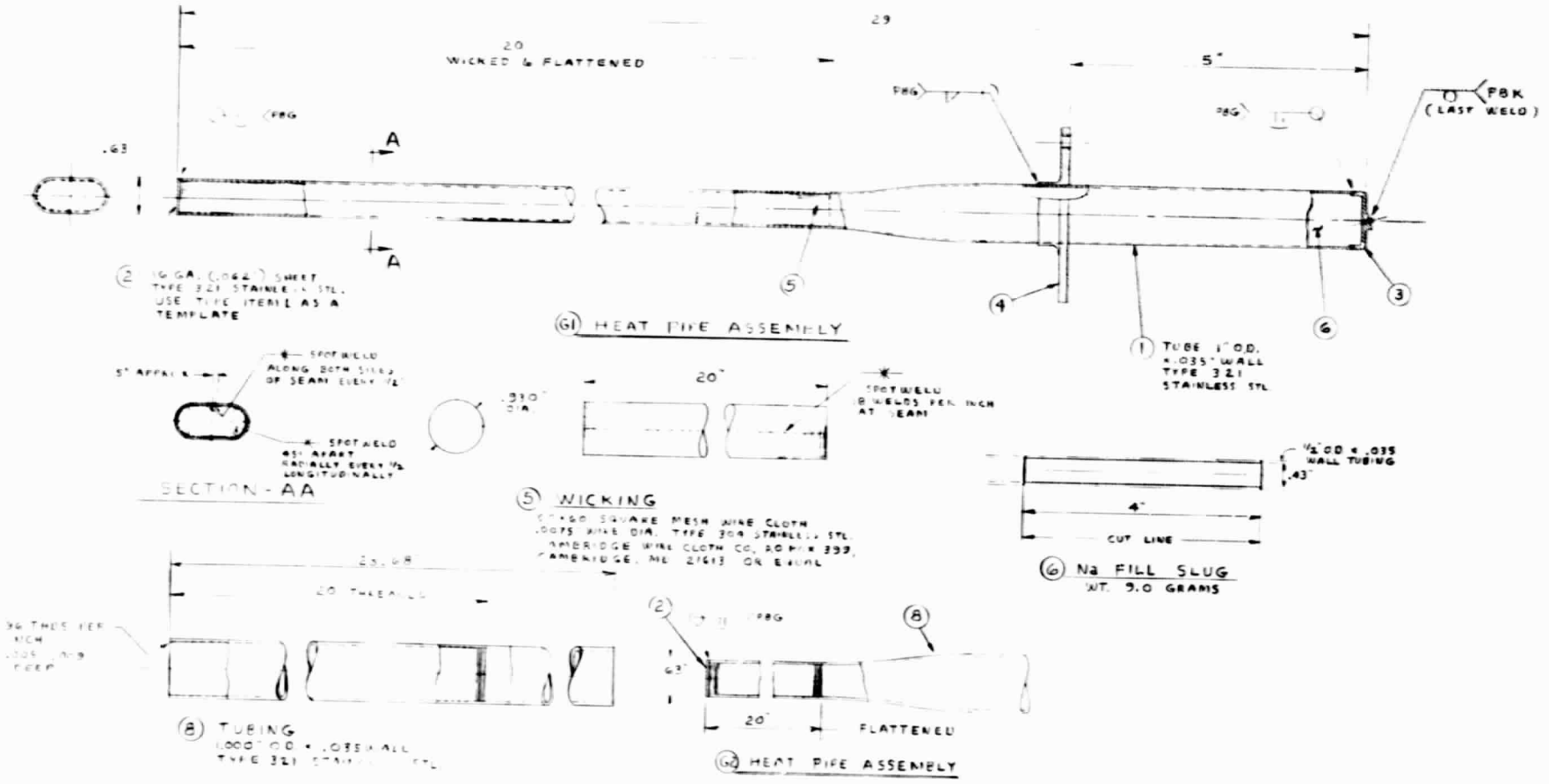

Figure 4-23. Primary Heat Pipe

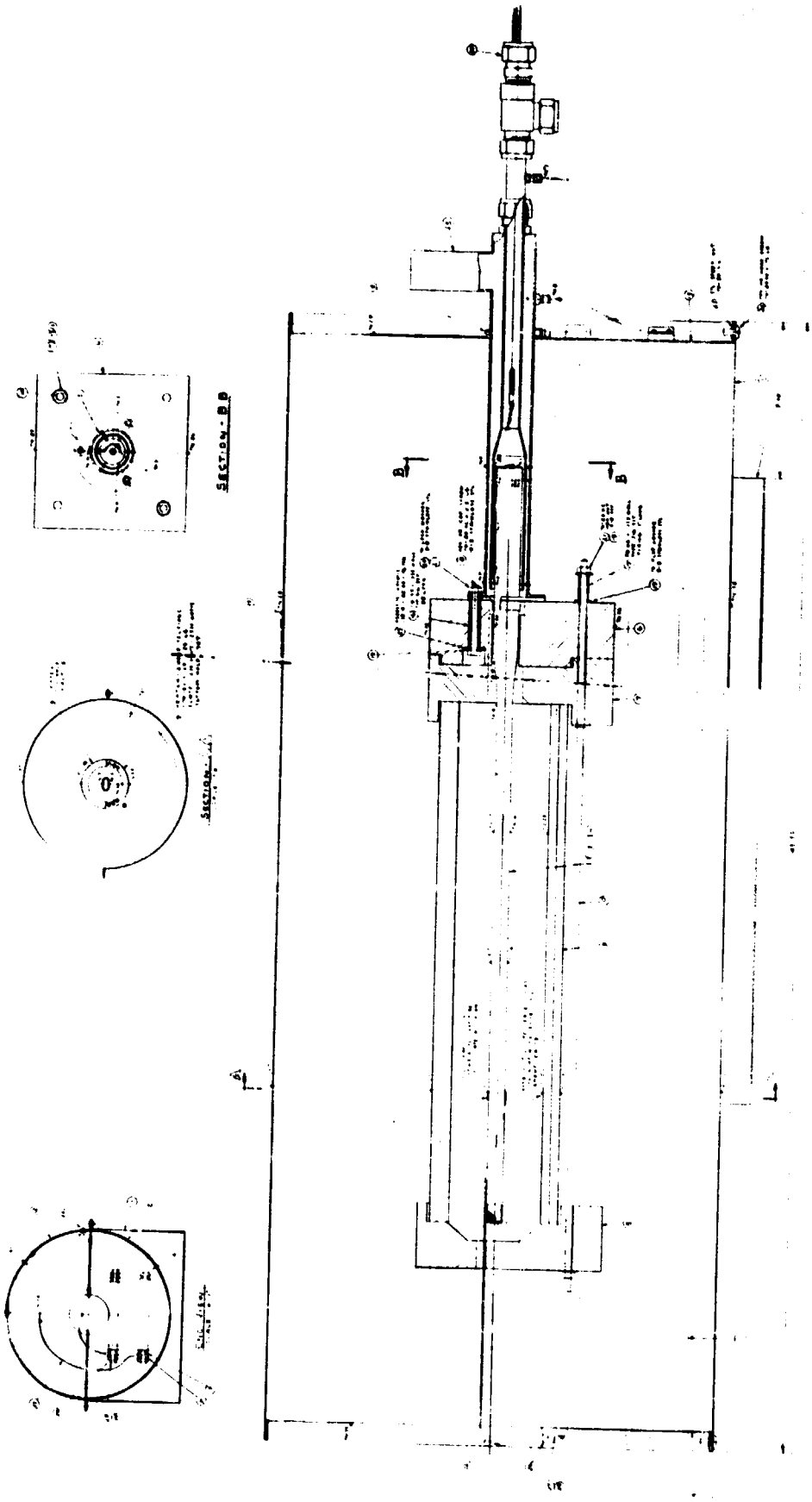

Figure 4-24. Heat Pipe Test Facility

Tests were conducted on all five heat pipes in accordance with a prepared test plan at various angles of inclination under steady state and transient test conditions. All the heat pipes except the third heat pipe in the above list with the simulated knurled surface operated successfully at the power input of 2.31 kW_t, which is the maximum solar heat flux expected at the evaporator surface; that third heat pipe could not be started, probably because of an undetected leak.

Typical heat pipe performance curves are given in Figures 4-25 and 4-26. The power input through clam shell electrical heaters was increased to 2350 watts in 2 hours time and the axial temperatures were observed and plotted at different times. Figure 4-25 shows this type of performance data at a heat pipe inclination angle 10° from horizontal. The startup conditions existed in the heat pipe until the power level was beyond 1000 watts. Temperature gradients occurred along the adiabatic and condenser sections even at 1000 watts, because of the low rate of heat transfer. However, the heat pipe operated isothermally at 2700 watts.

The effect of inclination angle was negligible in the operation of not only a gravity assisted heat pipe which had no wicking in the condenser but also in all the wicked heat pipes.

The fully wicked heat pipe had a higher temperature drop because of an additional drop across the condenser wick.

The nonflattened heat pipe showed hot spots present in the evaporator portion of the heat pipes, the location of which changed with the orientation angle,indicating the wicking did not maintain good contact with the wall. Flattening of the heat pipes in the other heat pipes seemed to avoid such hot spots in the evaporator.

In this particular solar thermal application of the heat pipes, the temperature drop from the evaporator external surface to the condenser external surface is of primary concern. Under two evaporator heat input rates, the total heat pipe temperature drops were compared. The reference design heat pipe and the grooved heat pipe (both flattened and wicked only in the evaporator region) had a 28-39°C (50-70°F) ΔT as compared to about 56°C (100°F) ΔT for the full-wicked and the non-flattened heat pipes.

A separate topical report* gives the details of the complete experimental work done on heat pipes which include basic theory of the heat pipes, heat pipe step-by-step manufacturing procedures with the inclusion of the cleaning and sodium-filling processes involved, the particulars on the experimental test setup and the results of experiments. For details on the experiments on each of the heat pipe the reader is referred to that report.

*Divakaruni, S. .. "Heat Pipe Design Confirmation Testing", DOE/JPL 1060-27, GEAP-55, September 25, 1979.

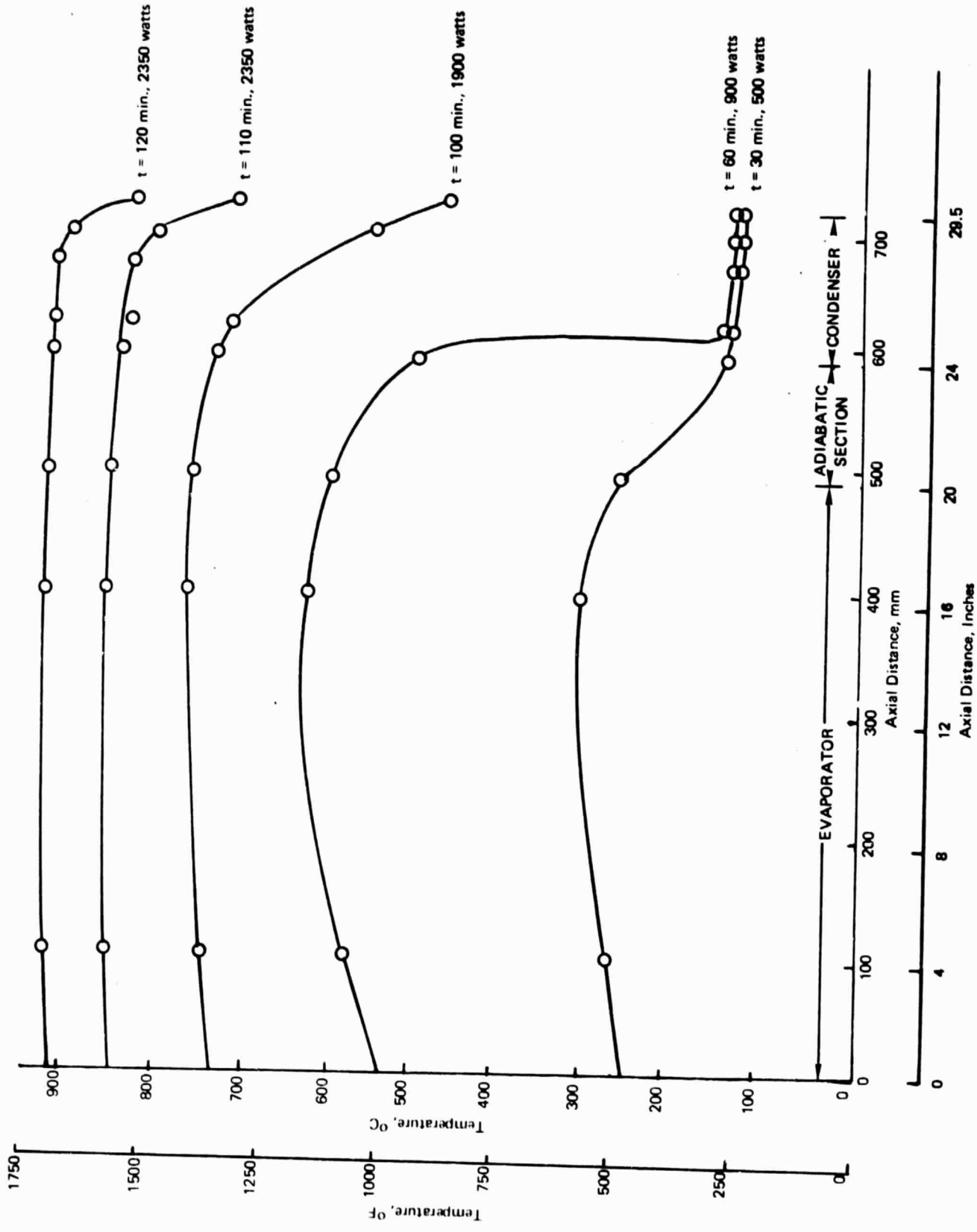

Figure 4-25. Start Up Performance at 10° Inclination

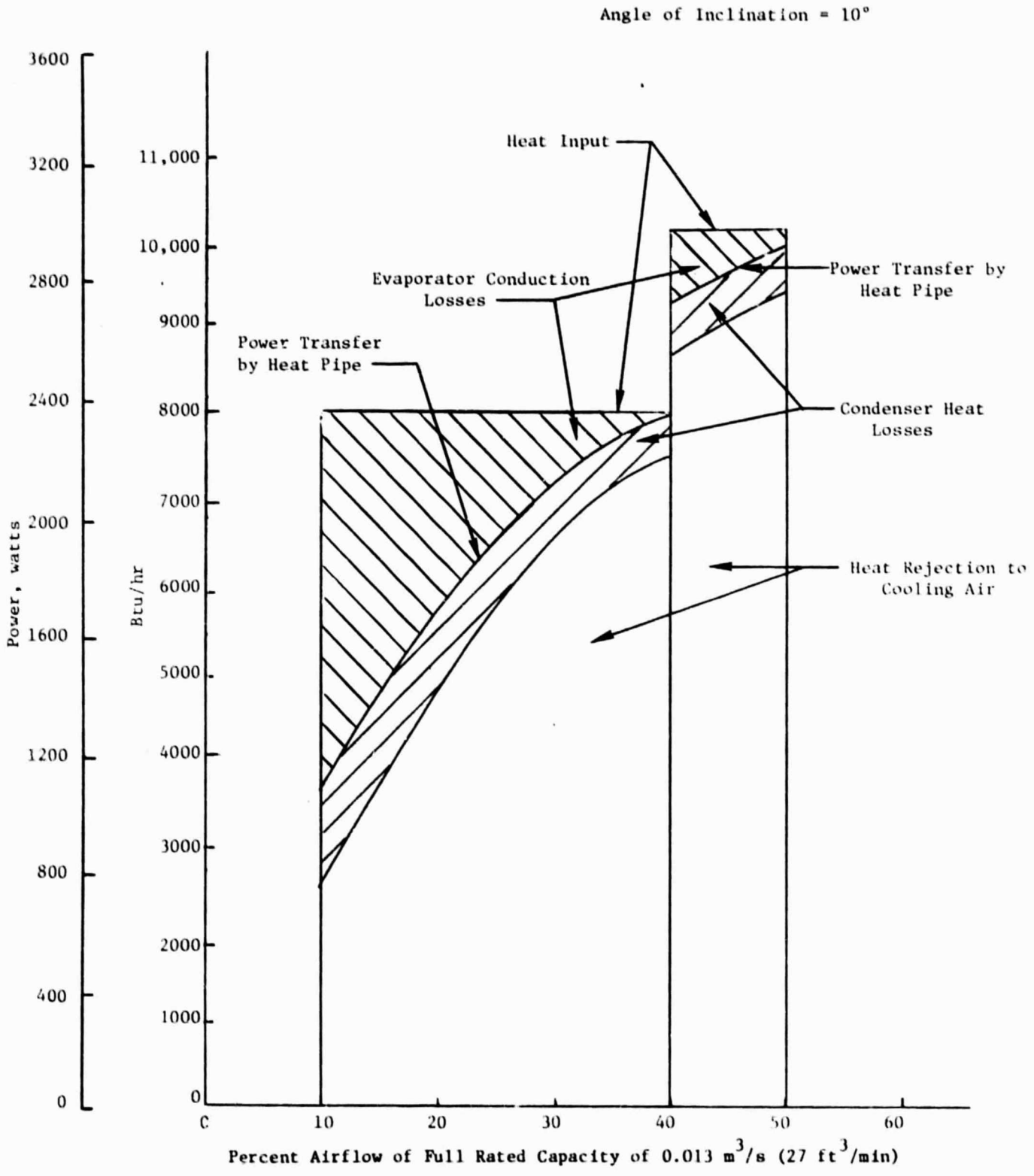

Figure 4-26. Heat Balance in Test Set-up for Heat Pipe #1

7. Easy Fluid Wicking Tests

a. Purpose and Scope. The wicking experiments undertaken in this study were intended to provide information on the capillary pumping capabilities and the associated flow rates in several stainless steel metal screens and the fibermetals. The experimental results obtained using easy fluids such as ethyl alcohol, methanol, and distilled water would form the basis for the prediction of the wicking capabilities in sodium environment of the potential wicks to be used in the design. The wicking experiments were also performed across joints between the fibermetals and the screens using these easy fluids.

An extensive literature search was conducted as part of the program to determine the extent to which the previous experimental efforts and the test methods could be used with easy fluids to study wicked flow in potential heat pipe experiments. The literature search consisted of general experimental methods used in determining the wicking properties of the stainless steel metal screens and fibermetals. Most of the methods used by prior investigators were utilized in this experimental program.

b. Test Fluids and Materials. The fluids used in the experiments to determine the capillary pumping heights included (1) distilled water, (2) ethanol, (3) methanol and (4) distilled water with a selected wetting agent.

The wicking materials selected for the experiments included (1) the AISI Type 316-304 stainless steel metal screens varying in mesh sizes and number of layers, and (2) several samples of stainless steel fibermetals. These materials were tested in the selected fluids at different stages in the specified cleaning procedures for the heat pipe materials.

c. Test Methods and Results. The capillary pressure experiments in wicks were conducted primarily by two different methods: (1) by observing the maximum wicking heights and (2) by determining the overpressure required to force an air bubble through the wicks.

The equilibrium wicking heights of stainless steel metal screens were measured in the four test fluids. No meaningful data could be obtained with single layer screens because of evaporation from the screens, even under highly controlled humidity conditions. The tests indicated that ethanol and methanol readily wet the stainless steel wick surfaces, but the distilled water formed contact angles in the range of 60°-80° with multiple layers of screens. These contact angles were calculated for the unoxidized metal screens by comparing the wicked heights obtained for unoxidized and oxidized metal screens; the contact angles of the oxidized metal screens were assumed to be zero. Also, the capillary pore radii estimated from the data obtained with distilled water were larger than those estimated from the data with ethanol. The discrepancy is attributed to imperfect wetting associated with distilled water.

The best method found for determining the capillary pore radii of metal screens was to measure the liquid column which could be supported by a single layer screen wick in air. The wicking experiments

were conducted several times in this fashion and produced consistent results in a rapid manner. An alternate method to the test was conducted in which the fluid vapor atmosphere was used; this method gave pore radii higher than the previous method and the experiments were time consuming.

Five Feltmetals®, FM1120, FM1103, FM1104, FM1107 and FM1108, were tested in ethanol and distilled water and the equilibrium wicking heights were measured. The rate of liquid rise vs. the reciprocal of the liquid height, for each wick material, was plotted. From this the permeability and the capillary pore radius were estimated. The capillary pressure measurements were also made on these materials by the above forced air-bubble method.

The estimates of wicking heights in sodium were based upon the experimental data for the materials tested. The capillary radius of the wick was first calculated using the following formula from the experimentally determined capillary pressure assuming complete wetting at a zero fluid contact angle in the easy fluid.

$$r_c = \frac{2\sigma \cos \theta}{\Delta P_c} \text{ (for easy fluids)}$$

where r_c = capillary radius

σ = surface tension

θ = wetting angle

ΔP_c = capillary pressure

The pumping pressure was then calculated for sodium at heat pipe operating temperatures using the above calculated capillary radius, the elevated temperature surface tension of sodium and a zero fluid contact angle. The calculated results indicated that fibermetals can be used to pump the liquid sodium well over the distances required in the secondary heat pipe application. Where smaller wicking heights are required, the capillary pumping of sodium can be very easily accomplished with the metal screens. Pumping heights estimated for screens in sodium ranged from 21 cm. (8.3 in.) for 60 mesh size to 111 cm. (43.7 in.) for 325 mesh size. It is to be noted that these wicking capabilities of the wicks are further aided by gravity return flow of the liquid sodium in most parts in the design of the secondary heat pipe wicking. The fibermetals were used only for radial distribution of the liquid metal where the maximum pumping height requirement was 46 cm (18.1 in.). Estimated wicking heights based on the present experimental data for fibermetals in sodium ranged from 125-196 cm. (49-77 in.). In general, the results indicated that the wicking requirements for TES containment vessel can be easily met with metal screens and fibermetals in liquid sodium. However, it is stressed that the wicking materials must be extremely clean using methods referenced earlier in the preparation of heat pipes.

® Trademark of fibermetals produced by Brunswick Corporation, Deland, Fla.

The analytical and experimental details of these wicking tests are covered more fully under a separate topical report*.

8. Sodium-Sialon Compatibility Tests

a. Purpose and Scope. Two tests of 1000 hours duration were conducted on samples of Sialon immersed in static sodium at elevated temperatures. The purpose of the tests was to indicate, at least in an initial sense, the compatibility of this material as a sensible heat storage material in sodium at temperatures in the 816-982°C (1500-1800°F) range.

b. Test Methods. The Sialon material used was prepared by the Jet Propulsion Laboratory and had the designation "Sintered Type 86 Sialon Poly type 15R". It had been presoaked in a nitrogen atmosphere and sintered in a graphite crucible at 1800°C (3272°F) one half hour without the use of sintering aids. The test sample was a pressed and sintered disc 63 mm (2.5 in.) in diameter and 6 mm (0.25 in.) thick. The material was chalk-like in nature and highly porous as evidenced by its moisture absorption characteristic. Lamination cracking was evident in the piece; cracking had occurred generally parallel to the cold pressed surface.

Four samples 16 x 16 mm (5/8 in. x 5/8 in.) and of random thickness in the pressing direction were dry cut with a jeweler's saw to avoid contamination of the porous material; thickness variations were caused by surface spalling. These specimens were dried overnight under vacuum at 121°C (250°F) and were allowed to cool in vacuum. Dry weights and wet weights, after boiling in distilled water for 15 minutes, were taken for record purposes and to determine the porosity of the material. The calculated porosities of these specimens ranged from 36.5 to 38.3 percent and were higher than appeared justified by later photomicrographs; nevertheless, substantial porosity was confirmed.

The four specimens were then air dried and replaced in the vacuum oven overnight at 121°C (250°F) to remove the retained water. Prior to loading the specimens in their capsules they were heated to 982°C (1800°F) in vacuum and, after cooling in argon, were transferred to the capsule filling facility in sealed, argon filled, polyethylene bags.

Eleven kilograms (25 lbs.) of sodium were procured in a sealed shipping container under a pressurized argon atmosphere. The analysis of this lot of sodium disclosed oxygen and carbon contents of 14 ppm and 36 ppm, respectively, and only a few ppm of other trace elements.

The sodium was transferred into a 305 mm (12 in.) long AISI Type 304 stainless steel tube with a 25 mm (1 in.) OD and 0.5 mm (0.020 in.) wall thickness. Transfer techniques were similar to those described elsewhere for the sodium to be used in filling heat pipes. After cooling of the transfer apparatus, the sample tube, filled with solid sodium, was removed from the apparatus, the ends were sealed with Swagelok fittings and the tube was placed in the inert atmospheric weld chamber.

*Divakaruni, S.M., "Easy Fluid Wicking Tests Related to Solar Receiver Heat Pipes", DOE/JPL 1060-26, GEAEP-53, September 25, 1979.

Stainless steel tubes of 25 mm (1 in.) ID were fabricated into three, 152 mm (6 in.) long capsules with a flat disk GTA welded to form the bottom of each capsule; a fitted disk with a 1.6 mm (0.0625 in.) vent hole was prepared as the top of each capsule. Capsule parts were cleaned, pickled in dilute nitric/hydrochloric acid, vacuum baked at 982°C (1800°F) for one half hour and cooled in vacuum.

The sodium transfer tube, three stainless steel capsules and their tops, and three preweighed Sialon specimens were installed in the inert atmosphere weld chamber with necessary tooling and the chamber was evacuated and back filled with high purity argon for capsule filling purposes. An identified Sialon specimen was placed in the bottom of each of the three serialized capsules. A tubing cutter was used to cut three 38 mm (1.5 in.) long tube sections from the sodium filled transfer tube. One section of tubing containing sodium was inserted inside each capsule, the vented capsule tops were installed on each capsule and GTA welded in place. A short length of stainless steel wire, flattened along one side, was inserted in each capsule vent hole and the area was temporarily sealed with tape.

The final sealing of the capsule was completed in vacuum inside an electron beam welding chamber. The capsules were quickly transferred from the argon atmosphere weld chamber to the EB weld chamber, the sealing tapes were removed from the tops of the capsules and the EB weld chamber door was immediately closed and the system pumped down to a vacuum of 10^{-5} torr. The capsules were held under vacuum for a minimum of 16 hours to completely vent the argon from the capsule. An EB weld seal was affected in the cap vent hole using the flattened wire as filler metal.

The vacuum sealed corrosion test capsules were pressurized under helium at 0.28 MPa (40 psi) and helium leak tested in a vacuum chamber to assure absence of leaks in the capsules.

Capsules were placed on test in an air furnace at 827°C (1520°F) and at 982°C (1800°F) to represent the nominal Stirling engine operating temperature and a 100°C (180°C) sensible heat temperature range above this temperature. The capsules were arranged in a vertical position to assure that the Sialon specimens were submerged in sodium. After 1000 hours of testing the capsules were removed and cooled to room temperature. The flat end caps of the 982°C (1800°F) capsule had bulged and the capsule gave evidence of leakage, indicating the vapor pressure at that temperature was sufficient to deform the capsule cap. The third, standby capsule was placed on test at a lower temperature of 954°C (1750°F) and was intact after a total of 1000 hours of testing.

Because of the porous and relatively weak nature of the Sialon samples, a concern existed that sodium entrapped within the pores of the Sialon would rupture the specimen when reacted with alcohol or water during recovery of the specimen. To avoid this, vacuum distillation was used in an attempt to condense the sodium at the end of the capsule opposite the specimen. A 427°C (800°F) heat source and liquid nitrogen heat sink were used over a 2 hour distillation period. After removal of the heat and continued cooling under liquid nitrogen, the heated end

of the capsule was cooled to room temperature and the capsule was opened with a tube cutter. In spite of this treatment sodium was still evident around the specimens.

The capsule end containing the specimen was filled with hexane to prevent gross oxidation and the sodium was reacted away by slowly adding propanol to initiate and control the rate of reaction. When all evidence of reaction had ceased under high propanol concentrations, the specimen was air dried and heated in vacuum for 1 hour at 538°C (1000°F) to assure the removal of any unreacted sodium.

c. Test Results. The specimen weights were compared before and after sodium exposure. Weight losses in sodium were very small, on the order of 4 percent. Because of the friable nature of the original specimens it is expected that some, if not all, of these weight losses occurred during the leaching and rinsing of the specimens during removal of sodium. These weight losses are considered inconclusive for this reason. The weight gain of the specimen tested in the 982°C (1800°F) test capsule, which leaked, was most likely the result of reaction of the sodium with the specimen and the inability of the solvents to remove these reaction products from the interstices of the Sialon after test.

Metallographic examination of a control specimen and of the specimens exposed at 827°C (1520°F) and at 954°C (1750°F) confirmed the high initial porosity. No significant changes were observed in the microstructures nor were any significant corrosion effects observed at the edges of the specimen exposed to sodium. It was to be expected that the sodium liquid and vapor had penetrated these porous structures much as water had been absorbed in the pretest water absorption measurement.

The corrosion testing of a lot of more densely sintered Sialon with higher strength and resistance to surface friability would provide more meaningful sodium corrosion test experience capable of detecting more subtle corrosion effects, if any. Nevertheless, these initial tests did indicate that significant corrosion should not be expected.

9. Stirling Engine Integration

The heat pipe solar receiver with TES is being considered for integration with a 4 cylinder P40 United Stirling engine and a single cylinder modified Phillips 1-98 type Stirling engine.

a. P40 Engine. Because of the present construction features of the P40 engine, which has a bolted head assembly with some bolts located at the center of the heat exchanger tube array, direct immersion of the heat exchanger tubes into the secondary heat pipe is not possible (the centrally located bolt heads cannot be sealed from the sodium vapor, but must be available for retorquing and disassembly of the balance of the engine from the heater head and regenerators).

To provide access to the heater head bolts it is necessary to duct the sodium vapor to a toroidal chamber surrounding the heat exchanger tubes and to locate the engine farther aft of the secondary TES than would normally be desired. The concept for this integration is shown in

Figures 4-27 and 4-28. Two possible engine arrangements are shown. The first assumes the engine can be run in the inverted position. The second assures oil drainage from the seals into a gravity oil sump. Both provide access to the center heater head bolts but, in the second, this access appears more convenient. Further analysis of this conceptual design and refinement of the structural support concept will be necessary under future work on the design, fabrication and test of a heat pipe solar receiver with TES for the distributed concentrator solar Stirling power system.

b. 1-98 Engine. Initial systems integration effort on this engine was initiated late in the program and involved heat exchanger definition, recommended selection of an electrical generator, structural support concepts for engine-generator, and definition of the weights and center of gravity of the engine-generator components.

Table 4-13 indicates the engineering definition of the modified 1-98 configuration. The heat exchanger tube configuration selected for the TES/heat pipe configuration was limited by the use of helium and an 1800 RPM generator speed. The stroke of the 1-98 engine and the existing rhombic drive were retained in this study; the engine power was increased by enlarging the piston bore. Note that the heat exchanger definition for this 20 kW_e Stirling power conversion system is different from that used in the earlier conceptual design.

Since the alternator represents a significant portion of the total weight, a significant effort was made to select the most appropriate unit. Contact with more than twenty alternator manufacturers was made to identify their present product line and their advanced design and fabrication capabilities. The units which are commercially available have been designed for high shock and heavy duty service for an industrial application; generally, they have not been designed using size and weight as constraints. Since these units are produced in a cost competitive environment, the use of low weight materials is precluded, and efficiencies are nominally low. An alternator designed specifically for a solar power system application could be manufactured with a much smaller external envelope, lighter weight and higher efficiency; however, costs would be higher. Specially fabricated water cooled alternators are recommended for later prototype developments since it is felt that higher manufacturing costs could be partly recovered in cost savings realized through lighter structural members and simpler interfacing with the engine.

Initial generator choices were limited to commercially available machines deliverable within 16 weeks. As indicated in the manufacturer's data, Table 4-14, a synchronous alternator is heavier, less efficient and more expensive than a comparably rated induction alternator.

The Stirling engine adds approximately 127 kg (280 lbs) to the above induction generator weight of 93 kg (205 lbs) for a total of 220 kg (485 lbs). This is heavier than the weight allowed in the earlier conceptual design, but generator weight reductions are possible as indicated above. The CG of the engine-generator assembly is located less than eight inches off the centerline of the receiver/TES/engine along the axial direction of the generator; this imposes a circumferential torque on the

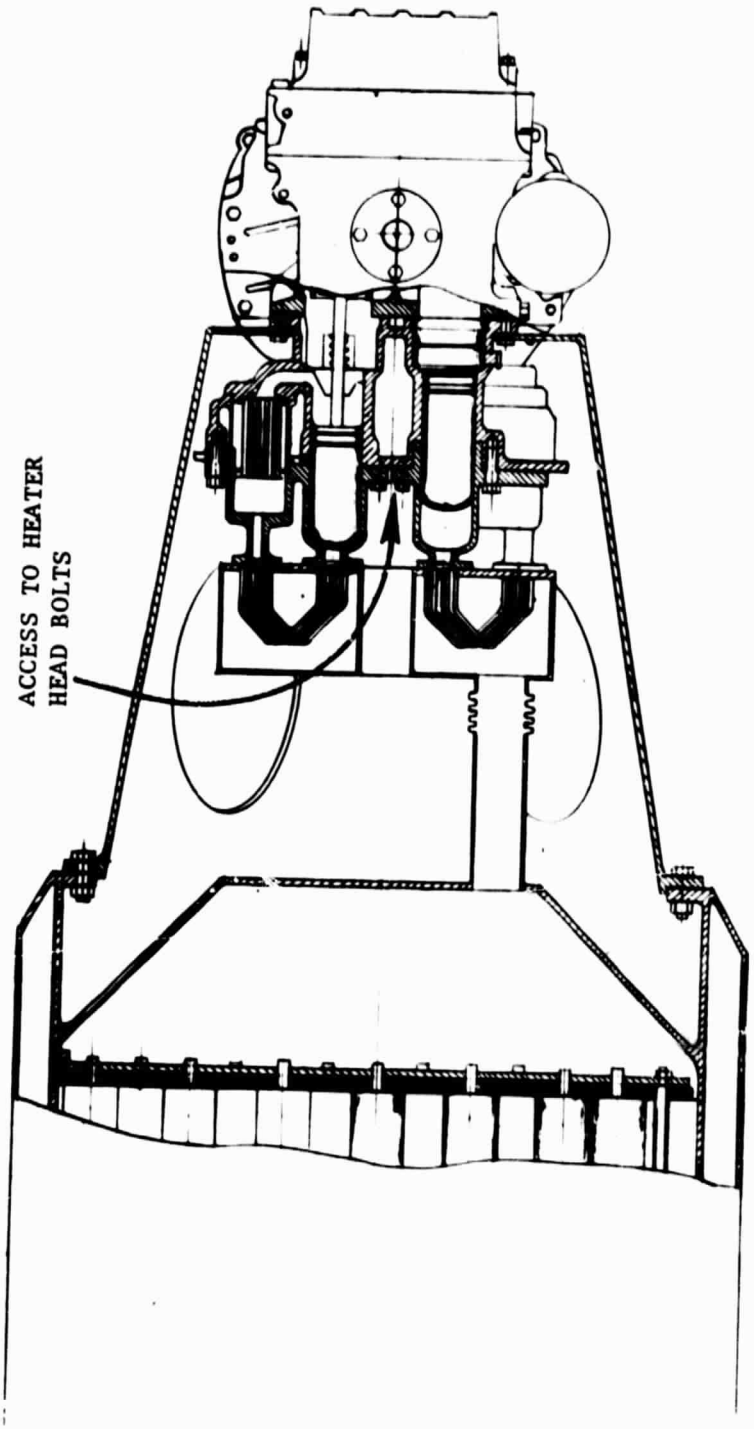

Figure 4-27. P40 Engine-Generator Integration with Heat Pipe Solar Receiver/ TES Subsystem (Engine Arrangement Does Not Permit Gravity Drain from the Oil Seals)

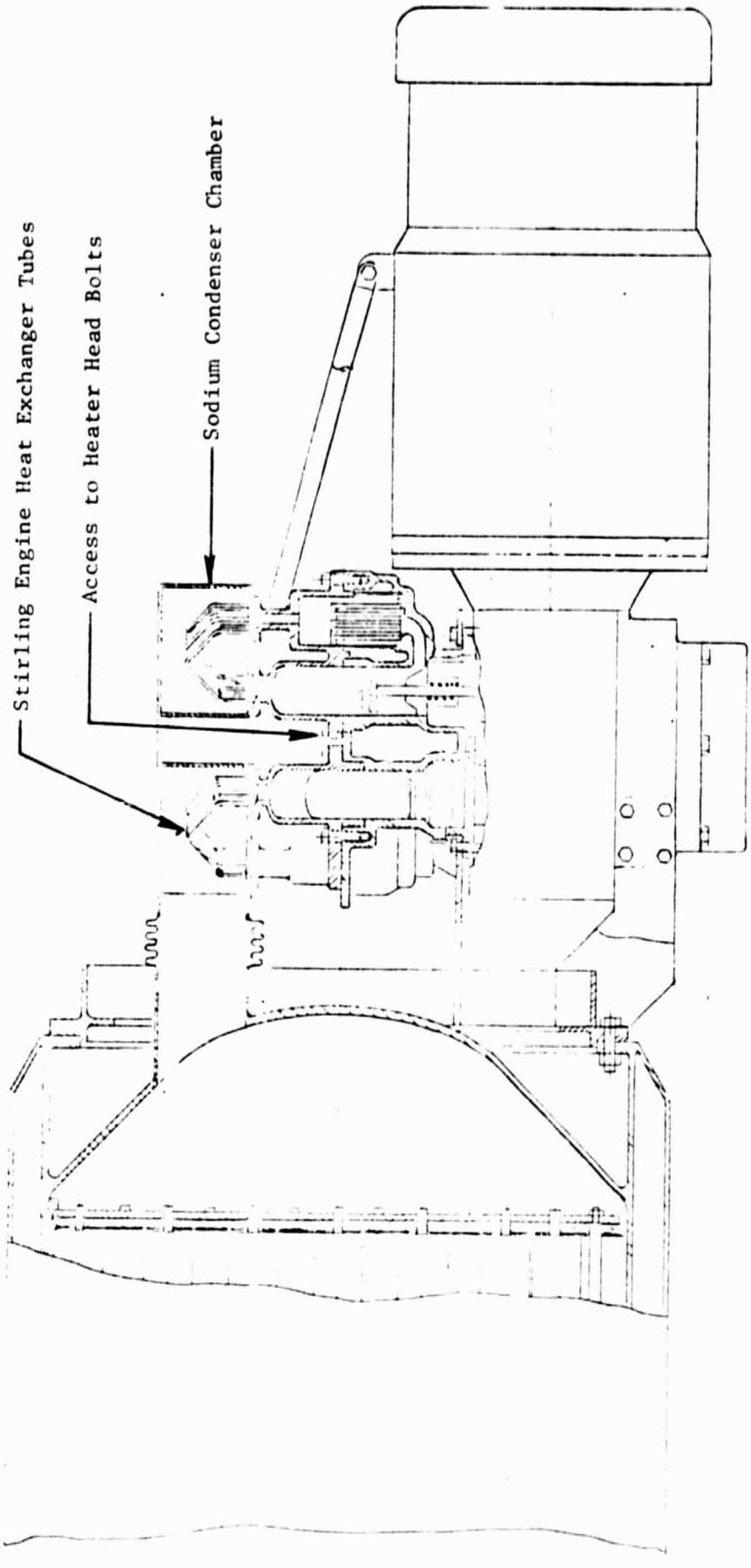

Figure 4-28. P40 Engine-Generator Integration With Heat Pipe Solar Receiver/TES Subsystem (Engine Arrangement Permits Gravity Drain From Oil Seals)

Table 4-13. Modified 1-98 Stirling Engine Configurations

Parameter	TES/Heat Pipe Config.	Direct Insolation
Nominal Electric Power Output	20 kW	
Operating Speed	1800 RPM	
Working Fluid Pressure		
- Mean, Atmos.	210	
- Cycle Variations, Atmos.	+66.6/-53.9	
Engine Stroke	28.9 mm (1.14 in.)	
Hot Side Metal Temperature (Max.)	825°F (1517°F)	
Coolant Water Temperature	65.5°C (150°F)	
Working Fluid	Helium	
Hot Side Gas Temperature	730°F (1346°F)	
Engine Bore	100 mm (3.937 in.)	
Swept Volume	227.4 cm^3 (13.88 $in.^3$)	
Void Volume	452.7 cm^3 (27.625 $in.^3$)	
Number of Regenerators	6	
Number of Heater Tubes	36	72
Inside Diameter	3.4 mm (0.132 in.)	2.9 mm (0.115 in.)
Length - Each	368 mm (14.5 in.)	238 mm (9.37 in.)
Pressure Drop	67.6 kPa (9.8 psi)	37.2 kPa (6.4 psi)
Method of Tube Attachment	Weld	Braze

Table 4-14. Generator Characteristics

Type	Power	Full Load Efficiency	Weight kg (lbs.)	Cost Factor	Size
Synchronous 1800 RPM 0.8 power factor	20 KW	90%	159 (350)	2.25	324 Frame
Induction* 1800 RPM 0.8 power factor	20 KW	91%	93 (205)	1	284 Frame

*Can be motored to start engine

engine-generator to receiver/TES mounting structure with the receiver in the horizontal position and a bending moment with the receiver in the vertical position. The integration of the modified 1-98 Stirling engine and its generator with the receiver/TES unit is shown typically in Figure 4-29. The heat exchanger tubes are immersed directly into the sodium vapor within the secondary, TES heat pipe and seal welded at a conical flange to complete closure of the TES sodium vapor space. Only axial loads are supported by this conical flange, which basically controls the axial position of the engine-generator. Radial and torsional loads are supported by struts at a transverse plane through the CG of the engine-generator; slotted clevis load connectors at this position allow for differential axial thermal expansion of the solar receiver and engine-generator. These load connectors also support radial and torsional loads. It may be desirable, later, to relocate these mounting connectors at an off-axis position such that the connectors are in the plane of the engine-generator CG in the axial and transverse planes in order to reduce bending moments on the structure while the axis of the receiver/TES/engine moves from horizontal towards the vertical direction.

Other operating integration requirements are discussed under Section VII-E.

C-2

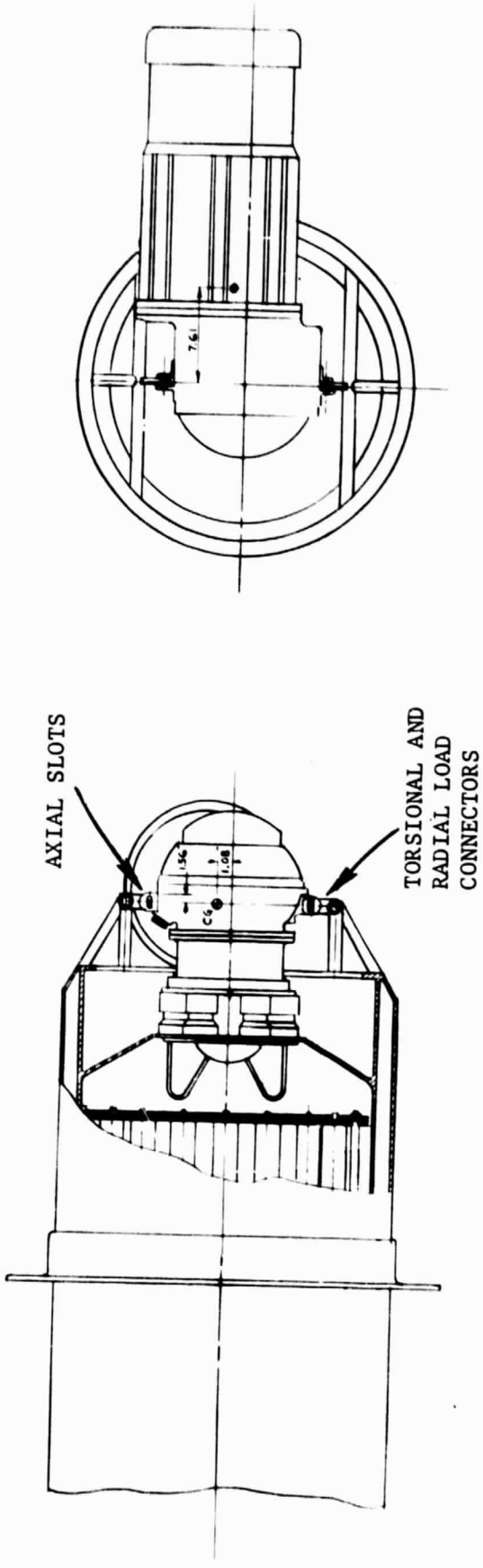

Figure 4-29. Phillips 1-98 Stirling Engine Interface with the HPSR/TES Subsystem

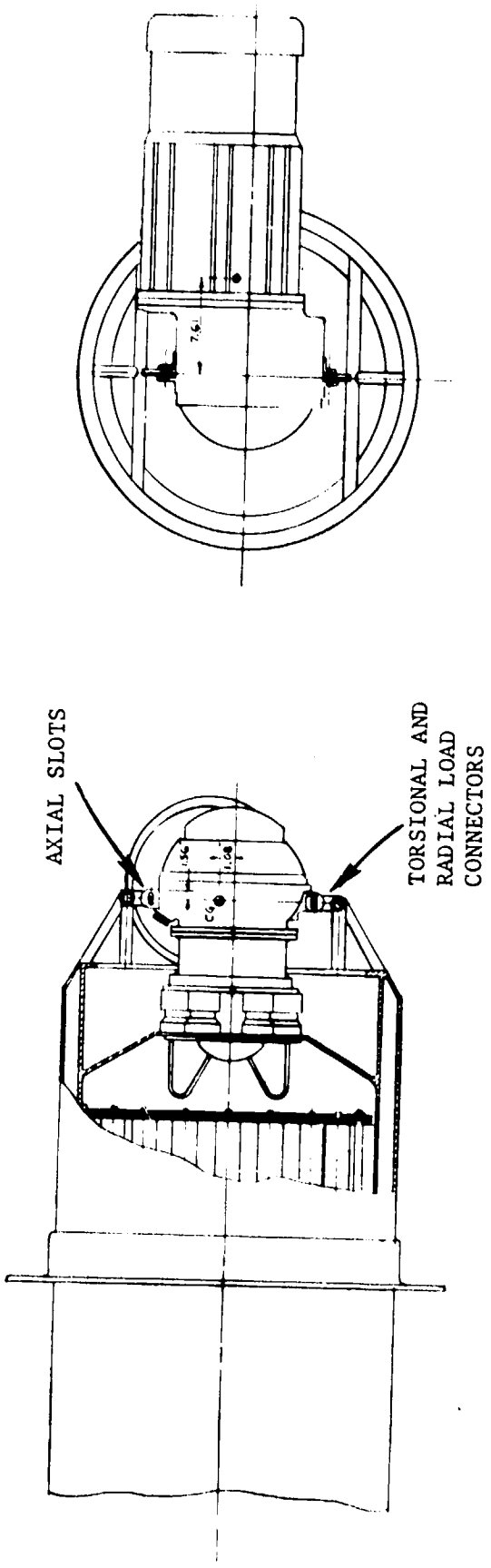

Figure 4-29. Phillips 1-98 Stirling Engine Interface with the HPSR/TES Subsystem

SECTION V

LIQUID METAL PUMPED LOOP SYSTEM

A. CONCEPTUAL DESIGN OF THE PUMPED LOOP SYSTEM

1. Design Approach

The design was based upon a single concentrator pumped loop system with a liquid metal cooled receiver located at the focal point and the TES Stirling engine heat exchanger, power conversion systems, EM pump and control valves located behind the concentrator. This arrangement was selected since alternatives were not as attractive. Mounting the entire system at the focal point would require substantial mass, and the thermal transport over these local short distances could be more effectively accomplished by heat pipes. Locating the TES and power conversion on the ground at the concentrator or at a central location serving several concentrators involved unacceptable heat losses and required the disadvantageous use of flexible bellows. By locating the TES, power conversion system, pump and control valves behind the concentrator, these disadvantages were minimized or avoided; greater TES weights and storage periods could eventually be accommodated behind the concentrator and the weight of these components could be used to offset some of the counterweights required at the rear side of the concentrator which are otherwise needed to counterbalance the receiver weight and its moment. This single concentrator liquid metal transport system layout is shown in Figure 5-1.

A single phase pumped loop rather than a boiling condensing loop was selected. This avoided the larger pressure drops, possible boiler instability and hot spot problems in a system operating at various pumped heads, boiler inclination angles and varying power input levels.

Two phase pumped loop power systems are best suited for steady state operation. A point focus solar power system must, by the nature of the power source, be a dynamic system, much like an automobile engine. For this purpose, a single phase system is better suited.

The single phase loop used electromagnetically pumped liquid sodium. Such systems operate most effectively with relatively large mass flows and a small pressure rise compared to mechanical pumps of similar power.

For purposes of making a direct cost comparison with the focus mounted heat pipe solar receiver, the pumped loop TES storage period and TES general design concept was similar to that for the heat pipe solar receiver. The employment of vacuum insulation resulted in the EM pump, TES control valves, Stirling engine heat exchanger, and all piping being contained within a vacuum tank; the long run of piping to and from the

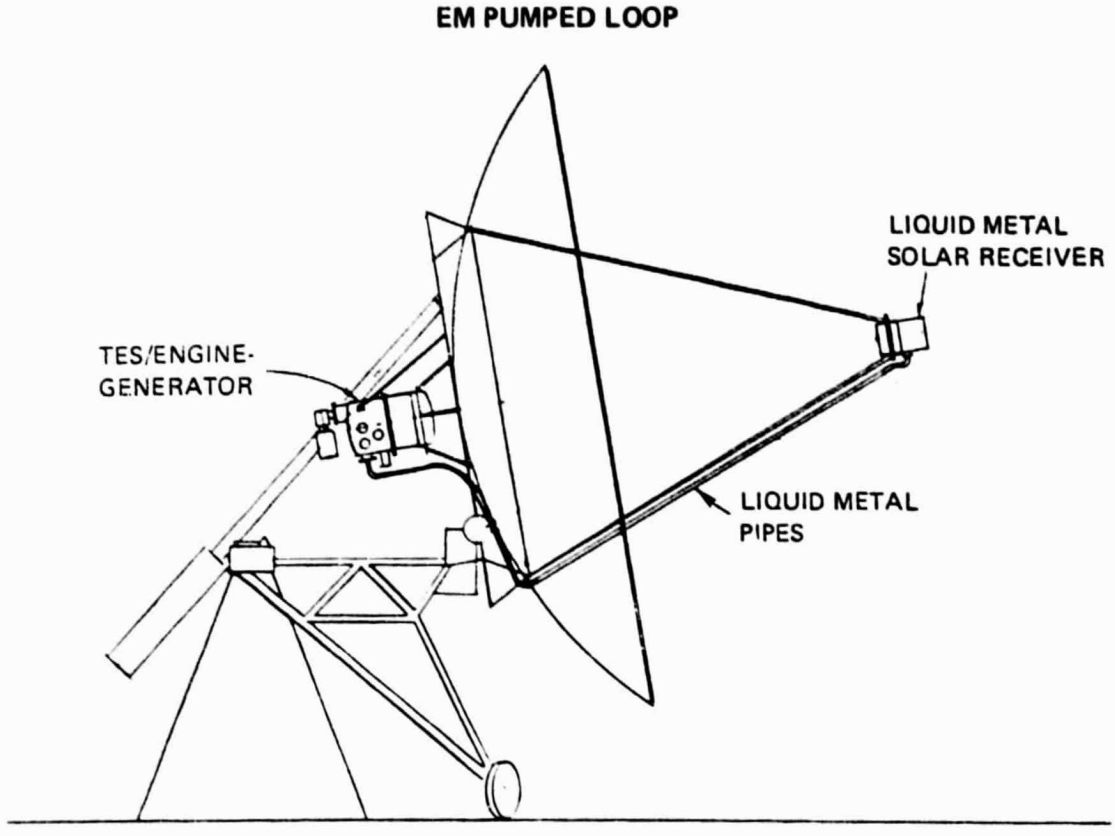

Figure 5-1. Pumped Loop Single Concentrator System Layout

focal point solar receiver were not vacuum insulated.

The use of flowing liquid metal for heat transfer required a determination of the mass flow and ΔT necessary to transport the required power, the sizing of pipes, the selection and arrangement of valves and the use of controls for regulating the performance of the system in various operating modes, the thermal analysis and mechanical conceptual design of the various components, the analysis of thermal losses and a determination of the weight and cost of the system.

2. Thermal Analysis

a. Solar Receiver. The solar receiver cavity and impinging flux distribution was assumed to be similar to that for the heat pipe receiver/TES system. Relatively high convective heat transfer coefficients for the liquid sodium were deemed to be sufficient to transfer the heat to the sodium without difficulty at the flow velocities in the required design. Since the planned design would have two concentric cylinders with the sodium flowing between them, turbulence inducers could be added to the flow if necessary to improve the single phase heat transfer.

b. Pumped Loop. Since the pump pressure requirements would vary as the reciprocal of the fourth power of the pipe diameter, it was desirable to have pipe diameters as large as possible to minimize the pump pressure and power requirements. Without a layout of the plumbing it was difficult to predict the actual pressure loss. Pipe diameter could not be increased without limit because the weight of the system would become too large. Experience with the heat pipe focal mounted TES system indicated that the system had to be well insulated. If vacuum insulation were to be used, the size of containment vessels could not be made too large from an elastic stability viewpoint.

In order to eliminate one of the vacuum vessels of a double walled vacuum insulation system, it was decided that the TES, pump, piping, valves and Stirling engine would operate in and be contained by a single large vacuum chamber. Within this chamber there would be sufficient insulation so that the wall of the chamber would operate at a temperature appropriate for mild steel. To minimize outer surface area, the vacuum cylinder would have a L/D ratio of about one. A 101.6 cm (40 in.) diameter cylinder appeared to have enough room for the TES and piping and also would be elastically stable with a reasonable wall thickness.

Because of the above constraints and after a consideration of sodium mass flow, ΔT and pressure drop, a pipe diameter of about one inch appeared initially acceptable. One inch diameter tubing was selected because it is a standard size and because information was available on the characteristics and costs of liquid metal valves for that tube diameter.

After later completing the plumbing layout it appeared that a more optimum pipe and valve diameter of 32 mm (1.25 in.) would be possible with some reduction in pumping power or a decrease in system ΔT. These changes would not significantly change the weight, cost and performance to a significant degree and this further design optimization was not pursued.

c. Thermal Energy Storage. The thermal design basis of the TES containers was identical with that used previously for the heat pipe solar receiver. The cans were spaced farther apart to allow for the necessary liquid metal flow required to meet convective flow heat transfer conditions.

d. Stirling Engine Heat Exchangers. In the Stirling heat exchanger the liquid sodium flows over the heat exchanger tubes again transferring heat by convective flow heat transfer. As with the receiver, relatively large heat transfer coefficients could transfer the heat to the Stirling engine heat exchanger tubes. If this later proved insufficient, turbulence inducers could be added.

e. Thermal Losses. This system, for comparability reasons, was designed with thermal losses similar to those for the heat pipe solar receiver/TES system. As with the heat pipe system, 6.9 kW_t would be lost from the receiver. The other losses were 1.1 kW_t from the TES/engine-generator unit mounted on the dish support ring and approximately 0.8 kW_t from the hot fluid transfer pipes connecting the receiver to the TES/engine-generator unit behind the concentrator. When compared to the focal mounted heat pipe TES system the total heat losses were only 0.2 kW_t greater.

3. System Engineering Definition

The definition of the system was guided by the above considerations regarding selection, location and sizes of components, system fluid mass flow, ΔT, and heat transfer considerations and the necessity for a regulated control system incorporating six valves and four unique modes of operation.

The piping schematic for liquid sodium control in these four operating modes is shown in Figure 5-2. In the first case heat is being transferred between the receiver and the Stirling engine; in the second, between the TES and Stirling engine; in the third, between the receiver and TES; and in the fourth between all three components, receiver, TES and Stirling engine. An interesting feature of this design is that only valves three and four need have variable flow capability. The other four valves need only be fully open or fully closed.

Table 5-1 defines the basic engineering parameters used to define the thermal performance of the system and to support the basis for the mechanical design. The mass flow of the loop, the loop ΔT at various operating power levels, the system ΔP and the definition of the TES system are shown. The operating temperatures of the loop components as a result of the stacking of the maximum and minimum ΔT's within the system are given in Table 5-2. A characteristic of the sensible heat pumped loop is that the accumulated temperature drop results in a much wider range of component operating temperatures than for the heat pipe system. It is possible that the receiver would be required to operate at 938°C (1720°F) while providing peak power directly to the TES. The Stirling engine temperature could fluctuate from 769°C (1416°F) to 799°C (1470°F).

A. Operating Mode with All Heat Flow Directed to Stirling Engine

B. Heat to Stirling Engine Supplied by TES Alone

C. Operating Mode for Charging the TES Alone

D. Mixed Operating Mode for Simultaneously Charging the TES and Operating the Stirling Engine

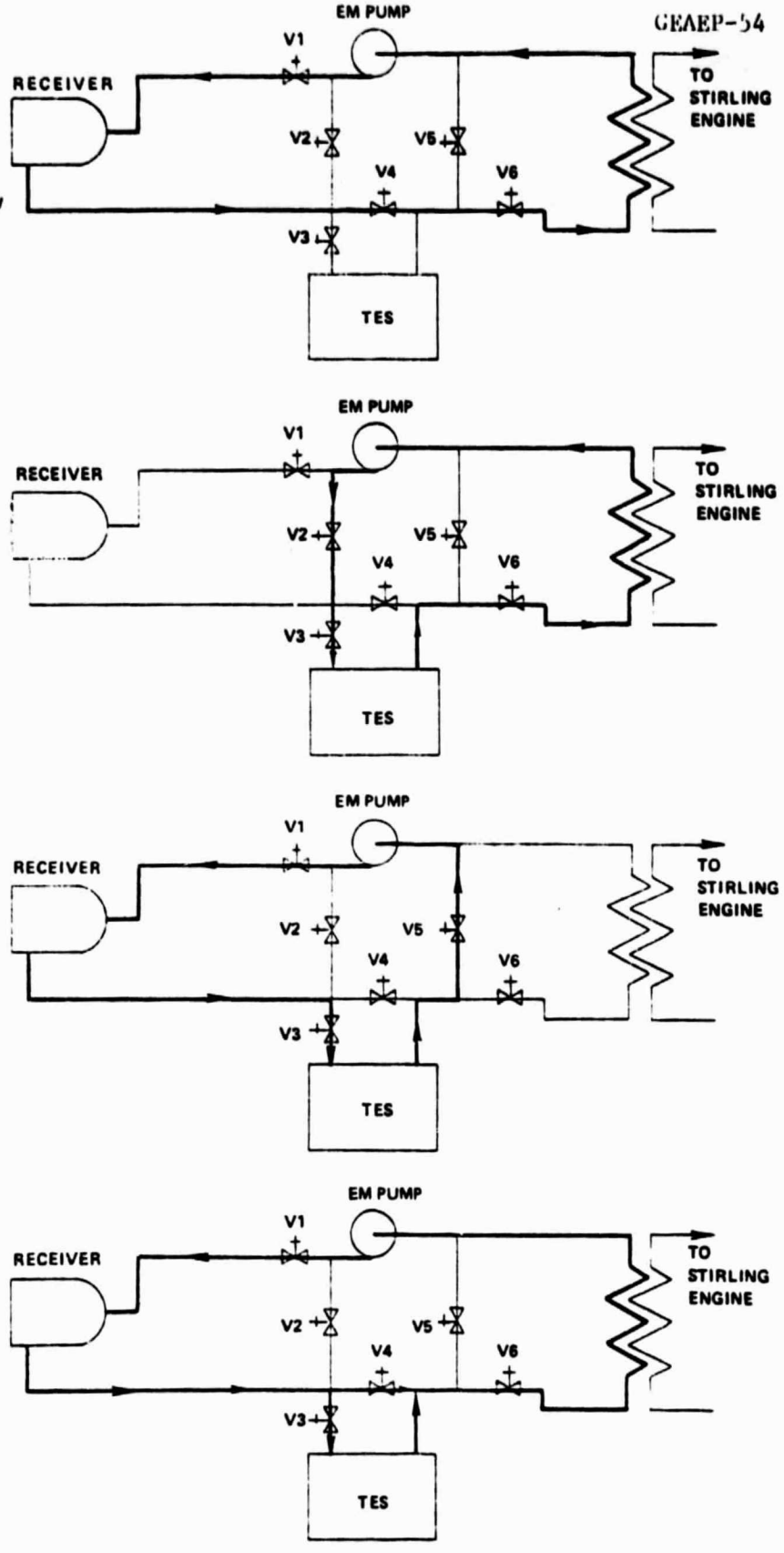

Figure 5-2. EM Pumped Loop Flow Schematic

Table 5-1. Pumped Loop Engineering Definition

Type of Salt	LiF
Weight of Salt	359 kg (792 lbs.)
Melting Temperature of the Salt	857°C (1575°F)
Number of Salt Containers	140
Diameter of Salt Containers	48 mm (1.9 in.)
Sodium Pipe Diameter	25 mm (1.0 in.)
Sodium Mass Flow (Nominal)	0.7 kg/s (15 gpm)
Sensible Heat Temperature Difference for Sodium To Deliver:	
52.5 kW_t	58°C (104°F)
62.1 kW_t	70°C (126°F)
Vacuum Chamber Diameter	1015 mm (40 in.)
Vacuum Chamber Thickness	6 mm (0.24 in.)
Number of Valves	6
Electromagnetic Pump*	
Weight	130 kg (287 lbs.)
Efficiency**	8%
Pressure Rise	27.6 kPa (4 psi)

*Engineering estimates only.

**Pump Power = 324 W plus possible extra power to cool the pump.

Table 5-2. Pumped Loop Operating Temperatures

LiF Melting Point	857°C (1575°F)
Sodium ΔT for 62.1 kW_t at 0.7 kg/sec	73°C (131°F)
Sodium ΔT for 52.5 kW_t at 0.7 kg/sec	58°C (104°F)
LiF ΔT for 52.5 kW_t at 95% Solidification	30°C (54°F)
LiF ΔT followed for Superheat	8°C (14°F)
Maximum Sodium Temperature in Receiver:	
(857°C + 8°C + 73°C)(At Peak Storage Temp.)	938°C (1720°F)
Minimum Sodium Temperature in Stirling Heat Exchanger:	
(857°C - 30°C - 58°C)(At Storage Discharge)	769°C (1416°F)
Normal Sodium Temperature in Stirling Heat Exchanger:	
(857°C - 58°C)(Storage Charged; Heat Supplied by Receiver)	799°C (1470°F)

4. Mechanical Design

Figure 5-3 shows a layout of the mechanical design of the TES/engine-generator unit of the pumped loop system. In this design the hot TES chamber is isolated thermally from the outer steel cylinder by non-metallic thermal bushings. Thermal expansion is accommodated by two telescoping sleeves at the generator end and a large pin at the other end. The Stirling engine exchanger is separate from the TES chamber and is free to grow thermally being only supported at one point.

A typical remotely actuated valve is shown to scale. Six such valves and their actuators extend into ports around the main vacuum cylinder.

The main vacuum chamber itself is bolted together in the middle during manufacture. Approximately one foot of fibrous insulation which surrounds the outer vacuum chamber is not shown. The temperature of the outer vacuum chamber shell operates at about 538°C (1000°F).

Figure 5-4 shows a schematic of the receiver. The aperture and depth are the same as that for the receiver for the heat pipe heat transport TES system. The receiver employs vacuum insulation just as does the heat pipe solar receiver system.

The two pipes that connect the receiver to the TES/engine-generator unit are insulated with standard high temperature insulation and are contained within concentric evacuated tubes to minimize both heat losses and shadowing.

Not shown in either drawing are the many bellows joints that would be necessary to accommodate the large thermal expansion of the pipes. Also not shown are the trace heaters on long pipe runs. These heaters would be necessary either to keep the sodium from freezing in the pipes when the unit first came on in the morning or to melt the sodium in the pipes prior to startup from a cold condition.

5. Weight Analysis

In preparation for costing the pumped loop system, an analysis of the component weights was made. The results of that analysis are presented in Table 5-3. Compared to the heat pipe solar receiver system, a smaller fraction of the total weight is devoted to actual thermal energy storage. The total weight of the EM pumped system is 3,550 kg compared with 1488 kg for the heat pipe TES system, a 239 percent increase. The reason for the large weight increase in the pumped loop system is evident in the compactness of the closely integrated focal mounted heat pipe solar receiver. This is in contrast to the dispersed nature of the pumped loop with its added weight in long pipe runs, heavy EM pump valves, larger TES chamber and large liquid metal inventory which are not found in the heat pipe system.

If a gas lift pump were used in lieu of the EM pump, which weighs approximately 136 kg (300 lb), the total system weight would be increased by 984 kg (2164 lb). The 1120 kg (2464 lb) weight of the gas lift pump

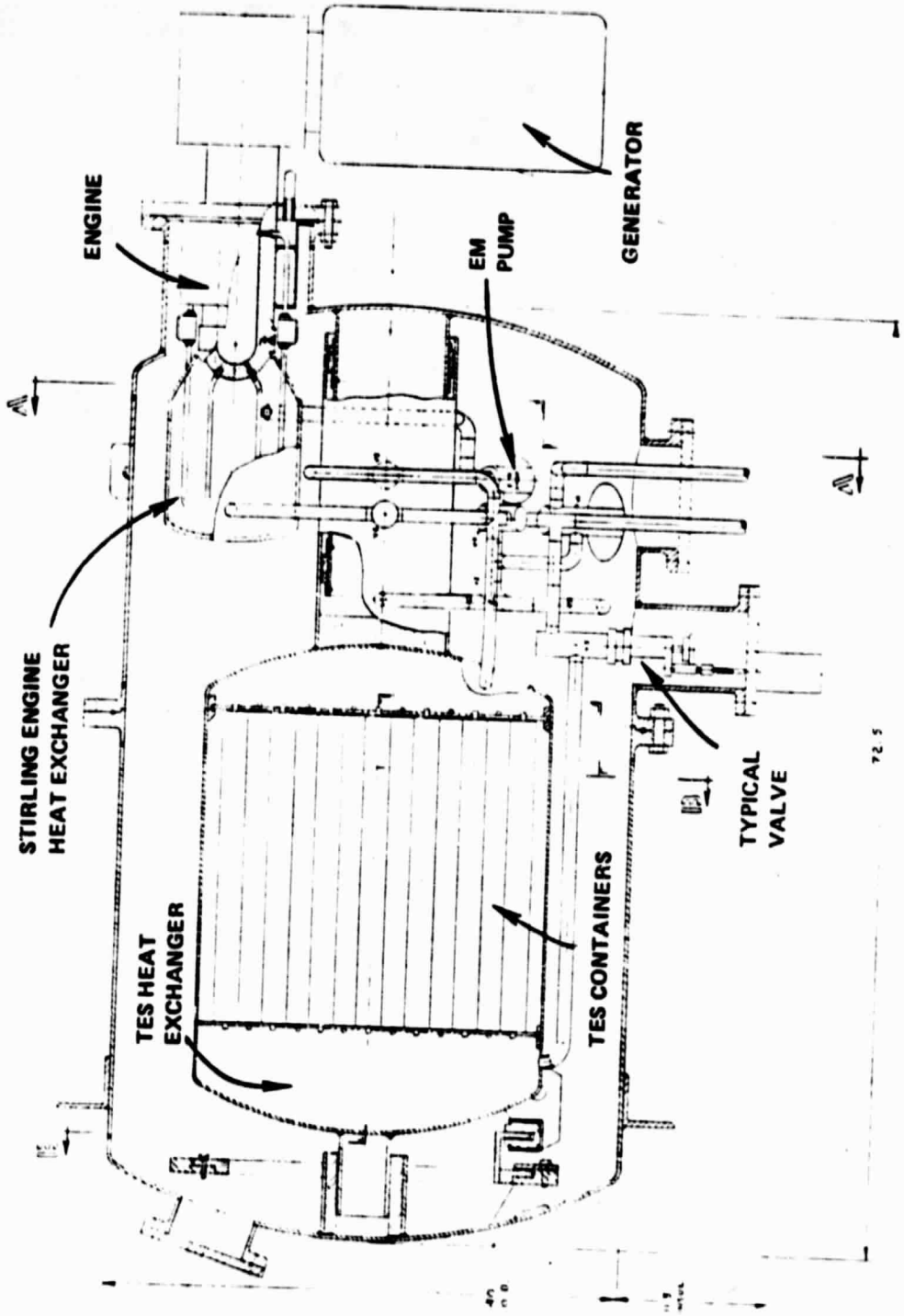

Figure 5-3. Single Concentrator Pumped Loop TES/ Engine-Generator Layout

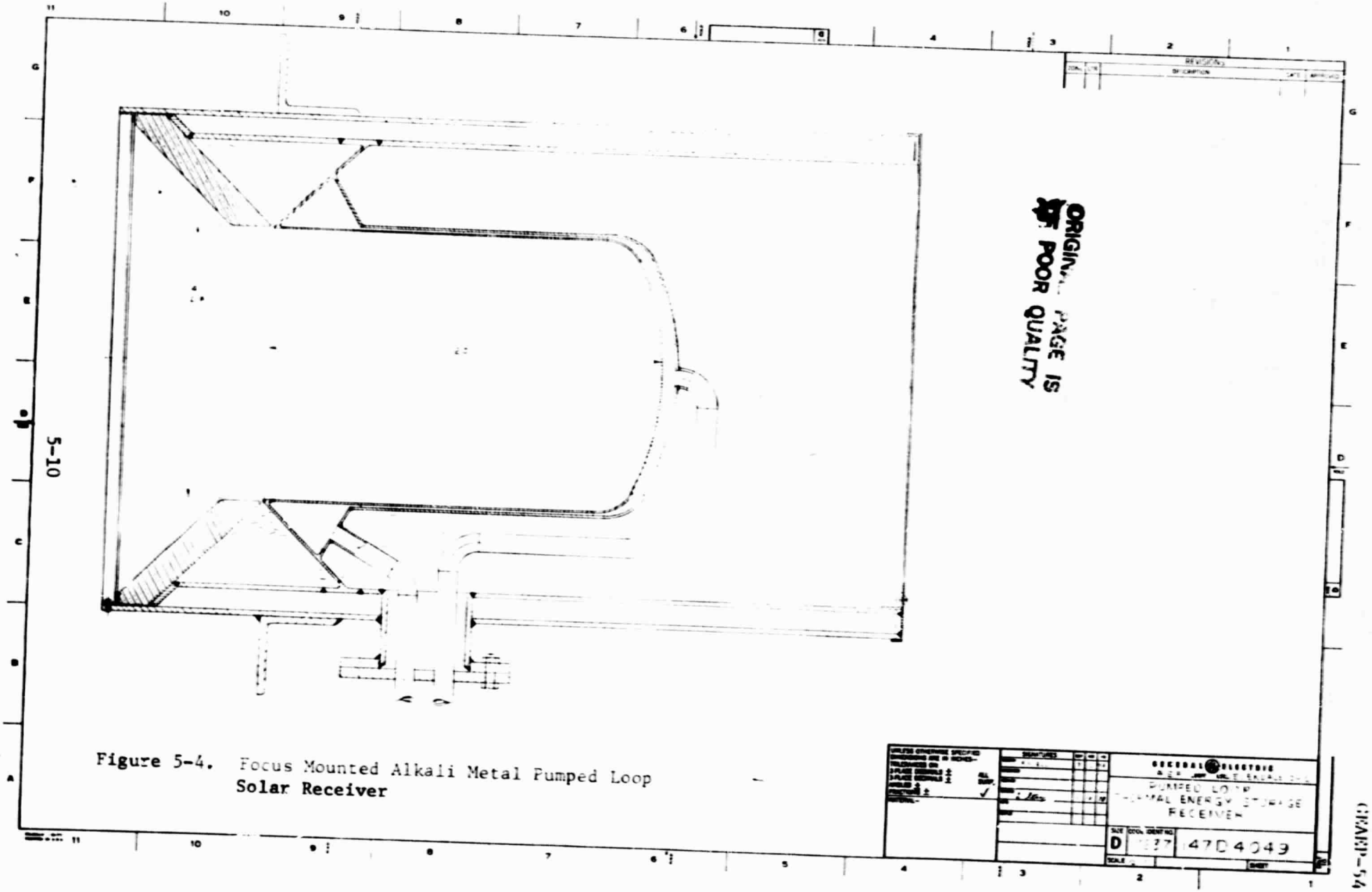

Figure 5-4. Focus Mounted Alkali Metal Pumped Loop **Solar Receiver**

Table 5-3. Mass Summary Table

	Mass kg (lb)	% of Total Wt.
Receiver	422 (930)	13
TES Salt	359 (791)	11
TES Cans	79 (174)	2
Piping and Valves	32 (70)	1
Vacuum Changer	640 (1411)	19
Exterior Insulation	430 (948)	13
TES Area Structure, Insulation & EM Pump*	657 (1448)	20
Sodium	218 (481)	7
Insulated Pipe Between Receiver and TES	500 (1102)	15
Total	3337 (7355)	
Stirling Engine (Est.)	147 (324)	
Generator (Est.)	68 (150)	
Total (With EM Pump)	3550 (7829)	
Total (With Gas Lift Pump)	4534 (9996)	

*EM pump weighs 136 kg (300 lbs.)
Gas-lift pump components without recuperator weighs 1120 kg (2464 lbs.).

includes the weights of the large diameter pipe and insulation along the length of the concentrator strut, the gas-sodium separators, inert gas recirculating pump, inert gas injector and increased sodium inventory.

B. DESIGN ASSESSMENT OF THE PUMPED LOOP SYSTEM

In addition to the specific component assessments discussed below, the pumped loop has several attributes worthy of note.

First, the pumped loop system offers the opportunity for significantly increasing the TES duration period by installing the additional storage material behind the concentrator where larger masses and volumes can be accommodated.

Second, a positive control of the heat flow is required with the need for sensors, control elements and valves.

Third, pumping power and the weight of pumps, pipe valves and liquid metal inventory add significant weight and cost.

Fourth, the use of a single phase liquid metal system for thermal transport requires mass flow and ΔT which inhibit system performance because the components operate over a wider temperature range affecting system efficiency and materials design capabilities.

1. Gas Lift Pump Assessment

A gas lift pump operates on the principal of fluid density differentials in the rising and descending legs of a vertically arrayed fluid loop. A gas is introduced in the lower portion of the rising leg of a fluid loop and reduces the density of that fluid. The gas is separated in a chamber at the top of the loop and recirculated by a gas compressor to the injection point. The system is basically simple in principle. The applicability of such a pump in liquid metal pumped loop applications for distributed concentrator solar systems is covered in more detail in Appendix A. The low density vertical rise portion of the gas lift pump in this case would be from the lowest edge of the concentrator dish to the focal point, a vertical distance of approximately 5.9 meters when the dish is at 10° elevation.

In terms of efficiency, the gas lift pump is comparable with the electromagnetic pump. The efficiency improves somewhat with the addition of a recuperator used to recover heat from the recirculating gas which must be recompressed at temperatures lower than the liquid metal temperature.

In terms of weight and cost, however, the gas lift pump is much less appealing. The gas lift pump would add some 984 kg to the total system weight and have an added materials cost of around $8300 excluding a gas recuperator. The gas lift pump adds a large diameter high temperature pipe to the system which must be insulated.

There are some technical questions that also remain about the gas lift pump. To avoid the need for flexible joints for pipes, the pump

must be attached to the dish itself. Questions then arise as to the ability of the pump to work at various angles with sufficient flow to keep the temperature rise within desired limits. Though the gas lift pump would use less electric power than the electromagnetic pump, the additional thermal losses through the insulation, separation, and recuperation systems result in an overall loss that is slightly greater than that of the electromagnetic pump.

Analysis indicates that the gas lift pump is an interesting approach to liquid metal pumping but it is associated with efficiency losses from 3.4 to 9 percent. Since the minimum loss of 3.4 percent represents the loss associated with ideal recuperation, such ideal recuperation is probably not economically feasible; thus the 9 percent loss would probably be a more reasonable one.

Further work would be required to answer more precisely the question of the relative cost of electricity to accommodate EM pump efficiencies versus the cost of a gas recuperator to improve gas lift pump efficiencies. Other questions also remain regarding the stability of gas-sodium bi-fluids contained in low angle inclined gas pump risers, the efficiency of separating large quantities of sodium and inert gases and the possible erosion and corrosion problems in pumping inert gases containing some sodium droplets. It appears that a gas lift pump would require more extensive development than an electromagnetic pump. Furthermore, the gas lift pump appears to have some fundamental characteristics associated with it such as size, weight, and thermal losses; these would tend to keep it less effective than an electromagnetic pump after similar periods of development.

2. EM Pump Assessment

Pumps for liquid metal service at a nominal 1100-1300°K (1500-1900°F) are not currently available, but represent an area of required development. Although liquid metal loops in this temperature range have been operated successfully, the usual practice has been to put the pumps in a relatively cold leg of the loop. In the present system, no such cold leg exists, and pumps must be designed for at least 1100°K (1500°F) service. This does not imply that such equipment cannot be developed, only that a development program will be required.

Both electromagnetic and mechanical pumps were considered. EM pumps have the decided advantage of requiring no rotating seals. It is probable that the mass-produced and unattended operation requirements of the overall system will eliminate rotating seals from consideration. Thus, the prime candidate for this application is the EM pump.

Estimates of the weight and efficiency of EM pumps were obtained. These showed weights of 50-250 kg (100-600 lb) depending on efficiency and design voltage, at efficiencies between 8 and 12 percent.

An assessment of the EM pump requirements and the available EM pumps was made by General Electric's Advanced Reactor Systems Department. The pump required for the solar power application was similar to a pump that was designed and fabricated for the Fast Flux Test facility

at Hanford, Washington. The pump is a helical induction electromagnetic type and is shown in Figure 5-5.

One very strong influence in selecting this pump is the cost of the stator. While an annular linear induction pump would be lighter and more efficient, its production costs would be on the order of 10 times that of the chosen pump due to lack of automated machinery. This kind of pump will have to be reconsidered if the quantities envisioned warrant mass production techniques.

The electromagnetic pump would be cooled by an air blower. Class H insulation, rated at 200°C (392°F),would be used for the stator windings and about 300 to 400 cfm of air would be required to cool the pump depending on the ambient air temperatures. With a pump duct carrying sodium at maximum temperatures near 857°C (1575°F) and a pump stator operating near 200°C (392°F),the pumping efficiencies will be low.

Performance and characteristics for the proposed low temperature statored EM pump are presented in Table 5-4.

Higher temperature EM pump stators designed to minimize heat losses have been demonstrated for space power application. A potassium boiler feed pump has been built and operated for 10,000 hours at 538°C (1000°F) at a flow rate of 1.47 kg/sec (3.25 lb/sec)*. This pump featured nickel clad silver conductors, Hiperco 27 laminations, 99% alumina slot insulation and top wedges, and "S" glass tape interwinding insulation. It was also operated with potassium at temperatures up to 760°C (1400°F) with the stator cooled by liquid NaK at 426-482°C (800-900°F). This technology demonstrates that tradeoffs in cost vs. performance for high temperature EM pumps can be achieved in pumping alkali metal fluids at high temperatures.

Rough estimation of the development cost and lead time to produce a low temperature stator and pump turned out to be approximately $200,000 and 16 months. Facilities for testing the EM pump are available within General Electric.

The estimate of unit cost for a mature system of a given design is based on an assumed production rate of about 300,000 units per year.

3. Liquid Metal Valve Assessment

Bellows sealed liquid metal valves have been used for alkali metal flow control in high temperature heat transfer loops for many years.

---

*Powell, A.H., Gahan, V.W. and Thompson, S.R., "Fabrication and Test of a Space Power Boiler Feed Electromagnetic Pump", Nuclear Systems Programs, General Electric Co., NASA Lewis Research Center Contract NAS 3-9422, MPR No. 28GESP-142, December 1968.

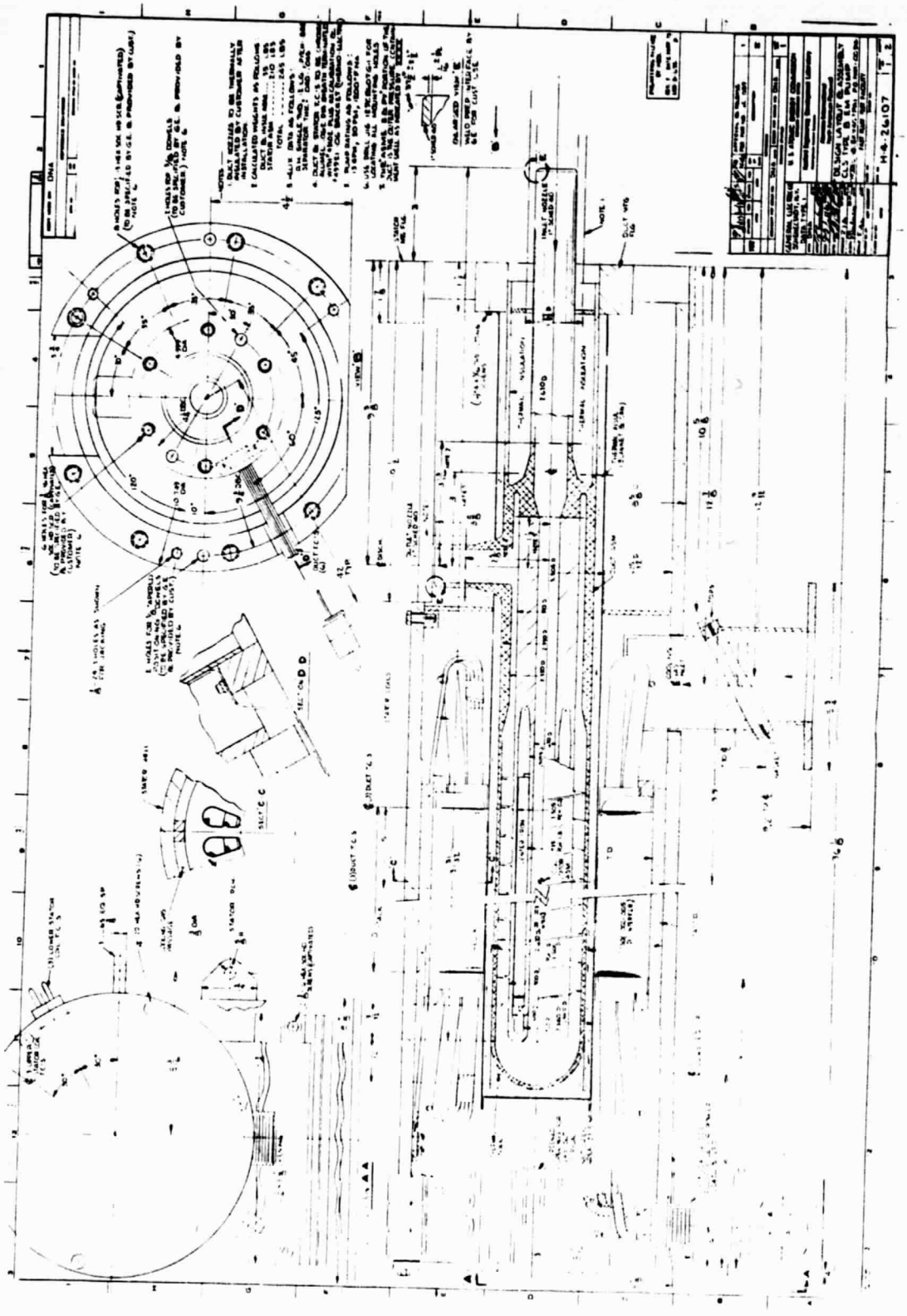

Figure 5-5. Pump Similar to the Proposed Electromagnetic Pump

Table 5-4. Electromagnetic Pump Performance

Capacity	0.7 kg/s (15 gpm)
Pressure	27.6 kPa (4 psi)
Temperature	816°C (1500°F)
Fluid	Sodium
Weight	90 kg (198 lbs) (including blower)
Efficiency	7%
Power Requirements	400 W 3ϕ 200-400 V
Cost	$\sim$ $850 F.O.B.

Applications have involved nuclear power conversion for naval propulsion, nuclear utility power and higher temperature nuclear power conversion in space. Stainless steel bellows valves are commercially available for the temperature range associated with alkali metal nuclear steam power conversion.

Higher temperature valves operating in the 870-1040°C (1600-1900°F) range have been built and tested for over 5000 hours for alkali metal Rankine space power systems*. Because of the operating temperature and the intended application in space, the valves were made using T-111 bellows, rhenium valve seats and W-25%Re valve plugs. The valve actuation mechanism featured a ball screw stem support with WC-6Co balls and a spur gear drive. The valve technology which was demonstrated in that work could readily be developed for use at lower temperatures appropriate to Stirling engine solar heat transfer systems using alternate, less expensive oxidation resistant alloys.

Although potential designs for use in the intended operating temperature range exist, no commercially developed source for such valves exists as off-the-shelf stock. For costing purposes, however, quotes were solicited from the major manufacturers of stainless steel, bellows type, alkali metal valves. Two quotations were received.

In the first quote, the cost for a one inch diameter pipe valve with a pneumatic operator was $930 less 20% for quantities over 100, or $744. The second quote was for $1520 in quantities over 1000. These costs are believed to be high when viewed in the light of 600,000 units per year. Since, in addition to the valve, some sort of actuation system and controls would be required, the cost of $744 per valve was used for cost calculations and was assumed to include these systems.

The production of these valves would require a developmental period and associated development costs. It is reasonable to assume that, given a large market on the order of 600,000 units per year, a reasonably competitive market situation would develop.

---

*Harrison, R.W. and Holowach, J., "Refractory Metal Valve for 1900°F Service in Alkali Metal Systems", General Electric Co., Cincinnati, Ohio, GESP-508, April 1970.

SECTION VI

COMPARISON OF PUMPED LOOP SUBSYSTEM WITH HEAT PIPE SUBSYSTEM

A. PERFORMANCE

Performance comparisons of the heat pipe solar receiver/TES and electromagnetic pumped loop TES subsystems are presented in Table 6-1. The efficiency advantage of the heat pipe subsystem is obvious. This advantage would probably be maintained by the fact that a technical improvement to reduce heat loss in any one system would, in most cases, apply to the other systems. Thus, a fundamental difference in the relative order of efficiencies will continue to exist regardless of how much improvement is made through technical advances in the specific values of efficiencies of each subsystem.

In Table 6-1 the thermal losses in the pumped loop scheme stand out as significant due to the long lengths of pipes. The heat pipe solar receiver system, being contained within one unit, does not suffer these losses.

The next significant difference between the pumped loop subsystem and the heat pipe solar receiver is in the Stirling engine efficiency. Since the pumped loop system must operate over a larger temperature range in the working fluid than the heat pipe subsystem, the mean operating temperature of the Stirling engine is lower, resulting in a less efficient engine and generator combination. Improved plumbing arrangements for the pumped loop design could conceivably reduce the difference, but it is difficult to envision a practical pumped loop in which this difference in the operating temperature of the Stirling engine would be substantially reduced.

Pump power poses the last item of significant difference between the two systems. Here the EM pump requires 3% of the output electric power compared to a negligible power (ΔT in the vapor space) for heat pipes.

Unless there should be an overriding reason to continue investigating pumped loop systems from the standpoint of extra thermal storage capacity or control flexibility, the heat pipe heat storage system represents the most cost-effective way to provide thermal energy storage for periods around an hour. The advantages of the pumped loop system lie first, in the larger thermal storage capacity that may be added by locating greater amounts of TES material and all the heavy components on the dish support ring, and secondly, in the added measure of control that may be exercised over the system as a whole. Its disadvantages lie: first, in that it requires much more supporting equipment, such as dump tanks,

Table 6-1. System Performance Comparison
Heat Pipe Solar Receiver Design
and Pumped Loop Design

	Heat Pipe Solar Receiver Design		EM Pumped Loop Design	
Average Thermal Power to Receiver, kW_t		62.1		62.1
Receiver Convective & Radiative Losses	6.85		6.85	
TES Convective & Radiative Losses	1.62		1.06	
TES-Receiver Connecting Pipe Loss	N/A		0.77	
Total Thermal Loss		8.47		8.68
Average Thermal Power to Stirling, kW_t		53.63		53.42
Stirling Engine Efficiency, %	35.0		33.2	
Generator Efficiency, %	90.0		90.0	
Overall Engine & Generator Efficiency, %	31.5		29.9	
Gross Stirling Electrical Power, kW_e		16.89		15.96
EM Pump Power	N/A		0.40	
EM Pump Cooling Power	N/A		0.10	
Total Electrical Loss, kW_e		0		0.50
Net Electrical Power		16.89		15.46
Overall Efficiency, %		27.2		24.9

expansion bellows along the pipe lengths, expensive valve actuation systems; secondly, that it is not a single compact unit as is the heat pipe solar receiver; and thirdly, that the long pipe runs pose additional heat losses and potential startup problems.

B. WEIGHT AND COST

Table 6-2 shows the weights for the primary design heat pipe solar receiver and the pumped loop TES systems. Both systems could be made lighter through redesign and the use of cellular insulation over the vacuum multifoil that was used; however, the relative difference would remain about the same since the same improvement would apply to both systems.

The result of the cost assessment between the two systems is presented in Table 6-3. These costs are the basic material costs only and do not include labor or overhead and profit margins. The difference in cost between the primary design and the pumped loop system would probably be even larger than indicated in Table 6-3 if these labor costs were added, since the pumped loop system is more complex and would require greater field assembly labor as contrasted to the compact, factory-produced heat pipe solar receiver with TES.

These systems are not cost optimized systems. This must be kept in mind. An example of this is that cellular insulation has already been shown to be more cost-effective than the vacuum multifoil insulation where size control is not a key factor. Considerable savings would result in all systems if the cost of insulation were reduced to only a few hundred dollars. Further cost optimization in other areas as well could be expected to reduce the base costs even further.

Table C-2. Comparison of Weights-Heat Pipe Solar Receiver Design and Pumped Loop Design

	Heat Pipe Solar Receiver Design		EM Pumped Loop Design	
	kg	lb	kg	lb
Receiver	210	463	422	930
Salt	359	791	359	791
Cans	79	174	79	174
TES Area Structure	181	399	-	-
TES Area Wicking and Sodium	86	190	-	-
Insulation	201	443	430	948
Outer Steel Shell/Vacuum Chamber	157	346	640	1411
Piping and Valves	-	-	32	70
TES Area Structure, Insulation & EM Pump	-	-	657	1448
Sodium	-	-	218	481
Insulated Pipe Between Receiver and TES	-	-	500	1102
Total	1273	2806	3337	7355
Stirling Engine*	147	324	147	324
Generator*	68	150	68	150
Total	1488	3280	3550	7829

*Estimates

Table 6-3. Materials Cost Comparison-Heat Pipe Solar Receiver Design and Pumped Loop Design

(Unit - Dollars)	Heat Pipe Solar Receiver Design	EM Pumped Loop Design
TES Salt ($NaF-MgF_2$)	327	327
Salt Supporting Structure	1153	5566
Cans		
Can Support Structure		
Tanks		
Valves and Actuators	N/A	4464
Piping or Heat Pipes (Not Incl. G.L. Pump)	1010	3383
Wicking	1954	N/A
Containment Structure - First Layer	3790	334
Inner Vacuum Cylinders, Vessels		
Flat Heads		
Containment - Structure - Second Layer	155	N/A
Outer Vacuum Cylinders		
Receivers (Separate)	N/A	3179
EM Pump	N/A	850
Insulation	2055	3446
Not Including Receiver in Pumped Loop		
Sodium	N/A	178
	10444	21727

SECTION VII

OPERATING, SAFETY AND RISK ASSESSMENTS OF THE HEAT PIPE SOLAR RECEIVER

The advantages of the heat pipe solar receiver in terms of compactness, manufacturability and operating characteristics have been discussed briefly in the Introduction. It is the purpose here to assess the operating, safety and risks associated with the heat pipe solar receiver, since that system appears to have the greatest potential for maximum efficiency and lowest cost in mass production. Because of the very minimal amounts of sodium involved, safety and risk consideration are not paramount. The self regulating thermal control afforded by the TES and the compactness of the design simplify the operating, maintenance and replacemen of this power storage and conversion subsystem.

A. SYSTEM OPERATION

1. System Startup

Prior to focusing the concentrator and allowing solar energy to enter the solar receiver, the TES containment vessel would be preheated to a temperature of approximately 149°C (300°F). This will insure that the sodium charge is in a liquid state (sodium melts at approximately 98°C (208°F) and thus is capable of being wicked throughout the TES vessel. This preheating could be accomplished via electrical heaters located inside the TES containment vessel. Temperature sensors, located at various positions inside the TES, would be monitored to determine when the TES system preheat cycle has been completed. Lock-out control systems would prevent focusing of the concentrator if the TES containment is below 149°C (300°F). Electrical heaters would be automatically energized any time the TES temperature is below 149°C (300°F).

The solar receiver/TES system may be at various angles of inclination and at various temperatures (including various power storage levels) at startup. The solar flux level (insolation) available may also be at various levels depending on the sky conditions and time of day. To study the various possible startup conditions the most usual conditions will be considered first and, later, the less usual conditions will be considered.

a. <u>Startup Condition #1</u>.

- Inclination Angle — 10°
- Solar Insolation — Typical - 8:00 A.M.
- TES Temperature — Approximately 816°C (1500°F) (approx. 21.7 kW_t sensible heat lost during 13 hour night; 42°C (76°F) temperature drop from a fully discharged TES system on the previous day)

- Focal unit was kept at positive inclination for some period of time at end of previous day (time enough to freeze Na in evaporator end of heat pipe) and then unit was placed in stowed position for the night.

The conditions outlined above can be considered usual. The solar tracking system would be allowed to focus the concentrator as soon as adequate solar insolation was available. When the TES system reached a predetermined temperature, the electrical breaker connecting the induction motor/generator to the grid would be actuated. The generator would operate as a motor starter for the Stirling engine and would bring the Stirling engine up to the motor synchronous speed. The Stirling engine would then start driving the motor above synchronous speed at which point the motor would operate as a generator supplying power to the electrical grid.

b. Startup Condition #2. Same as Condition #1; however, the concentrator was not placed in stowed position overnight. The unit was left at the same position (inclination) overnight.

Under this condition, startup would be the same as discussed in Condition #1. Overnight heat losses from the TES would be expected to be somewhat less than those calculated with the receiver in the stowed position.

c. Startup Condition #3. Same as Condition #1 or 2 but startup would be made at a time when maximum solar insolation was available. Under this condition the inclination angle would be approximately 80° (typical 12:00 noon). The higher solar insolation available would result in a faster heat up of the solar receiver heat pipes. Thermal energy storage temperature would be continuously monitored and the Stirling engine started as outlined in Startup Condition #1.

d. Startup Condition #4. For this cold startup condition it is assumed that the TES system has been depleted, the unit has been out of service for maintenance or other reasons and is ready to be placed back in operation. The electrical preheaters would first be energized and the TES brought up to a temperature of 149°C (300°F). This would insure the sodium is in a liquid state in the TES. When the unit is shutdown, the sodium would be allowed to freeze in the TES and heat pipes. Receiver inclination at shutdown would allow the sodium in the heat pipes to freeze in the evaporator end. The concentrator would be focused on the sun and the heat pipes and TES would gradually heat up. At the predetermined TES temperature the Stirling engine would be started as indicated in Condition #1.

2. Intermittent Solar Power Operation

Cloud passage, of course, can result in intermittent solar power being supplied to the solar receiver. The present design concept provides a TES system capable of operating the Stirling engine-generator at a rated power output of approximately 17.2 kW_e for approximately 1.2 hours. Assuming no solar power is available at the end of this time period, the TES temperature will decrease and the power to the Stirling engine will

also start to decrease; the Stirling engine output torque would decrease and the generator speed would start to fall toward synchronous speed (at which no power would be produced).

However, as long as the Stirling engine is producing net power, even at a reduced rate, the generator will continue to provide its power to the grid. Conventional load management will be required to prevent the load from exceeding the generator output. As the TES temperature declines by means of sensible heat loss below the melting point of the TES material, the system would continue to produce useful power at lower power levels. At some temperature and power output level it would be necessary to decide to shut the system down in order to retain the thermal energy in the TES system for later restart. At this point, the circuit breaker feeding the electrical load would be opened, disconnecting the generator from the load, and either the working fluid pressure in the Stirling engine would be reduced to prevent transmission of power to the generator shaft or a brake might be utilized to stop the engine. The latter would require electrical power, gas pressure or some other form of power to actuate the brake.

Once cloud passage is complete and solar insolation again is available at the receiver, the TES system temperature will start to rise. As soon as the temperature reaches a preset value the electrical breaker to the grid can be closed and the Stirling engine started. If desired, the TES system may be partially or completely charged before placing the engine-generator unit on the line. As the TES salt stores latent heat by melting the TES material, the ΔT required to charge the capsules increases requiring a higher sodium vapor temperature in the TES for a given charging time. Sodium vapor temperatures would be monitored throughout this time as a means of sensing the need for regulating power to the TES or to the Stirling engine.

Were a fossil fuel combustor to be added to the system, its operation, in a highly efficient on-off manner, could be actuated by the temperature in the TES system. The TES would maintain a smooth flow of constant temperature and power to the Stirling engine; the combustor would merely recharge the TES if necessary without the necessity of providing programmed variable thermal power inputs to the Stirling engine to compensate for varying solar input or power demands.

B. OVERNIGHT SYSTEM THERMAL LOSS

During overnight storage the conduction and convection losses mentioned in Section IV still persist but the convection and radiation losses from the cold receiver no longer occur. Over the course of a 13 hour night the heat losses from the TES area would result in a sensible heat temperature drop of approximately 42°C (76°F) which corresponds to an energy loss of about 21.7 kW_t. This is small enough not to significantly affect the performance of the Stirling engine on subsequent startup. It also indicates that the unit might be kept for several days without having to go through any unique startup procedure.

In the proposed storage mode the large dish would be inverted to protect its surface. In this inverted position, if the sodium in the primary heat pipes were still liquid, the primary heat pipes would continue to operate rejecting heat from the TES to the receiver, and subsequently, by continuing radiation and convection, to the atmosphere. By allowing the solar receiver to cool in the operating position and the sodium to freeze in the heat pipes near the receiver aperture, such losses by reverse heat flow in the primary heat pipes could not occur. It was necessary to determine what amount of time it would take for the liquid sodium in the primary heat pipes to freeze in the cold end.

A finite element steady-state analysis of a primary heat pipe bounded the problem between two extremes. The first extreme assumed that the sodium in the heat pipe did nothing to increase the conductance of the heat pipe and the second extreme assumed that the conductance of the heat pipe was infinite. Figure 7-1 shows the results of the analysis. When the assumption is made that the sodium in the heat pipe does nothing to conduct heat, that is, the sodium does not transfer heat in the vapor phase, the heat pipe will, sooner or later, cool below the freezing point of the sodium. This also indicates that once frozen, by any means, the sodium in the lower foot or so of the primary heat pipes will not thaw until it is heated by the sun. If the assumption is made that the sodium continues to circulate through the wicked portion of the heat pipe and efficiently transfers heat in the vapor phase, then the solid line shows that the heat pipe would not freeze. The answer lay between these two extremes.

Since an accurate transient analytical model of a heat pipe was difficult, the question was decided by experiment. In the experiment a heat pipe at a slope of approximately 10° was heated uniformly to 816°C (1500°F). Half of the heater on the evaporator section of the heat pipe was then removed and the other half turned off. Air flow at approximately 3 mph was then directed on the heat pipe which cooled to temperatures below the freezing point of sodium within 30 minutes. When the air flow was increased to 9 mph the time for sodium solidification was less than 10 minutes. Figure 7-2 shows the experimental results for cooling air flow at 3 mph.

The results of this experiment provide strong indication that, after shutdown, the heat pipes will cool to a temperature below the freezing point of sodium at the aperture end of the evaporator section. The concentrator could be moved to the stowed position after a wait of about half an hour during which time the sodium in the primary heat pipes would solidify preventing reverse heat flow from the TES to the cold receiver.

C. CONTROL REQUIREMENTS

1. Energy Extraction Control

The approximate 1.2 hours of TES allows the Stirling engine to operate at near constant power input. At startup the control system must decide at what time the electrical breaker tying the induction generator to the load will be energized. This decision can be based on

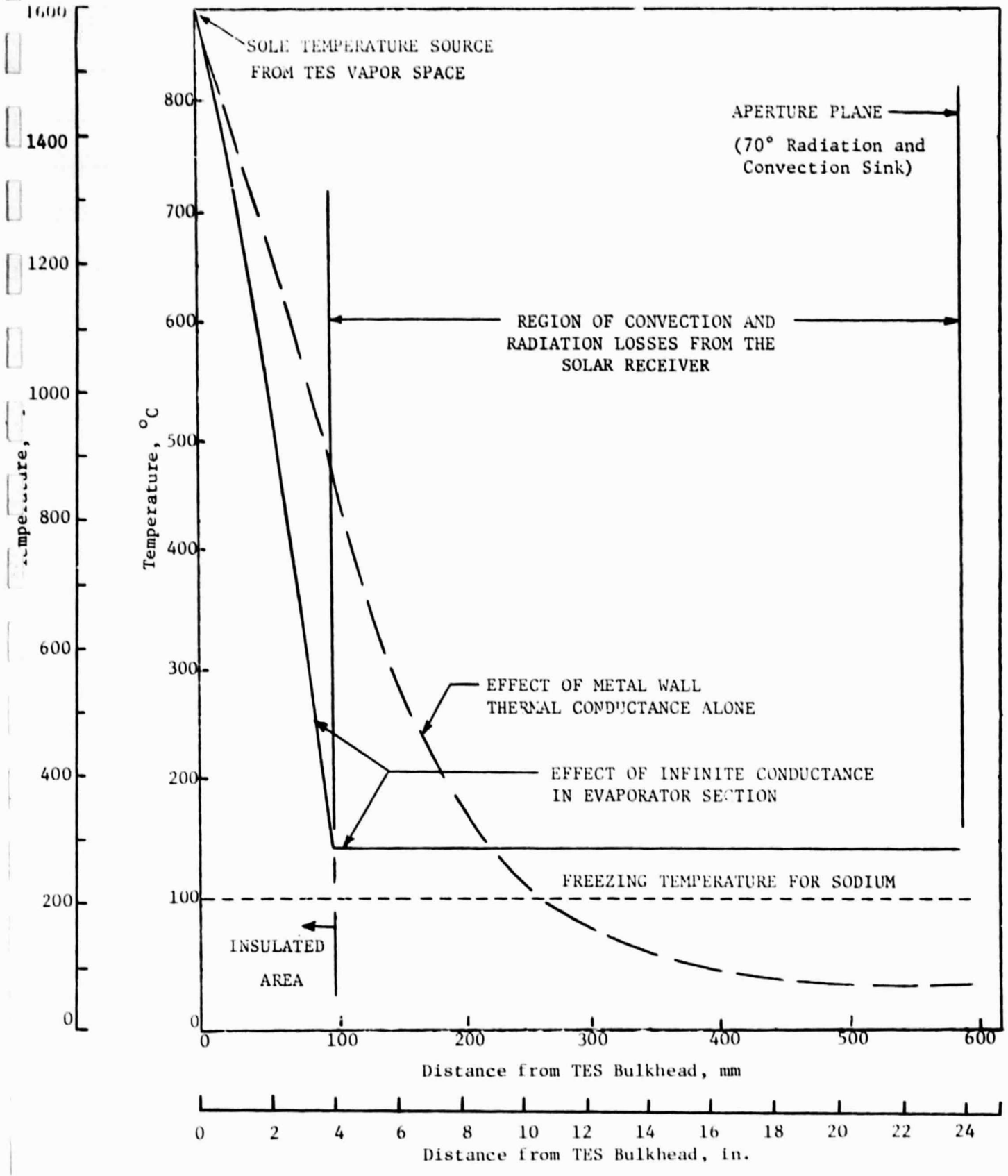

Figure 7-1. Night Time Steady State Temperature Distribution for a Primary Heat Pipe in the Solar Receiver

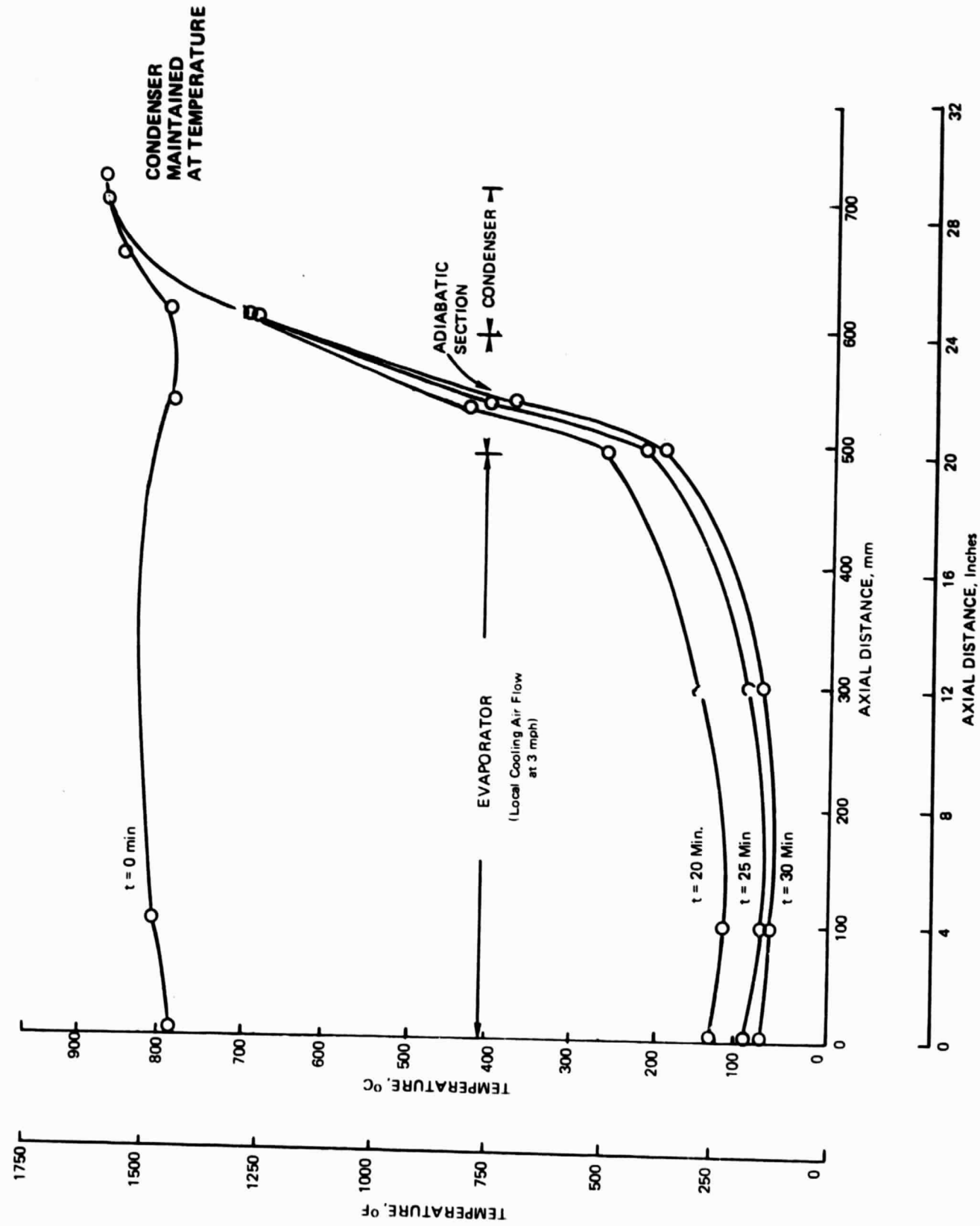

Figure 7-2. Experimental Simulation of Primary Heat Pipe Cooling Prior to Overnight Storage. (Sodium Solidifies in Evaporator and Prevents Reverse Heat Flow)

the status of the TES as indicated by the temperature of the secondary heat pipe vapor space and as monitored by a solar flux meter capable of integrating the flux input. A means of insuring that the TES system is not overcharged, resulting in excessive primary heat pipe temperature, must be incorporated through the secondary heat pipe vapor space temperature. Assuming power to the Stirling engine is to remain constant, defocusing of the concentrator must be accomplished when this temperature indicates the TES is superheated above 8°C (15°F). Shutdown (disconnect from the electrical power system) may be determined by TES temperature and/or Stirling engine speed and power output.

Although the kinematic-Stirling engine is capable of operation at various speeds as a function of system fluid pressure, this type of control appears complex and is not required when an induction generator is utilized. Electrical power conversion for better storage or load dispatch control for the utility grid is beyond the scope of this assessment.

2. Required Controls and Instrumentation

The focal mounted system with approximately 1.2 hours of TES will require a minimum of control and instrumentation. Table 7-1 lists required instrumentation based on a very limited analysis. The type of sensor, its location, and function are indicated.

Pressure type sensors for use in alkali metal systems normally contain a bellows or diaphragm of some sort. This must be kept heated since damage to the sensor can result if pressure were accidently applied when the sodium was frozen. For this reason pressure sensors are not recommended for control system actuation.

Initial developmental units would require considerably more instrumentation to monitor system operation. These would be primarily temperature sensors. Vibration monitors would also be employed. The Stirling engine would probably require a fluid flow meter for measuring lube oil and coolant flow rates. Loss-of-flow type switches and pressure gages or switches also appear necessary. Oil or coolant flow loss would automatically actuate the defocusing system, stop the engine and disconnect the generator from the load.

The induction generator instrumentation would consist of voltmeters, ammeters and a 3-phase wattmeter. A generator overload condition would result in a Stirling engine shutdown and defocusing action.

A conceptual control schematic is shown in Figure 7-3.

D. SERVICING REQUIREMENTS

Maintenance work will fall into the planned (routine) and unplanned categories. The solar receiver and TES system are basically static systems and, therefore, maintenance would be expected to be minimal on these components. The Stirling engine would require routine oil changes and, possibly, coolant system cleaning. A major engine overhaul would, no doubt, be required after a prescribed number of operating hours. Cer-

Table 7-1. Required Control Instrumentation

Sensor Type	Location	Function
1. Temperature T/C	Primary HP	Over temperature protection. Activate defocusing system.
2. Light sensors (Fiber Optics)	Around heat pipe receiver aperture	Feedback for tracking system.
3. Temperature	TES system vapor space	Startup and shutdown control.
4. Temperature	TES system interior structure	Control pre-heating (electric) system.
5. Tachometer	Stirling engine shaft	Actuate defocusing system, brake and determine shutdown.
6. Integrating solar flux meters	Concentrator	Monitors TES charge level.
7. Pressure level	Stirling lube system	Loss of oil pressure; shutdown Stirling engine
8. Temperature level	Stirling engine coolant system	Loss of coolant or high temperature shutdown Stirling engine.
9. Electrical Voltmeter Ampmeter	Generator Control	Monitor output and provide protection from overload.

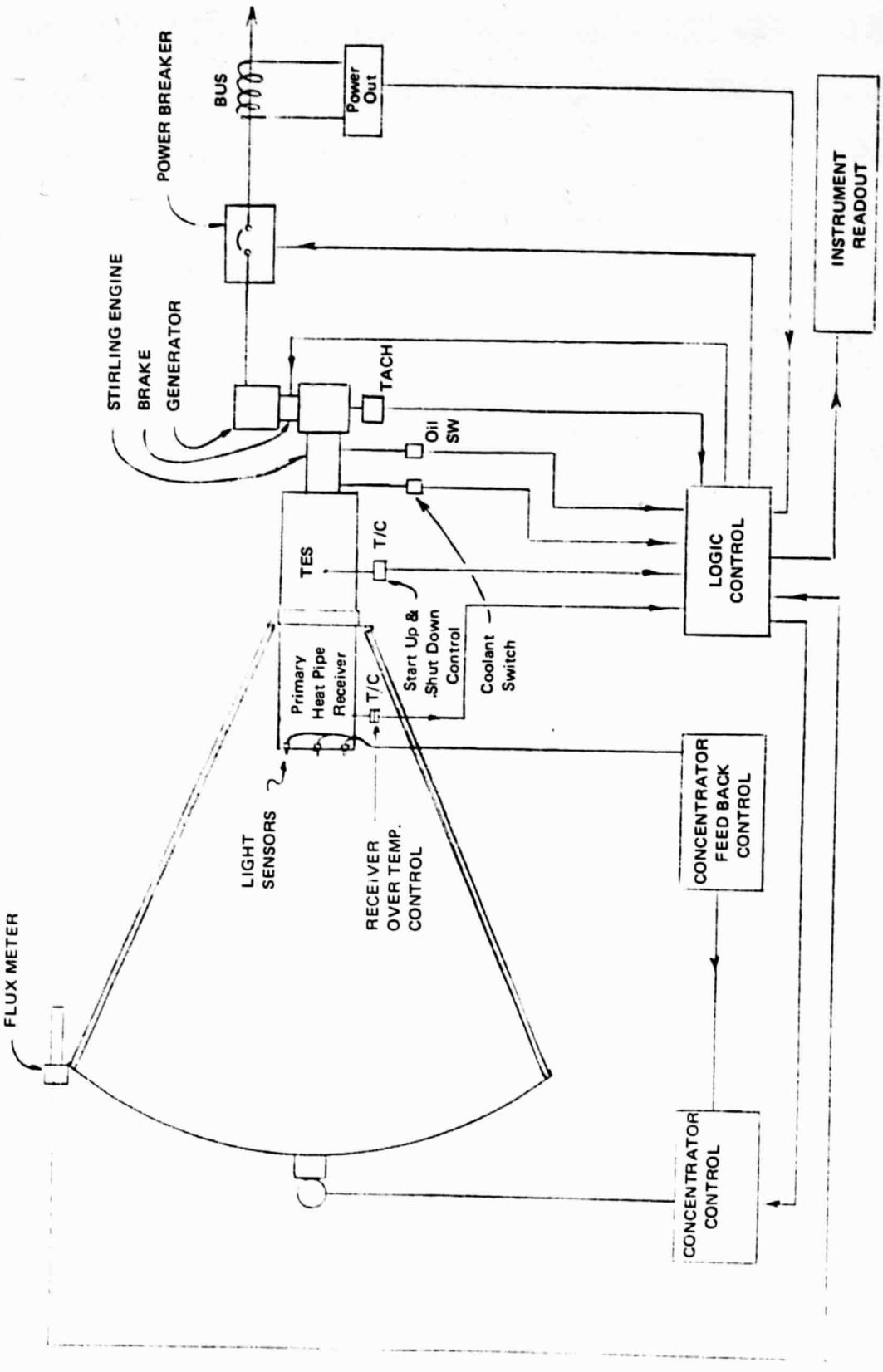

Figure 7-3. Control Schematic

tain minor maintenance to the engine would be done in the field. Major engine overhauls would be expected to require removal of the focal-mounted system to an overhaul depot. Removal and replacement of the compact and integrated heat pipe solar receiver/TES/engine-generator could be quickly and easily accomplished by means of a few simple disconnects.

The failure of a single primary heat pipe in the evaporator or adiabatic section, from a thermal cycle fatigue crack or something else that allows air into the heat pipe, will result in a power loss to the system but not necessarily a shutdown, since the thermal energy carrying capability of each of the heat pipes is well above its maximum normal operation requirements. The repair need not be affected immediately; however, at some point the pipe would have to be removed from the TES system containment and replaced.

Routine inspection of control systems and periodic actuation of safety systems to insure that their operation is satisfactory will be required. Control systems maintenance is expected to be the major portion of this type of work done at the site.

Life limitations with regard to component replacement cannot be accurately predicted at this time since most of the system components have no past operating data to utilize for reference. The solar receiver and TES system life will be dependent, to a large extent, upon material properties such as oxidation resistance, creep strength and thermal cyclic fatigue. The Stirling engine will probably perform similar to other types of reciprocating machinery and require a major overhaul every 4000 operating hours (normally once a year).

The generator is inherently a very reliable mechanical device and with the exception of routine lubrication should require little maintenance. The generator life will depend largely on lubrication of bearings. An overhaul is estimated at every two years.

Repairs to the solar receiver heat pipes or TES containment vessel will require inert gas welding chambers, sodium filling facilities, and evacuating equipment. These facilities would be located at the overhaul depot or factory where the system was originally manufactured.

E. PRELIMINARY FAILURE MODE EVALUATIONS

Possible failure methods and estimates of the probability of occurrences, consequences, methods of failure avoidance, repair methods, relative cost of repairs and safety aspects are presented in Table 7-2 for each of the focal-mounted major components. As with most systems, failures might result from any one or more of four major areas: design, manufacture, operation or accident. The program implementation plan should, therefore, include the detailed study of how potential failure or defects can be eliminated in each of these areas.

Experience from previous work in the development of alkali metal systems operating at high temperatures provides some insight into failure modes for the Na filled heat pipe and TES system as indicated in Table 7-2. The analysis covers only the components of the focal mount system.

Table 7-2. Failure Mode Analysis and Effect

Component Description	Failure Method	*Est. Prob. of Occurrence	Consequences of Failure	Methods of Avoiding or Detecting Failure	Repair Method & Relative Cost	Safety Aspects
1. Primary Na Heat Pipe	Heat Pipe Failure From:					
	Weld Thermal Cycle Crack	5	Possible small fire as Na makes contact with air. Loss of sys. power 1/27th; possible damage to adjacent HP's; power loss low unless secondary failures occur.	Good design, proper matl. selection; high quality welding; and other processing during manufacture. Visual inspect occasionally for indication of Na leaks; performance depreciation.	HP must be removed, repair welded, refilled with Na and reinstalled into containment shell; factory repair, moderate cost.	Single HP; slight safety hazard
	Exterior Oxidation	2				
	Interior Na Corrosion	< 1				
	Rupture/Long-Time Creep	< 1				
	Rupture/Internal Pres.	1				
	Rupture/External Pres.	< 1				
	Wick Plugging	2				
	Pinhole/Porosity Leak	3				
2. Secondary Heat Pipe Containment Shell	Shell Failure From:	5	Potential fire as Na contacts air; dense white oxide smoke; attacks paints and metals, damage to insulation, etc. Complete loss of power, burnup of heat receiver, etc., if not defocused.	Good design, matl. selection and high quality control during manufacturing. Monitor power output; locate NaO smoke detectors at several points, defocus activation on sudden performance change.	Unit would probable be scrapped; decontamination required before disposal of hardware; salvage Stirling and gen. high cost.	No major hazard since amount of Na small. NaO smoke quickly dispersed in atmosphere.
	Weld Thermal Cycle Crack	2				
	Exterior Oxidation	< 1				
	Internal Na Corrosion	1				
	Rupture/LT Creep	< 1				
	Rupture/Internal Pres.	1				
	Rupture/External Pres.	2				
	Porosity Leak					
Wicking	Mechanical Failure	1	Gradual reduction in performance.	Redundant wicking in present design.	Rebuild TES hardware only if performance deteriorates significantly	Possible overtemperature of primary heat pipes; slight safety hazard.
3. TES Containment Capsules	Weld Failure	3	Dependent on TES matls. used; failure of one capsule not expected to be significant.	Good design and QC in manufacturing, filling, etc.; detection of failure not practical. Determine salt/sodium compatability.	Difficult to repair; factory repair required; moderate cost; repair may not be necessary with good sodium/salt compat.	No safety problem with proper TES matl.
	Exterior Na Corrosion	< 1				
	Interior Salt Corrosion	1				
	Rupture Internal Pres./ Vacuum	1				
	Cracks, Porosity, Pinholes	2				
4. Stirling Hx Tubes	Stirling Tube Failure From:		He leakage into containment vessel resulting in sudden loss of sys. power, incr. pressure in containment shell. Shell must be designed to handle press.	Good design and QC in manufacturing; press. switch in containment shell activated; visual and audible alarm; Pres. relief actuated; limited He replacement rate and engine safety controls	Return to factory; remove Stirling, repair Hx and reinstall Stirling on TES. Moderate cost.	TES chamber pressure increase; rating must handle; no major hazard from small amount of sodium. NaO smoke quickly dispensed in stmosphere
	Exit Na Corrosion	1				
	Cyclic Fatigue Base Metal and Welds	5				
	Rupture Internal Pres.	2				

*Based on prob. scale of 1-5, 5 being highest probability.

Table 7-2. (Continued)

Component Description	Failure Method	*Est. Prob. of Occurrence	Consequences of Failure	Methods of Avoiding or Detecting Failure	Repair Method & Relative Cost	Safety Aspects
5. Stirling Engine Cylinder Head Engine to Containment Shell Joint	Cracked Head	< 1	Same as (4) above	Same as (4)	Same as (4)	Same as (4)
	Weld Failure	2	Same as (2) above	Same as (2)	Same as (2)	Same as (2)
	Bellows Cyclic Fatigue	5				
6. Insulation Jacket Outer and Inner Shells, Bellows	Insulation Vacuum Loss From:		Fast of slow loss of vac. resulting in greater heat loss to atmos. Atmospheric water vapor entry to TES chamber unlikely.	Good design & QC in manufacturing. Press. sensor alarm in insulation jacket; temp. detector.outer shell temperature alarm.	Depending on location of failure field repair possible; evacuation after repair required; periodically could be done in field. Relatively low cost.	No safety problem.
	Weld Cracks	1				
	Rupture Collapsing	1				
	Porosity Leak	3				
7. Focal Mount Support Ring	Cyclic Fatigue	<< 1	Separation of the power system from the focal mount and major damage to collector or power system.	Good design and QC in manufacture; proven design by vibration testing. Vib sensor terminates operation before major damage.	Focal mount collector system probably damaged. Moderate collector repair cost; replacement of power system.	Negligible
8. Heat Rec. Insulation (Blanket Type)	Moisture Entry	5 (Reducible by Design)	Damage to insulation; loss of insulating value. Excessive heat losses.	Utilize good sealing design and QC in manufacture; analysis of performance deterioration.	Replace insulation in field; relatively low cost.	Negligible
9. Aft End Insulation (Blanket Type)	Moisture Entry	5 (Reducible by Design)	Same as (8) above	Same as (8)	Same as (8)	Same as (8)
10. Other Parts of Stirling Generator or Accessories	Of Any Type	5	Defocus system or loss of power; no adverse effect on Rec/TES unit.	As prescribed by Stirling design; open elec. beaker to disconnect from load.	Probably factory disassembly and repair. Rel. low cost	Negligible
11. Stirling Engine Stall or Sustained Solar Power input Above Rated Engine/Generator Capacity	Of Any Type	5	None, overtemperature of Stirling engine requires time to overcome thermal inertia	Rise in temperature of TES chamber over maximum triggers defocussing.	None	None
12. Collector Tracking System Failure	Of Any Type	3	Possible melting of metal components and cordierite ceramic around heat receiver aperture. Possible loss of vacuum thermal insulation	Use of high temperature ceramic; design analysis of transient heat flux; analysis of performance deterioration.	Replace non-critical components; relatively low cost.	Negligible

Table 7-2. (Continued)

Component Description	Failure Method	*Est. Prob. of Occurrence	Consequences of Failure	Methods of Avoiding or Detecting Failure	Repair Method & Relative Cost	Safety Aspects
13. Primary Heat Pipes	Failure to Solidify Potassium in Primary Tubes Prior to Stowing.	1	Thermal loss from TES chamber through primary heat pipes during overnight periods.	Loss in overnight temperature in TES chamber; utilize long cooling period before stowing; alternative design using thermal switch in secondary heat pipe.	Thermal loss is only problem; no repair required.	None

A failure of the concentrator solar tracking system (failure to defocus concentrator in the event of a loss of load) could result in the over-temperature and destruction of the focal-mounted system; however, the thermal energy storage provides additional time for corrective action even when the TES system is fully charged since the sensible heat of the system will slow the rate of temperature increase.

In reviewing the information in the table certain things become apparent. First, structural failure from thermal cyclic fatigue ranks highest on the occurrence probability scale. Second, the result of the failure would generally be either a relatively small decrease in performance or a relatively sudden and complete failure to perform. The latter conditions are usually associated with loss of sodium from the system or the entrance of air into the sodium-containing portions of the system, particularly the TES vapor spaces. Failure of this type would entail significant repair costs or possibly replacement of the unit. Design, manufacturing and quality control procedures will require the utmost attention to avoid such failures during normal operation.

The loss of sodium to the atmosphere will normally result in a limited fire. The sodium will self-ignite from the moisture in the air. When this occurs a dense white smoke, NaO, is produced and NaOH is found around the leak. The TES system will operate at a pressure slightly under atmospheric so that a leak will allow air to enter the containment vessel. The air being noncondensible will stop the heat transport system normal operation and NaO will be found throughout the inside of the system. In this event the complete TES unit would require a thorough cleaning before it could be placed back in operation.

Contact between fluoride salt and molten sodium causes no observable reaction*.

It will be necessary to continue failure analysis efforts as establishment of the system proceeds to insure that a high degree of reliability is provided in design, manufacturing and operation.

F. HEAT PIPE RELIABILITY

In assessing the expected operating life and reliability of alkali metal heat pipes in the heat pipe solar receiver expected to operate for many years in the 788-871°C (1450-1600°F) temperature range, the following factors must be considered:

- Oxidation resistance of heat pipe materials.
- Strength of materials used in heat pipes expressed as allowable stresses versus temperature.
- Low Cycle Fatigue both as to imposed thermal conditions and to LCF thermal transient analysis of components.

*Bozer, O., "Safety Considerations for High Temperature Thermal Energy Storage in Fluoride Salts"; Repro. No. 779092 IECEC Record 1977, pp 575-582.

- Alkali metal materials compatibility as evidenced in long term operation of alkali metal test capsules and power conversion systems.

- Heat Pipe Life Tests reviewed from the background of limited prior test experience.

- Embrittlement of materials which might occur in the presence of hydrogen.

A definitive discussion of these factors and of prior testing experience in both heat pipes and alkali metal pumped loop systems is contained in a separate document*. Based upon prior operating experience with alkali metal heat pipes at lower temperatures and on long term pumped loop alkali metal operating experience in this temperature range, the development of heat pipe thermal transport systems for high temperature solar applications appears warranted.

The use of weldable, fabricable, solution strengthened alloys without significant ductility limiting aging reactions will be required.

Oxidation and thermal fatigue will be more severe in the solar receiver which operates at the maximum temperature and is more subject to thermal fluctuation. There, oxidation resistant stabilized grades of stainless steels or superalloys will be required. The flexibility of the solar receiver constructed of free-standing parallel tubes should be helpful in minimizing the effects of thermal gradients; the high internal thermal conductance of the heat pipes themselves is also beneficial. In the secondary TES heat pipe, the isothermal nature of the heat pipe and the thermal inertia provided by the TES will limit, significantly, the possibility of low cycle thermal fatigue. Because of the relatively low vapor pressure of sodium, high pressure stresses are not anticipated, but creep strength considerations and allowable design stresses must be considered in detailed designs.

An extensive background of alkali metal compatibility testing suggests that proper control of heat pipe cleanliness, careful control of alkali metal impurities and the use of appropriate handling, transfer, loading and sealing techniques can assure more reliable long term operation. Alkali metal heat pipe endurance tests have been successfully conducted for periods over 35,000 hours in duration; lithium fluoride fused salt storage systems have also been operated for longer than 10,000 hours in primary and secondary sodium heat pipe systems at temperatures in the 816-871°C (1500-1600°F) range in a reliable manner. No hydrogen embrittlement has been experienced in these tests. Methods have been developed for minimizing the diffusion of hydrogen into heat pipes and of clearing hydrogen from heat pipes during testing. Hydrogen embrittlement by means of gross hydrogen impregnation is not to be expected; the use of helium rather than hydrogen in the Stirling engine should be chosen to avoid this concern.

---

*Zimmerman, W.F. and Stearns, J.W., "Heat Pipe Operating Reliability for the Solar Stirling Receiver", DOE/JPL 1060-29 (To be published).

Overall, sufficient evidence is available to indicate that heat pipes can be made to operate reliably for long periods of time in the 593-871°C (1100-1600°F) range using the most economical materials for the intended temperature. The exact lifetime and temperature levels for which specifically designed heat pipe systems can be used will, however, require further system study conceptual design verification and component life testing.

G. SAFETY CONSIDERATIONS

1. Sodium Safety Considerations

Sodium, like other alkali metals, rapidly oxidizes when exposed to the atmosphere. When exposed to air of relatively high humidity spontaneous ignition occurs and a dense white smoke is produced, (NaO). An oxide film then normally forms on the surface causing the flame to be extinguished. Removal of the oxide film will allow the sodium to flame up again. Continued exposure to the atmosphere results in the formation of sodium hydroxide. This substance on the surface of a metal has a greenish color.

The spontaneous ignition of sodium can result in the ignition of adjacent combustible material; the heat generated during rapid oxidation can produce damage to containment or other adjacent hardware; the oxide smoke can produce corrosive damage to machined parts, paints, etc., and also have adverse effect on the lungs and eyes of system operating personnel. The extent of these effects is, of course, a function of the amount of oxide smoke and the time one is exposed to the smoke.

From the above, one would surmise that although sodium is an excellent high temperature heat transfer media it presents some hazards to system construction, operation, and maintenance. Recognizing this fact, the extent of the hazard is then a function of the system design, quality control during construction, operating and maintenance procedures and last, but most importantly, the quantity of sodium utilized in the system.

Since each heat pipe in the receiver contains a negligible amount of sodium, the failure of any primary heat pipe produces no significant safety hazard. The hazard from loss of sodium from the secondary heat pipe is similarly limited because of the relatively small quantity of sodium contained therein and the dispersed nature of the solar concentrator power collection system. Thus, the possibility of damage to adjacent equipment or hazards to operating personnel is almost nonexistant.

One of the main advantages of sodium as a heat transfer media is its very low vapor pressure at high temperature. Only at maximum operating temperature will the system pressure rise slightly above atmospheric pressure. Furthermore, for the heat pipe solar receiver, there are no requirements to pump sodium in a liquid state at pressures above atmospheric. Thus, for the most part, leakage of air into the system will be the result of a containment vessel failure. If the leak is in a region which contains liquid, the sodium can, however, flow from the vessel or heat pipe via gravity and cause a minor fire. Significant damage to the system via oxygen contamination can result from the in-leakage of air; however, hazards from fire or smoke are reduced to a minimum.

2. Solar Flux Missed Aperture Analysis

A finite element heat transfer analysis of the consequences of the solar flux missing the aperture was performed for system survivability, for material selection confirmation and for system control purposes. Under the peak solar flux the analysis determined the maximum temperature vs. time that might be expected on the ceramic solar heat barrier which surrounds the aperture. The surface temperature distribution was also calculated after equilibrium was reached.

This analysis predicted a maximum temperature of about 1316°C (2400°F) on the ceramic and about 466°C (870°F) on the steel outer case in the unlikely event the sun spot remained in a fixed position on the ceramic surface. A peak temperature gradient along the ceramic surface was 320°C (575°F) per inch. Figure 7-4 indicates the transient temperatures at the point of maximum equilibrium temperature. At a concentrator slew rate of 400° or more per hour the sun spot would remain on a given position on the ceramic for less than one minute; thus it appears that the front outer surface of the solar receiver exposed to this moving sun spot would only reach a maximum temperature of around 427°C (800°F) during focusing and defocusing of the receiver for solar heat control purposes. The low expansion Cordierite ceramic which is exposed to these conditions could readily tolerate this condition and no significant damage would be done to the solar receiver itself even if the sun spot were allowed to remain fixed on the outer ceramic surface of the solar receiver.

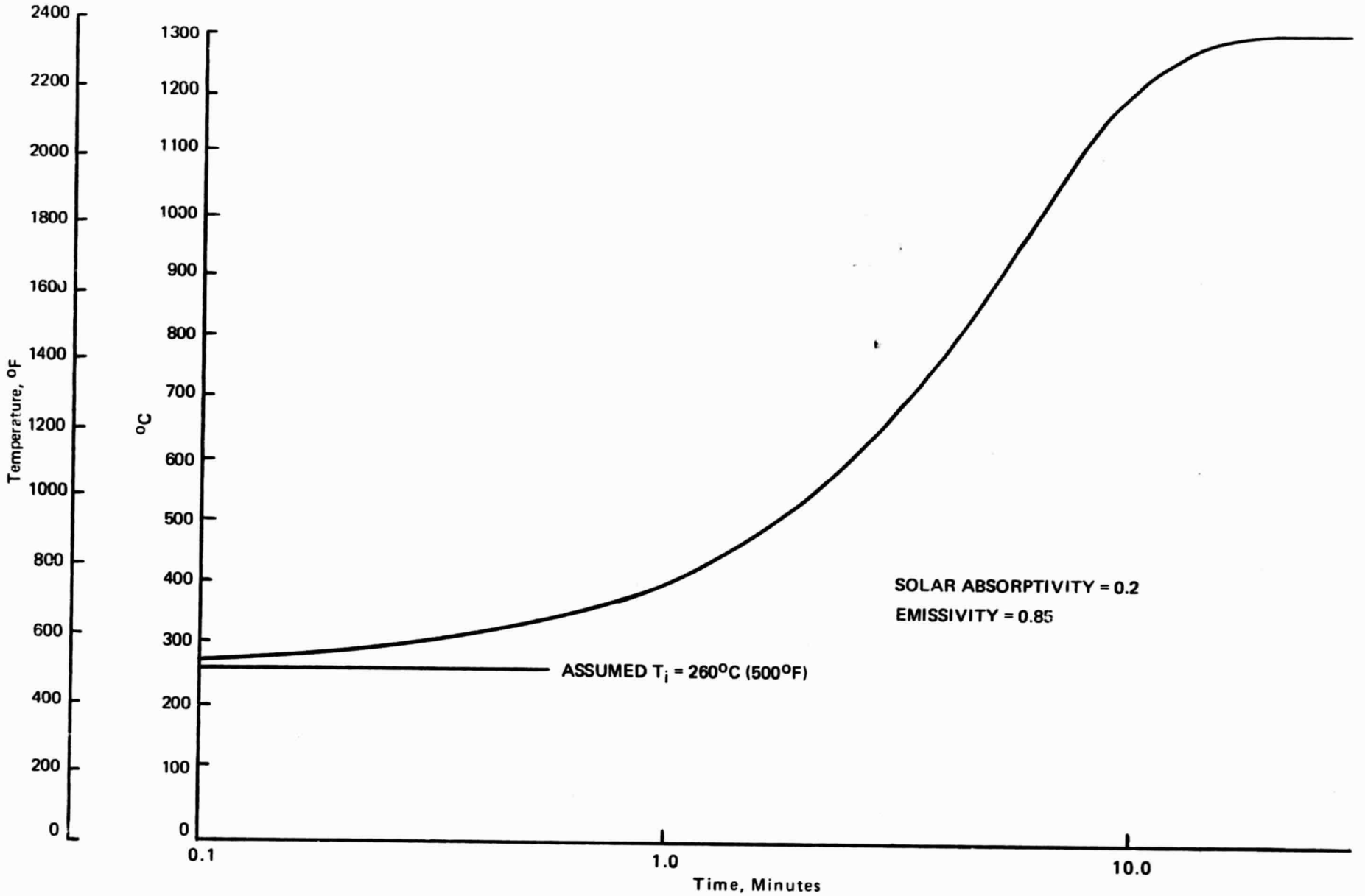

Figure 7-4. Cordierite Ring Time - Temperature Plot

SECTION VIII

ECONOMIC ASSESSMENT OF HEAT PIPE SOLAR RECEIVER

A. RATIONALE FOR ECONOMIC ASSESSMENT

Even in the conceptual design phase of a project, it is necessary to estimate the final cost of components. A concept which is shown to be much too costly at an early stage of conceptualization can be eliminated and effort placed on more viable ones. Analysis of cost early in a program also leads to the identification of areas where significant cost reductions are possible. Thus, the estimated cost of heat pipe solar receivers and components has been performed on all concepts for assessment purposes.

Several factors are significant in performing such an assessment. These include the goals to be achieved for cost, the methods used to estimate costs, and the degree of product maturity assumed. There are subtle problems of extrapolation and of predicting future technical and economic scenarios.

The goals for receiver costs are based on the goals for the cost of the entire Stirling power system, including the costs of the concentrator, power conversion system, controls, and, of course, the receiver. For this assessment, JPL determined the breakdown in cost targets for each component subsystem, and these are discussed below. Since these subsystem goals are interrelated, the subsystem designer does not, and should not, have full freedom. For example, lowering the receiver temperature might make it much cheaper, but, since the Stirling engine would then be less efficient, more concentrator area would be required for the same power, and the overall economics might suffer. Hence it is important to investigate low cost receivers within the total external restraints imposed by the development program goal established by JPL.

Cost estimation methods vary widely depending on the objective. Since this project is aimed at a mass produced product, at the rate of several hundred thousand units a year, equivalent to several thousands of megawatts of installed power or several large coal or nuclear powerplants, the methods used are based on true mass production economics. At this production scale typical costing structures merit attention. Table 8-1 shows the breakdown for a typical mass produced automotive product. The key point is that direct materials make up approximately 50 percent of the selling price. A similar materials cost to selling price ratio was assumed for mass production cost estimates of the heat pipe solar receiver. The method used for cost analysis for this project consisted of calculating component materials weights, calculating the cost of materials and then doubling the total material cost to get an estimated selling price.

Table 8-1. Typical Mass Production Cost Breakdown

Direct Labor (Factory Floor)	3.8%
Direct Material (In appropriate forms)	50.0
Overhead (Including Supervisors and Foremen)	22.0
Labor-Overhead-Materials	75.8
G&A	7.5
Production Cost	83.3
Margin (Facilities amortization, profit, etc.)	16.7
Selling Price	100.0%

Based on automotive practice, including the use of dedicated facilities, multi-shift operation, and a thoroughly mature product.

It must be emphasized that the resulting selling price is a long range forecast. In no way does it represent the price for a unit in the near future.

The determination of material prices in mass production quantities requires special attention. Except for common materials such as rolled steel, aluminum, concrete, etc., this information represents another estimate. This is because many materials and components simply are not now produced at the required level. Vendors are generally unwilling to even estimate costs at levels several orders of magnitude greater than present production. General Electric's approach in these cases was to apply judgement for the more significant components based on the history of other materials, such as aluminum. The ultimate availability of materials, such as chromium and cobalt, was also considered.

Another key consideration is the influence of design improvements. Usual industrial practice is based on continual product improvement, including substitution of materials, redesign to permit the use of lesser quantities of the more expensive materials, and development of low cost materials for a specific application. General Electric has assumed a certain amount of this type of improvement. However, no "breakthroughs" have been assumed.

B. SYSTEM WEIGHT AND COST OBJECTIVES

The weight and cost objectives for the heat pipe solar receiver are shown in Table 8-2. Initial objectives were $\$400/kW_e$; later specific solar receiver and TES cost objectives shown in the table were incorporated which, for the conceptual design provided a cost target of $\$110/kW_e$. Only 20.5 percent of the unit cost is associated with the receiver function, while 79.5 percent is determined by the TES function. Cost reductions appear possible in both areas but the TES area should be capable of the greatest potential reductions. The weight objective was based on projected concentrator design concepts and assumed that the Stirling engine and generator weigh about 265 kg.

C. MASS PRODUCTION COST ESTIMATES

Three designs have been analyzed for cost and weight. The first is the original conceptual design. Its features included vacuum insulation, much use of high-cobalt alloys, and wick covered salt capsules. It is shown earlier in Figure 2-1. It represents little attempt to achieve low cost and is essentially a low risk, one-of-a-kind design. Since it was clearly too expensive, a second design was made. It featured fibrous insulation, low-cost TES salt, substitution of stainless steel for high-cobalt alloys and, generally, a simpler, more efficient structure. The third design decreased the amount of structure required to support the salt and reduced the wicking requirements substantially. Even lower cost insulation was used, and advantage of possible mass production tooling was taken.

Figure 8-1 shows schematically the approach to product improvement and cost reduction.

Table 8-2. Cost and Weight Objectives

Solar Receiver Output	62.1 kW_t
TES Output	52.5 kW_t
Engine Generator Output	16.5 kW_e
Maximum Focal Mount Weight	1365 kg (3010 lbs)
Allowable Receiver & TES Weight	∿1100 kg (∿2420 lbs)

	Per Unit	Per kW_e	%
"Receiver" @ \$6/kW_t	\$ 372.60	\$ 22.58	20.5
"TES" @ \$15/kW_t	787.50	47.72	43.4
"TES" (1.25 hrs. @ \$10/kWh_t	656.25	39.75	36.1
Total Unit Cost Objective	\$1816.35	-	100.0
Total Cost per kW_e	-	\$110.05	100.0
Material Cost Objective*	\$ 908.00		

*Based on material cost equal to 1/2 of the selling price.

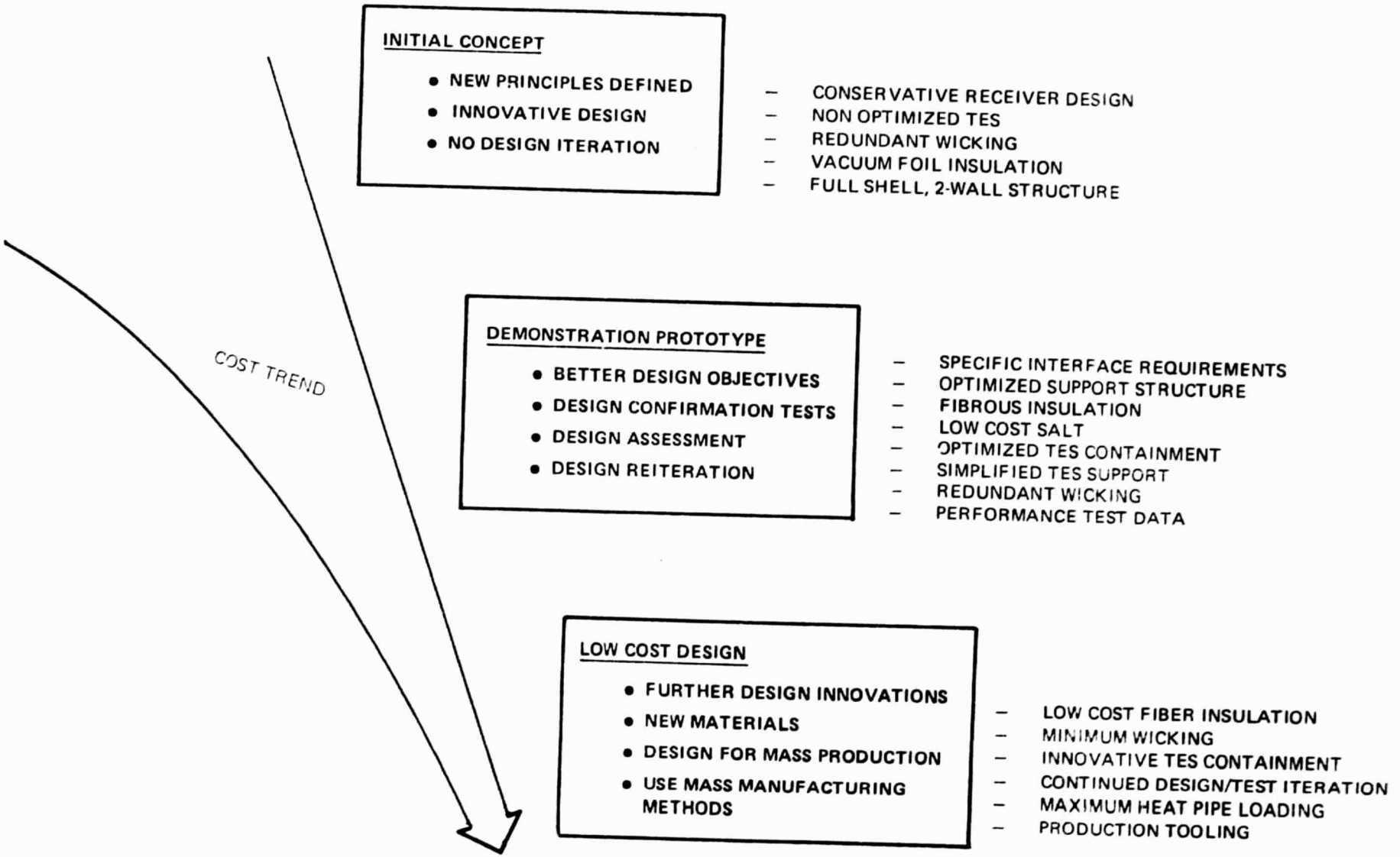

Figure 8-1. Approach to Receiver/TES Cost Reduction

Table 8-3 shows the results. Clearly the original concept does not meet the cost and weight objectives. The second design nearly meets the weight objective, but is still much too costly. The third design meets the weight objective, and is near the cost objective.

This cost reduction process is now being performed under a subsequent contract. It is clear that the goal is potentially attainable, but that more work is still needed.

Table 8-3. Cost and Weight of Heat Pipe Solar Receiver

Parameter	Initial Concept (HA-188 - LiF)		Demonstration Prototype (S. Steel NaF-MgF_2)		Low Cost Design (Tube and Header)	
	kg	lb	kg	lb	kg	lb
Receiver	210	463	210	463	26	57
Salt	359	791	359	791	359	791
Cans	86	190	79	174	29	64
TES Area Structure	212	467	181	399	56	123
TES Area Wicking & Sodium	86	189	86	189	42	93
Insulation	201	443	201	443	188	414
Outer Steel Shell & Support Structure	157	346	157	346	84	185
Total	1311	2890	1273	2805	784	1727
Stirling Engine	147	324	147	324	147	324
Generator	68	150	68	150	68	150
Total	1526	3364	1488	3279	999	2201
Materials Costs Est. (1978 Dollars)	$14,972		$10,440 (~$8760 with cellular insulation)		$2,380	

SECTION IX

CONCLUSIONS

The following significant conclusions are made regarding the use of alkali metals for thermal transport and thermal energy storage in point focusing, distributed concentrator Stirling solar power conversion systems:

1. Thermal transport in focus mounted, compact and fully integrated solar receiver/TES/Stirling engine-generator subsystems is best effected through the use of alkali metal heat pipes. Heat transfer fluid pumping losses are negligible. The temperature drop from solar receiver to Stirling engine is minimal because of the high alkali metal evaporating and condensing heat transfer coefficients. Reverse heat flow from the TES is avoided. The compactness afforded by the use of heat pipes is a significant factor: it aids in the reduction of thermal losses; it minimizes focal point mass; it makes the unit readily mass producible and testable at the factory and it permits simple low-cost field installation and change-out for local repair and maintenance or for re-shipment to a major overhaul center. Even without the use of TES, this heat transfer method minimizes receiver and Stirling engine heat exchanger hot spots and temperature variations which can adversely affect engine life and performance.

2. Latent heat thermal energy storage is preferred over sensible heat storage. The near constant operating temperature of the TES heat source avoids the energy degradation associated with the operation of sensible heat storage over a wide temperature range. It permits the Stirling engine to operate at a steady, near maximum operating temperature without significant fluctuations in power level or losses in efficiency at off-design operating temperatures. The efficiency of latent heat storage at high cycle operating temperatures is particularly effective in that it minimizes the weight and cost of high temperature materials required to contain both the TES material and the heat transfer media.

3. The availability of latent heat storage and alkali metal thermal transport offer significant advantages to the addition of fossil fuel hybridization. Fuel combustion can be accomplished in a highly efficient on - off mode at high combustion efficiencies. The need for special

controls, variable combustion rates and a high turn-down ratio required to supplement variable solar insolation rates which would be required in a direct solar receiver, can be avoided. The combustor could be installed on the secondary heat pipe thus avoiding reradiation losses from the receiver during fossil fuel combustion. The relatively large external surface areas of the secondary TES heat pipe are adequate for combustion-side convective heat transfer; and, the high evaporative heat transfer film coefficient in the alkali metal minimizes both temperature differentials in the secondary heat pipe and the possible overheating of the heat transfer surfaces.

4. Heat pipe design confirmation tests indicate the actual heat pipes will perform as predicted at all operating angles of inclination and that the heat pipes will not allow significant reverse heat flow during intermittent operation or during overnight periods in the stowed position.

5. Wicking design confirmation tests indicate the selected wick configurations have the pumping capacities and flow capabilities across wick joints required by the conceptual designs.

6. The heat pipe solar receiver with TES permits an optimum orientation of the Stirling engine. The engine can be oriented so as to provide ready accessibility to all engine components and to permit positive gravity drainage of the engine oil seals at all angles of inclination of the solar concentrator during normal operation. It is not necessary that the centerline of the Stirling engine heat exchanger be concentric with the solar receiver.

7. The conceptual design of the focus mounted heat pipe solar receiver with TES provides a basis for the early fabrication and test of a highly efficient distributed concentrator solar Stirling power conversion system and for the progressive development of lower cost systems in mass production.

8. Pumped loop liquid metal thermal transport and storage systems have significant disadvantages compared to the focal mounted HPSR but may have possibilities where larger TES is required. For long pipe runs between several concentrators and a common TES engine-generator, the piping heat losses are prohibitive. The system requires pumps, valves, controls and large masses of alkali metal which are heavy, which add appreciable cost and which will, in some cases, require development of components not currently available. For single phase pumped loops, significant sensible heat temperature differentials are required to transport thermal energy. This results in the operation of various components in the system over a wider range of

temperatures than necessary with resultant losses in operating efficiencies; it also produces higher operating temperatures in the solar receiver than would be required using heat pipe thermal transport. The system might have some marginal utility for a single concentrator if significantly larger TES periods were required and the TES mass was utilized to replace some of this concentrator counterbalance mass.

SECTION X

RECOMMENDATIONS

The following recommendations are made regarding continuing efforts related to the further development of point focussing, distributed concentrator Stirling solar power conversion systems with liquid metal thermal transport and latent heat thermal energy storage:

1. The design, fabrication and test of a focus mounted heat pipe solar receiver with TES is recommended.

2. Additional conceptual design effort is needed to continue the process of cost reductions in heat pipe solar receivers in order to achieve minimum capital cost in mass production; such effort should be initiated both to identify these design concepts and to define the experimental design confirmation and modular test efforts necessary to implement them.

3. Other TES supportive technology programs should be continued to more accurately characterize the physical, thermal and corrosion compatibility properties of TES materials applicable to solar Stirling engine operating temperatures.

4. An application requirements study should be undertaken to assess the economic value of distributed concentrator solar Stirling power in conjunction with thermal energy storage and fossil fuel hybridization. The study might use as inputs such factors as size of the concentrator unit, TES duration, extent of fossil fuel utilization, utilization of the power on a utility grid, swing load power requirements, effect of solar Stirling market penetration and alternate utility power operation options.

APPENDIX A

DESIGN ANALYSIS OF A GAS LIFT PUMPED LOOP

INTRODUCTION

Gas lift pumps operate on the combined principles of density difference and entrainment of a fluid behind rising gas bubbles. Their great attractiveness lies in that a pump is not needed that actually pumps the liquid through which the gas is bubbled. This analysis investigates the applicability of such a pump for pumping a liquid metal around a loop on a paraboloid solar concentrator/receiver between the receiver and a thermal energy storage unit. A method of simplified analysis is derived herein and compared with the results of more accurate analysis.

The liquid metal pumped loop thermal transport portion of the single concentrator solar Stirling power presently under study for the JPL Solar Stirling Engine can be designed in a variety of ways. One of the most intriguing is the gas lift pump design suggested by Elliott[1]. This approach uses bubble driven circulation to drive the heat transfer fluid through the thermal system. While such gas lift pumps are unfamiliar to many in the heat transfer community, they have a respectable provenance. In Marks' Handbook[2] there is a discussion of such pumps applied to municipal water systems. Water lifts of 91.4 m (300 ft) with efficiencies of 36 to 48 percent are reported.

One of the attractions of this mode of pumping is that it may, as suggested by Elliott, solve the pumping problem in a materials/temperature regime where mechanical pumps are not available. For this reason, a design analysis for the use of a gas lift pumped loop was carried out. The results of that analysis follow.

DESIGN DEFINITION

The sketch of Figure A-1 describes the design configuration analyzed. This configuration may differ in detail from the precise design under study at JPL, which was unavailable to us at the time of this work, but it represents with sufficient accuracy the salient geometrical requirements. In this sketch, the concentrator parabola is 11 meters in diameter, has a support ring at 60% of its radius, and has a tripod supporting the receiver at the focal point. The focus is at 0.6 times the diameter. There is shown, in addition to the basic components, a line designated the High Rise Pipe which runs from the lowest point on the dish to the receiver. Not shown are the heat storage tank, nor the vertical extent of the gas/liquid separation tank which will extend somewhat above the receiver.

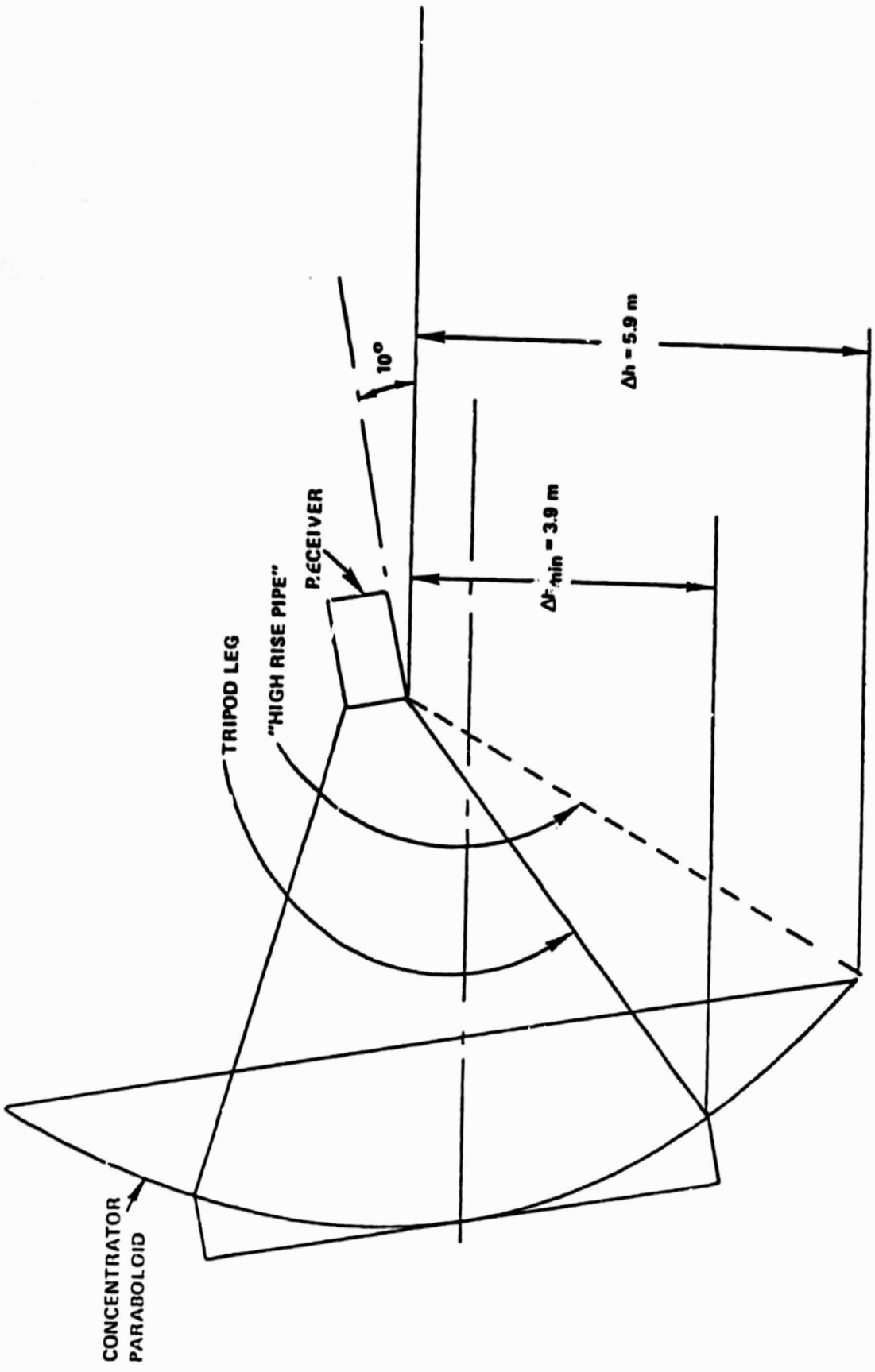

Figure A-1. Gas Lift Pump Configuration (Effective Pumping Height is Shown at 10^{o} Inclination)

Gas lift pumps provide pressure, as will be discussed below, in proportion to their vertical height. The critical design condition, from the pressure rise point of view, is, therefore at the lowest elevation, which is 10°. The 10° horizon is indicated. The vertical height of the tripod leg in the vertical plane is 3.9 m (11.9 ft.), while that of the high rise pipe is 5.9 m (18 ft.). These dimensions limit the pressure available from the gas lift pump.

Further characteristics of related components can be found in Reference 3. The heat transfer fluid is sodium. The pump gas is argon. The operating temperature is 871°C (1600°F). Using the piping, heat exchanger and storage tank characteristics supplied in Reference 3, an estimate was made of the circuit pressure drop coefficient, $K = \Delta P/q_o$, where q_o is the dynamic pressure of the flow in the piping. Details of this analysis are provided in Reference 4. The results of this analysis provide a value of K = 20. However, implied in this result is the assumption that the flow velocities inside the Stirling engine heat exchanger are sufficiently small so that they do not contribute to the pressure drop of the system. This assumption seems reasonable with the present configuration, however, it might require modification if, for example, the mass flow were substantially reduced. In this case tight baffling might be needed to insure adequate heat transfer and this, in turn, would increase the pressure drop in the heat exchanger with respect to that in the piping.

From the above analysis, the chart of Figure A-2 was prepared. The specific weight of sodium was taken to be 720 kg/m^3 (45 lb/ft^3) at the operating temperature of 871°C (1600°F). A range of pipe diameters of from 25-50 mm (1-2 in.) was used and the resulting relationships between the system pressure drop and the system weight flow calculated and plotted. Clearly shown in this figure is the variation of the pressure drop with the second power of the flow. Less clearly is indicated the inverse fourth power variation with pipe diameter. Earlier design calculations employed larger 76 mm (3 in.) piping. However, layouts of the corresponding receiver designs quickly devolved upon 25 mm (1 in.) piping. Larger sizes cause rapid increases in cost, particularly of insulation, size and weight. It will be difficult, from a systems point of view, to entertain piping much larger than 25 mm (1 in.).

STATIC ANALYSIS OF THE GAS LIFT PUMP

The diagram of a gas lift pump based on the suggestion of Elliott is shown in Figure A-3. Annotated upon this figure are the pressure defining equations around the liquid loop. By straightforward substitution of these equations we can arrive at an expression for the pressure P_1 as

$$p_1 \simeq \Delta P + \rho_\ell \, g h_1 \left[\left(\frac{h_f}{h_1} \right) \left(\frac{\bar{\rho}_1}{\rho_\ell} \right) - 1 \right] \qquad (1)$$

where the two loop pressure drops, Δp_1 and Δp_2 have been combined into ΔP. (Note that the density ρ_1 refers to the average density of the two phase fluid over the height h_f, while the density $\bar{\rho}_2$ refers to the density over the height $(h_f - h_1)$). However, p_1 is also

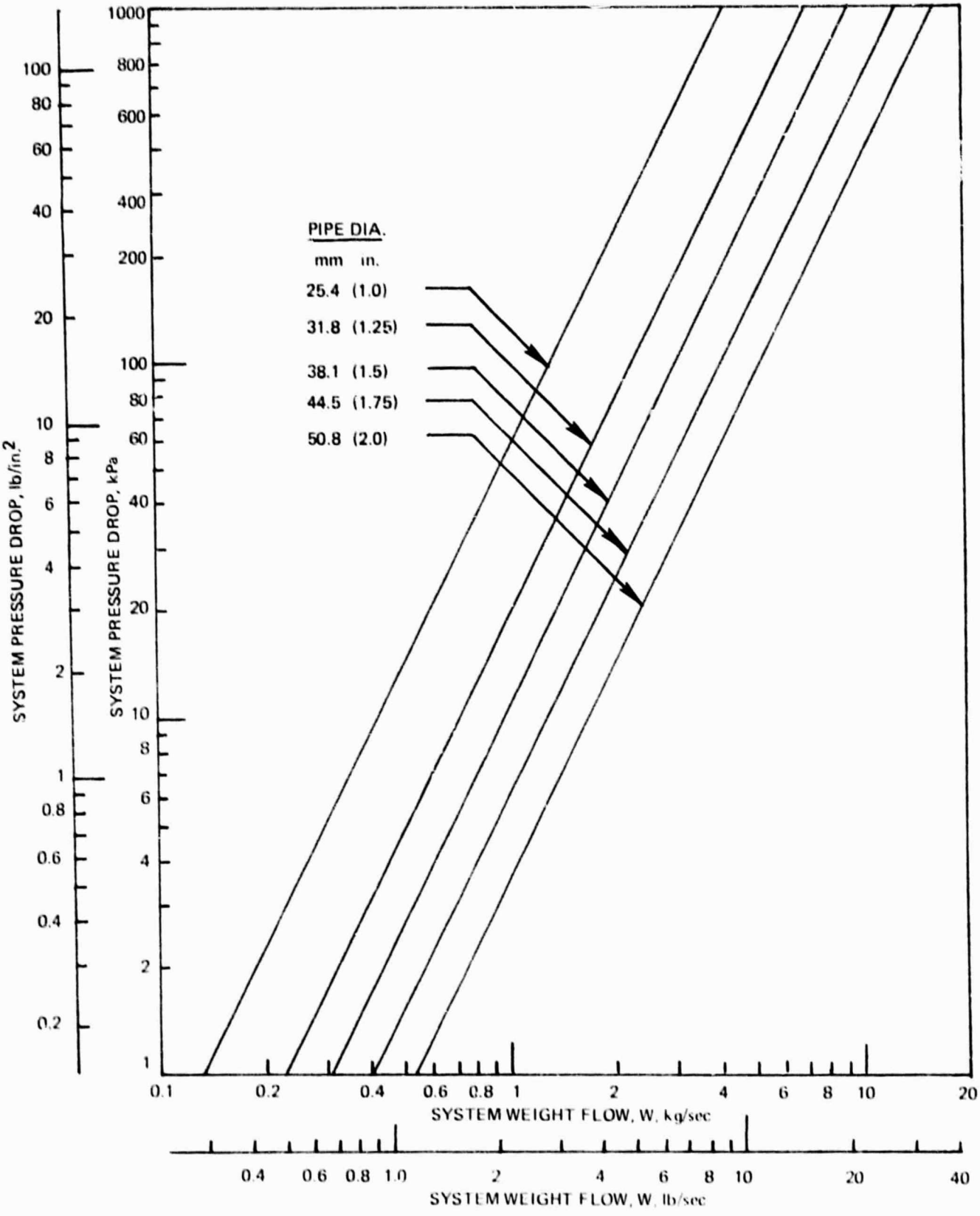

Figure A-2. Sodium Mass Flow vs. Pressure Drop for Various Pipe Sizes

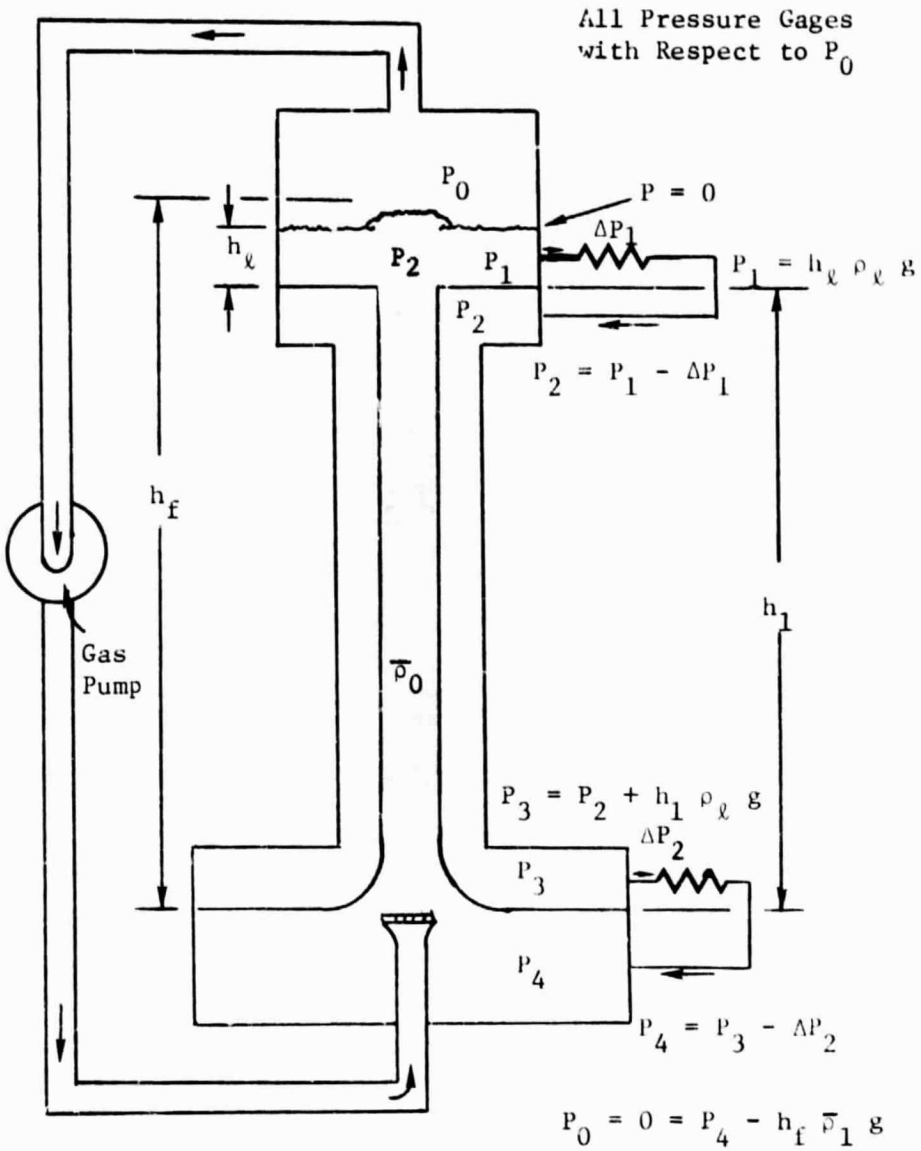

Figure A-3. Diagram of Gas Lift Pump (From Elliott).

$$p_1 = \rho_\ell \, g h_\ell \tag{2}$$

combining (1) and (2) and simplifying leads to

$$\Delta P = h_\ell \, \rho_\ell \, g - h_\ell \, \rho_\ell \, g \left(\frac{h_f}{h_1} \frac{\rho_1}{\rho_\ell} - 1 \right) \tag{3}$$

We introduce the notion of the static height, h_s, defined as

$$h_s = \frac{\Delta P}{\rho_\ell g} \tag{4}$$

which is the head of liquid of density ρ_ℓ which must be supplied by the pump. Introducing this definition in (3) produces

$$h_s = h_\ell + h_1 - h_f \frac{\bar{\rho}_1}{\rho_\ell} \tag{5}$$

But $$(h_f - h_1) \, \bar{\rho}_2 = h_\ell \, \rho_\ell \text{ (see Fig. A-3)} \tag{6}$$

So that $$h_f = h_1 + h_\ell \times \frac{\rho_\ell}{\rho_2} \tag{7}$$

If (7) is substituted into (5), the result can be reduced to

$$h_s = h_1 \left(1 - \frac{\bar{\rho}_1}{\rho_\ell} \right) + h_\ell \left(1 - \frac{\bar{\rho}_1}{\rho_2} \right) \tag{8}$$

Now if the pressure drop from p_4 to p_1 is small compared to the reservoir pressure, p_0, i.e.,

$$\left(\frac{p_4 - p_1}{p_0} \right) << 1 \tag{9}$$

which is a reasonable case, then $\bar{\rho}_1 \approx \bar{\rho}_2$* and

$$h_s = h_1 \left(1 - \frac{\rho_1}{\rho_\ell} \right) \tag{10}$$

(Note we can now drop the subscript on ρ).
Equation (10) provides a simplified explanation of the pressure developed

*This is equivalent to the assumption that the gas in the pump is incompressible.

by the gas lift pump. The pressure arises from the difference in densities between the liquid in the downcomer and the mixture in a corresponding length of two phase flow pipe. The absolute limiting pressure that can be developed is the static head in the downcomer, but that only if the average density in the two phase flow is zero.

An expression for the density ratio $\bar{\rho}/\rho_\ell$ can be constructed as

$$\frac{\bar{\rho}}{\rho_\ell} = \frac{\rho_g A_g + \rho_\ell A_\ell}{\rho_\ell (A_g + A_\ell)} = \frac{\frac{\rho_g}{\rho_\ell} + \frac{A_\ell}{A_g}}{1 + \frac{A_\ell}{A_g}} \tag{11}$$

It is reasonable to assume that $\frac{\rho_g}{\rho_\ell} << \frac{A_\ell}{A_g}$* for a wide variety of cases of interest. For such cases,

$$\frac{\bar{\rho}}{\rho_\ell} = \frac{A_L}{A_L + A_G} = R_L = (1-R_G) \tag{12}$$

Substituting (12) in (10) provides

$$h_s = h_1 R_G \tag{13}$$

From this we define a standpipe effectiveness of the gas lift pump as the ratio of the pressure developed by the pump to the height of the downcomer. For the static analysis

$$\varepsilon_s = \frac{h_s}{h_1} = R_G \tag{14}$$

From this relationship it can be inferred that it will be difficult to achieve effectiveness factors approaching unity since with equal volumes of gas and liquid the static effectiveness is 0.5. The actual gas lift pump has further losses.

A comparison was made between this completely simplified static analysis and the results calculated by Elliott. In order to make this comparison the two-phase empirical relations of Hughmark[5], for determining the gas mass flow rate, used by Elliott were also used here. The comparison shown in Figure A-4 is remarkably good with Elliott's calculations showing pressure losses with respect to the static analysis at the high gas fraction, i.e., high gas flow rates. This is to be expected since the static analysis is unaware of the frictional pressure

*The ratio $\frac{\rho_\ell}{\rho_g}$ is typically of the order of magnitude 10^{-3} while ratios $\frac{A_L}{A_G}$ much less than 10^{-1} would be of little practical interest.

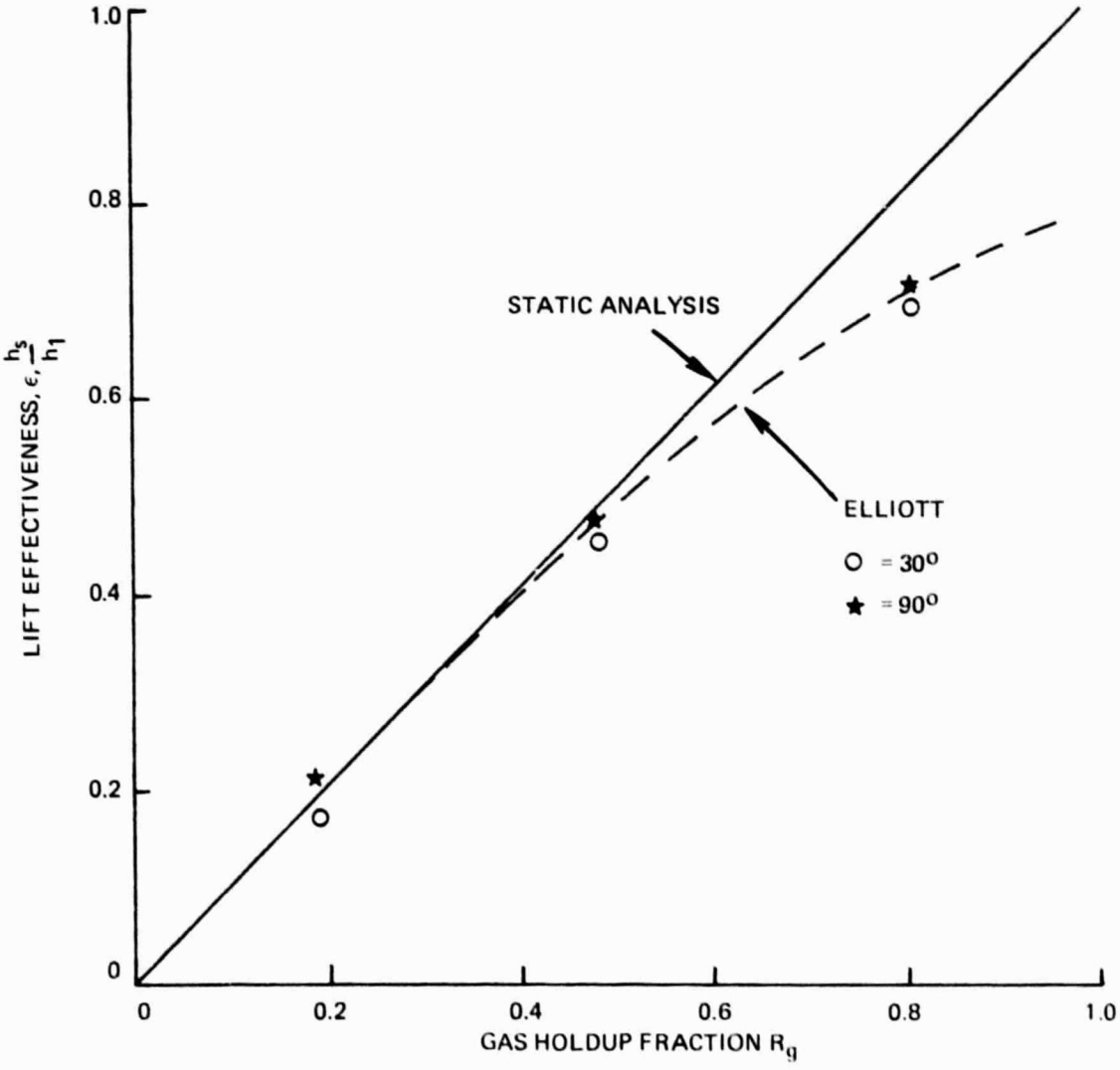

Figure A-4. Gas Lift Pump Effectiveness vs. Gas Holdup Fraction

drop. This comparison serves two purposes, it provides an outside check on Elliott's analysis and it provides an extremely simple analytical approximation for the effectiveness as a function of the gas holdup fraction.

ESTIMATE OF THE EFFECTIVE STANDPIPE HEIGHT, h_1, AVAILABLE FROM THE MAXIMUM DOWNCOMER

The analysis of Elliott and the static analysis above makes the assumption that the density of two phase flow will be uniform throughout. With pipes inclined substantially from the vertical, as will be the downcomer in this apparatus at its design point, this assumption becomes questionable since separation of the gaseous and liquid phases could occur. This doubt is especially true when the gas holdup fraction, R_g, is substantial.

Intuition leads one to believe that in such situations, the bubbles will tend to rise vertically, not along the axis of the downcomer. As a result of this preferential motion, the originally uniform distribution of gas and liquid will become skewed with the gas tending to collect at the top and the unbouyed liquid at the bottom. To the extent that this unmixing occurs, the performance of the pump will be impaired. The amount of gravitational (bouyancy) separation effected would depend upon the L/D of the pipe, the inclination angle and the ratio of the vertical component of the bubble terminal velocity with respect to the liquid velocity. Hughmark comments that his correlation works as well for horizontal pipes as vertical ones but he had eliminated the Weber number (the bubble convection parameter) before he analyzed the horizontal data. The point remains unclear.

In order to estimate the pressure rise available from the gas lift pump, we must make some preliminary assumption as to the maximum value of R_G which we may prudently use. Since the performance estimates we now make are not based on test data it is wise to leave some headroom for performance degradation with respect to the theoretical estimates. In Figure A-5 there is a plot of the Hughmark correlation of the gas holdup fraction as a function of mass flow for an argon driven pump. The selection of argon will be discussed below. In this figure it can be seen that $R_g \propto$ log in. in the central region but drops even below the logarithmic rate at higher flow rates. Notice that for an order of magnitude increase in gas flow, from 3×10^{-4} to 3×10^{-3}, the gas holdup fraction increases from 0.3 to 0.7, that is, it barely doubles. This fact and the fact illustrated in Figure A-4, that the accountable losses increase at an increasing rate with gas flow (and R_G) suggest that we select a value of R_G not unduly great. We have assumed a value of $R_G = 0.6$. From Elliott's curve in Figure A-4, we find a value of $h_s/h_1 = 0.56$ and we apply a factor of 0.9 to this to account for pressure losses not included in Elliott's analysis. From which

$$\Delta P = \rho_\ell \, g \, h_1 \times 0.56 \times 0.9$$

$$= [766 \times 9.8 \times 5.9] \times [0.504]$$

$$= 44.3 \times 0.504 = \underline{22.3} \text{ k Pa. } (\underline{3.24} \text{ psi}).$$

A line corresponding to this, the available pressure, has been added to Figure A-2.

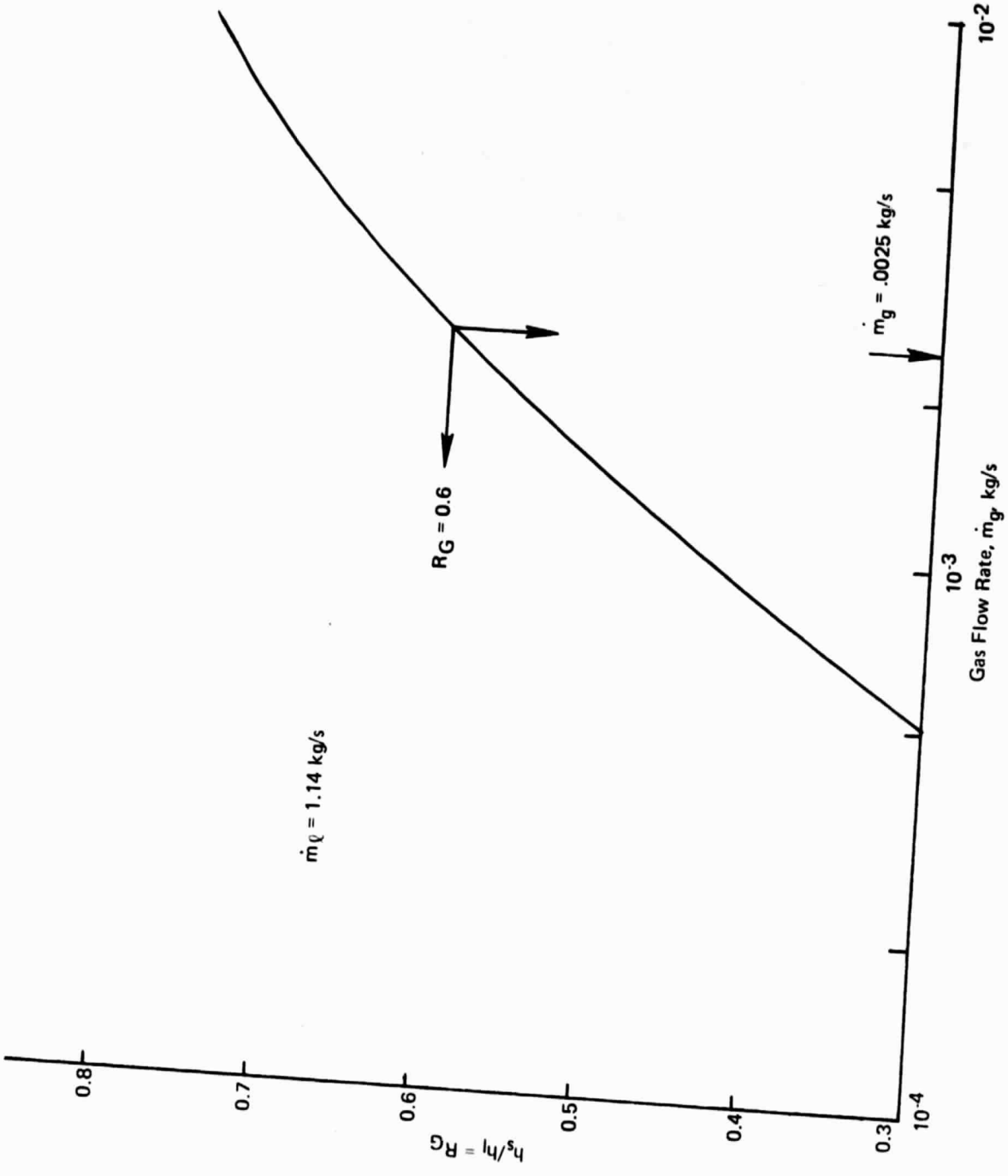

Figure A-5. Gas Holdup Fraction from Hughmark for Argon Gas Lift Pump

The above calculation assumes that all of the "high rise pipe" is allocated to the downcomer, i.e., we are using the maximum value of h_1, the gas/liquid separation chamber would have to be installed above the receiver. This chamber must be very effective since the pump is presumed to be in a cold leg. Sodium carried over into the cold leg will solidify creating both maintenance and reliability problems. The impact of the separation chamber has not been evaluated.

By reading the intersections of the available pressure line with the various pipe diameters, we can determine the corresponding flow rates. These various flow rates are required to deliver the same amount of heat, 52.5 KW, to the SEHX*. Naturally, the temperature drop needed to deliver this constant heat will vary inversely with the flow rate. The temperature drop can be computed from the following.

$$q = 52.5 \text{ KW} = 34.12 \frac{\text{Btu}}{\text{sec}}$$

$$q = \dot{\omega} C_p \Delta T \tag{15}$$

$$\Delta T = \frac{q}{\dot{\omega} C_p} \quad C_{P(Na)} = 0.30, \text{ hence} \tag{16}$$

$$\Delta T = \frac{34.12}{0.3 \times \dot{\omega}} = \frac{166}{\dot{\omega}} \ ^\circ F$$

This relationship is plotted in Figure A-6 where $\dot{\omega}$ has just been determined above.

It is readily apparent that increasing the flow rate decreases the temperature drop in the SEHX and correspondingly increases the SE operating temperature while on the other hand it increases the pressure drop and the pump work. In the case of the gas lift pump these last factors may be crucial. It is of interest therefore to establish a quantitative estimate of the effect of the flow rate on the SE efficiency so that the conflicting interests can be reasonably compromised. Therefore, an estimate was made of the effect of operating temperature on the SE efficiency. Their estimates showed that effect of decreasing the SEHX wall operating temperature from 871°C (1600°F) causes a decrease in SE efficiency of 0.022 percentage counts/°F from which we can evaluate the impact of changes in the flow rate and SEHX wall temperature on the SE efficiency.

ESTIMATION OF THE PUMP POWER

Since the gas flow is essentially incompressible, see (9), the gas and liquid pumping requirements can be considered together. That is,

$$P_P = \frac{Q_T \Delta P}{\eta_P} \tag{17}$$

*Stirling Engine Heat Exchanger.

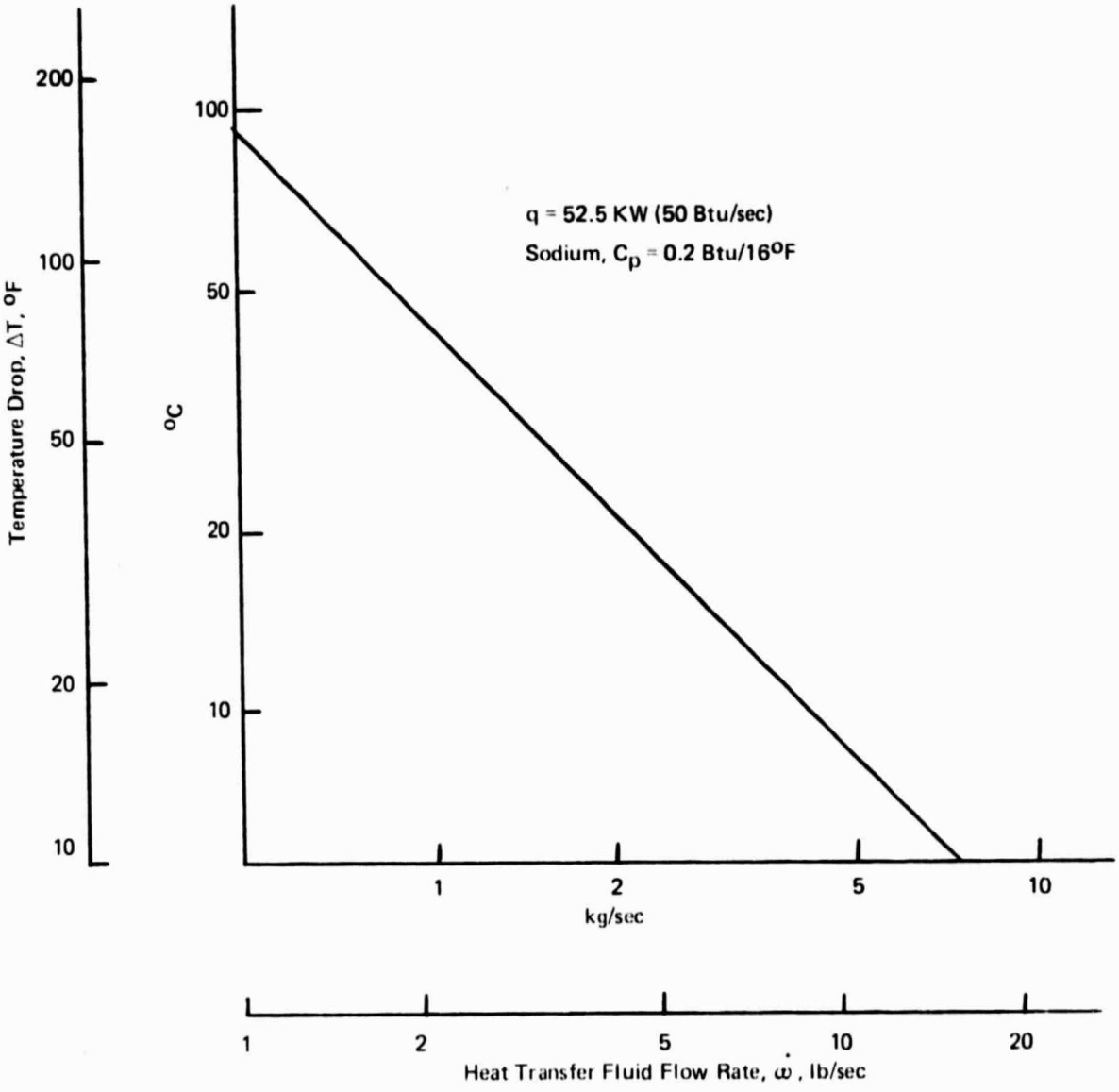

Figure A-6. The Heat Transfer Fluid at the Stirling Engine Heat Exchanger

where $Q_T = \frac{\dot{m}_\ell}{\rho_\ell} + \frac{\dot{m}_g}{\rho_g}$ (18)

if we assume the pump efficiency to be 75%.

$$P_P = \frac{4}{3}\left(\frac{\dot{m}_g}{\rho_g} + \frac{\dot{m}_\ell}{\rho_\ell}\right) \quad (19)$$

The fraction of their pump work which is lost to the system can be computed by considering that the pump power was provided by the Stirling engine, the generator and an electric motor. That is, the total thermal energy expended on the pump is

$$P_{TOT} = \frac{P_P}{\eta_m \eta_g \eta_{st}} \quad (20)$$

where the subscripts should be self-explanatory.

Since all of the pump energy is deposited in the fluid, the energy lost is

$$P_{LOST} = P_{TOT} - P_P = P_P\left(\frac{1}{\eta_m \eta_g \eta_{st}} - 1\right) \quad (21)$$

If we assume for present purposes that in these sizes, $\eta_m = 0.80$, $\eta_g = 0.80$, and $\eta_{st} = 0.45$, $P_{LOST} = P_P \left(\frac{1}{.8 \times .8 \times .45} - 1\right)$

$$= P_P\ (3.47 - 1) = 2.47\ P_P$$

$$\Delta\eta = \frac{2.47\ P_P}{52.5}$$

HEAT REJECTED TO THE GAS COOLER

The central idea of using the gas lift pump is to be able to use the pump in a cold leg, thereby eliminating the need for the expensive development of an expensive hot pump. The pump gas leaves the separation chamber of the pump at the liquid temperature 871°C and must be cooled to essentially room temperature to use an inexpensive pump. The heat rejected in this gas cooler is

$$q_c = \dot{m}_g\ C_{P_2}\ \Delta T \quad (22)$$

For purposes of this analysis, we shall assume that the mass flow of gas required to pump a given ΔP is proportional to the mass flow of liquid pumped. Therefore,

$$q_c = \left(\frac{\dot{m}_g}{\dot{m}_\ell}\right)_o \times \dot{m}_g \rho_g C_p \Delta T \qquad (23)$$

Argon is selected as the pump gas since, of candidate gases, it has the lowest value of ρC_p, thereby minimizing this loss.

Using this relationship the receiver heat supplied and efficiency can be corrected by this loss. A recuperator can be used to reduce this expense at some equipment cost. The effect of a recuperator has not been evaluated.

In Table A-1 the performance characteristics for the gas lift pump outlined above have been tabulated for piping sizes from 25-50 mm (1-2 in.) in diameter. From this table it can be seen for the preliminary design undertaken, that 25 mm piping is of approximately the correct size and that the gas pump installation (without recuperator) costs the system about 10% in performance. With an ideal recuperator, the optimum pipe size would be somewhat larger, but the increased system cost for the recuperator and the larger, heavier, and more costly receiver have not been evaluated.

SUMMARY AND CONCLUSIONS

A preliminary analysis has been carried out of a gas lift pumped thermal subsystem for the solar Stirling engine. Results of this analysis indicate that the gas lift pump is a feasible approach but that associated with it is an efficiency loss of between 3.4 and 9 percent. The former value probably cannot be achieved with an economic design. The latter value is probably a reasonable target figure.

Problem areas have been uncovered which would require design and development problems. Among these are:

An analysis will have to be carried out to resolve the relative COE with and without a recuperator. Without a recuperator, the losses (~9%) seem too great to be allowed for a pump. On the other hand an effective recuperator will bring added costs.

A resolution of the problems of a pump operating with sodium in perhaps liquid, vapor and solid phases poses pump design problems which must be resolved through development.

The gas lift pump is feasible at some cost in system efficiency, and development cost and risk. The impact of the gas lift pump on COE can not be discerned at present.

Table A-1. Performance Characteristics of the 23.4 kPa (3.24 psi) Argon Pump

Pipe Diameter mm	Pipe Diameter in.	$\dot{\omega}$ kg/s	$\dot{\omega}$ lb/s	SEHX Loss ΔT °C	SEHX Loss ΔT °F	SEHX Loss "Counts" $\Delta\eta$	SEHX Loss $\Delta\eta$ %	Pump Loss $\Delta\eta_2$ %	Cooling Loss $\Delta\eta_3$ %	Total Loss No Recup. $\Sigma\Delta\eta$ $\Sigma\Delta\eta$ %	Total Loss Ideal Recup. $\Sigma\Delta\eta$ Δ
25.4	1.00	0.63	1.39	68	123	2.7	6.0	0.5	2.5	9.0	6.5
31.8	1.25	1.11	2.45	38	68	1.5	3.3	0.9	4.4	8.6	4.2
38.1	1.50	1.50	3.3	28	50	1.1	2.4	1.2	6.0	9.6	3.6
44.4	1.75	1.95	4.3	21	38	0.8	1.8	1.6	7.8	11.2	3.4
50.8	2.00	2.59	5.7	16	29	0.6	1.3	2.1	10.3	13.7	3.4

REFERENCES

1. Elliott, D.G., Informal Communication, "Gas Lift Pump for Solar Heat Transfer", JPL, Sept. 28, 1978.

2. Baumeister, T. et al., Marks' Standard Handbook for Mechanical Engineers, Eighth Edition, McGraw-Hill, New York, 1978.

3. Zimmerman, W.F., "Conceptual Design Study on the Application of Liquid Metal Heat Transfer Technology to the Solar Thermal Power Plant", DOE/JPL Semi-Annual Progress Report on Advanced Technology Development, Oct. 1, 1978 - March 31, 1979, GESP-819.

4. Unpublished Notes - Lew Feldman, General Electric Co., Advanced Energy Programs, Dec. 22, 1978.

5. Hughmark, G.A., "Holdup in Gas-Liquid Flow", Chemical Engineering Progress, Vol. 58, No. 4, pp. 62-65, April 1962.